Simulation and control of denitrification biofilters described by PDEs Simulation et commande d'un biofiltre de dénitrification décrit par des EDP

Jesus Ixbalank Torres Zuniga

Université Paul Sabatier

Laboratoire d'Analyse et d'Architecture des Systèmes - CNRS

Thèse

présentée en première version en vue d'obtenir le grade de Docteur,

spécialité *Systèmes Automatiques*

par

Ixbalank TORRES

Simulation and control of denitrification biofilters described by PDEs

Thèse soutenue le 31 mai 2010 devant le jury composé de :

Frédéric MAZENC	INRIA	Rapporteur
Antonio A. ALONSO	IIM-CSIC	Rapporteur
Isabelle QUEINNEC	LAAS-CNRS	Directrice de Thèse
Alain VANDE WOUWER	Université de Mons	Co-directeur de Thèse
Lucie BAUDOUIN	LAAS-CNRS	Examinatrice
Jean-Louis CALVET	LAAS-CNRS	Examinateur

J'aime le chant du cenzontle,
oiseau aux quatre cent voix,
j'adore la couleur du jade,
et le parfum entêtant des fleurs,
mais plus que tout j'aime mon frère: l'homme.

Nezahualcoyotl
Roi poète de Texcoco, 1402-1472

Avant-propos

Depuis le début de ce travail de recherche, notre but principal a été de concevoir un correcteur pour un biofiltre de dénitrification décrit par un ensemble d'équations en dérivées partielles. Dans un premier temps, nous avons profité de l'expertise du groupe Méthodes et Algorithmes en Commande du Laboratoire d'Analyse et d'Architecture des Systèmes - CNRS dans la commande et la résolution de problèmes d'optimisation sous des inégalités matricielles linéaires. Ainsi, nous avons pu synthétiser des correcteurs par retour de sortie formés par une loi de commande par retour d'état complétée par un observateur de Luenberger.

Durant mon séjour au Service d'Automatique de l'Université de Mons en 2008, j'ai travaillé sur la modélisation, la réduction du modèle et la simulation des systèmes à paramètres distribués pour représenter le biofiltre sous une forme classique en espace d'état en considérant les modes, représentant l'information temporelle du système, les plus importants. Ainsi, cette nouvelle représentation a été utilisée pour synthétiser un correcteur par retour de sortie à partir d'un système d'ordre réduit.

Finalement, nous avons fusionné les méthodologies de simulation des équations à dérivées partielles et la commande non-linéaire maîtrisées par les deux groupes de recherche précédents. Comme résultat, nous avons conçu une loi de commande à retour qui linéarise les dynamiques du biofiltre en boucle fermée complétée par un observateur à paramètres distribués.

Il ne me reste donc qu'á remercier les MAC pour l'accueil et le support durant ces trois ans et demi, spécialement Isabelle qui m'a guidé et qui m'a beaucoup appris et conseillé lors du développement de mon travail de recherche. Le premier groupe de thésards, Wilfried, Christophe, Yassine et Pauline (même si elle est DISCO) qui m'ont super bien accueilli dès mon arrivée à Toulouse. Giorgio, Luiz et Thomas pour leur amitié pendant mon séjour au LAAS. Sandy qui a donné la touche féminine au bureau et qui m'a beaucoup aidé à rédiger en français et en anglais. Tous les autres

jeunes du groupe, Nedia, Carlos, Fernando, Mounir, Bogdan, Josep, Carlo, Akin, Tung et Jean François qui ont fait l'ambiance dans le LAAS, skyMAC et seaMAC. Enfin, les permanents, M. Calvet, Didier, Germain, Denis, Fred, Sophie, Dimitri, Lucie, les deux Christophe, les deux Vincent, tous très sympa et toujours prêts à discuter lorsque l'on est bloqué.

Je tiens également à remercier toute l'équipe du Service d'Automatique de l'Université de Mons, surtout Alain qui m'a beaucoup appris durant mon séjour à Mons et Carlos Vilas qui m'a beaucoup aidé à acquérir les aspects techniques des méthodes FEM et POD. Cristina et Francisca pour leur amitié pendant mon séjour à Mons. Enfin, les autres doctorants, Johan, Oleksandr, Guillaume, Laurent et Bob, tous très sympa.

Je suis très reconnaissant à M. Frédéric Mazenc de SUPELEC-CNRS et M. Antonio. A. Alonso de IIM-CSIC pour avoir accepté d'examiner cette thèse et d'en être les rapporteurs.

J'adresse mes plus grands remerciements au CONACyT pour le soutien financier lors du développement de cette thèse de doctorat, á l'UPS pour le soutien financier lors de mon séjour à Mons, au LAAS-CNRS pour l'accueil dans le laboratoire et á tout le personnel qui m'a aidé à résoudre les différentes situations auxquelles j'ai dû faire face.

Je n'oublierai jamais tous les copains de l'équipe de foot-ball du LAAS, de l'équipe de snowboard de l'UPS, les amis bolivariens et les interminables discussions dont Juan Pablo, Anibal, Eduardo, David, Hugo et Gibran. Tous les amis du monde avec qui j'ai passé des bons moments et appris le meilleur que j'ai pu de leur cultures, et très chaleureusement ma *polola*, qui a rendu la dernière année en France très spéciale.

Je ne peux pas finir sans faire mention à la France, ce beau pays que je tiendrai toujours au coeur. Sa campagne, ses vins et sa cuisine me manqueront toujours.

Il est ainsi, dans cet environnement et avec la motivation de commander un procédé de traitement des eaux usées que ce travail de recherche est arrivé à bon port.

Résumé

1. Introduction

Le nitrate est un contaminant présent dans les nappes aquifères et dans les rivières qui n'a cessé d'augmenter ces dernières décennies principalement en raison de l'utilisation intensive d'engrais azotés et de traitement inadéquat des eaux usées issues de l'activité humaine. La dénitrification (réduction de l'azote nitrique en azote gazeux) est alors une étape importante dans le traitement biologique des eaux usées des systèmes d'élimination de nutriments. Elle peut être classiquement menée dans des systèmes complets de nitrification-dénitrification par boues activées ou par biofiltration. La biofiltration est une technologie basée sur une réaction biologique qui utilise des micro-organismes immobilisés formant des biofilms ou couches biologiques, où les bioréactions sont mises en place autour de particules solides. Ces particules immobilisées sont emballées dans une colonne connue sous le nom de biofiltre. Le développement de la biofiltration a été favorisé par ses avantages par rapport à d'autres technologies alternatives. En effet, il s'agit d'une méthode environnementale effective, facile à mettre en oeuvre et rentable du fait de à sa compacité, de son efficacité et de sa faible consommation d'énergie. Avec l'avènement de normes plus strictes pour rejeter des eaux usées, dans le but de leur réutilisation en eau potable ou non, une meilleure compréhension et l'amélioration des performances d'un tel réacteur est une étape primordiale. C'est dans ce contexte que le développement des correcteurs efficaces pour optimiser la conduite de ces procédés doit être envisagé.

Plusieurs modèles mathématiques ont été proposés pour décrire la dynamique d'un biofiltre sous la forme d'un système d'équations différentielles en fonction des variables de réaction (concentrations des substrats, de biomasse, etc). Par ailleurs, il faut identifier différents paramètres (porosité, cinétiques des réactions, constantes de saturation, etc). Les variables d'état du biofiltre peuvent être distribuées dans le temps et dans l'espace. Par conséquent, il faut les décrire par des équations aux dérivées partielles (EDP). L'ensemble d'équations aux dérivées partielles obtenu à

partir du bilan de masse pour toutes les variables d'état constitue un système à paramètres distribués (SPD).

Dans cette thèse, nous nous intéressons à la transformation des concentrations de nitrate et de nitrite en azote gazeux lors de la traversée d'un réacteur de dénitrification, en présence de perturbations externes. Le réacteur considéré est un biofiltre modélisé par un ensemble d'équations aux dérivées partielles. Le modèle le plus général considère à la fois un terme de diffusion (dérivée spatiale de deuxième ordre) et un terme de convection (dérivée spatiale de premier ordre), conduisant à un système d'EDP paraboliques. Toutefois, le terme de diffusion est parfois négligé, auquel cas le système devient un système d'EDP hyperboliques.

2. Biofiltre de dénitrification

La biofiltration est une technologie prometteuse pour le traitement des eaux usées [24], [63] ou de l'eau potable [58], [12], mais aussi dans l'aquaculture ou pour le contrôle de la pollution atmosphérique. La biofiltration est effectuée par un réacteur tubulaire appelé biofiltre. Un tel dispositif est compact, relativement simple à construire et à exploiter. Par ailleurs, il montre une bonne efficacité pour le traitement biologique associée également à une faible consommation d'énergie. Un biofiltre est caractérisé par la distribution spatiale des micro-organismes fixés sur un support solide [66]. Il est décrit mathématiquement par un système à paramètres distribués (SPD) et est donc représenté par des équations aux dérivées partielles (EDP) [22].

Le procédé de dénitrification auquel nous sommes intéressés est un biofiltre rempli d'un matériau poreux pouzzolane. Des concentrations de nitrate et de nitrite émis par des eaux usées sont considérées à l'entrée du réacteur. Une source supplémentaire d'approvisionnement d'éthanol peut être utilisée comme une action de commande d'entrée ou pour assurer un rapport suffisamment élevé de carbone source par les nitrates (C/N), tel que la composante carbonée ne limite pas la croissance. La dénitrification est realisée dans des conditions anaérobies, cela signifie, en absence d'O_2 dans l'état gazeux. La réaction biologique est une réaction en deux étapes. La

première étape est la dénitration qui transforme les nitrates (NO_3) en nitrites (NO_2), tandis que la deuxième phase transforme le nitrite en azote gazeux (N_2). La population de micro-organismes (bactéries) est impliquée dans les deux étages, avec de l'éthanol en tant que co-substrat. Cette biomasse s'accumule sur le support solide de surface, due à la filtration des bactéries présentes dans l'eau d'alimentation et à la croissance nette. Ainsi, la biomasse constitue un biofilm autour des particules du filtre, qui s'épaissit avec le temps. Nous considérons alors que toute la biomasse est fixe et ne bouge pas au long du réacteur. Au contraire, les composés solubles (nitrates, nitrites et l'éthanol) sont transportés tout le long du biofiltre.

L'objectif est d'éliminer les nitrates et les nitrites tout au long du biofiltre. Les bactéries utilisées prennent le carbone organique comme source d'énergie. La route métabolique de la dénitrification est constituée de plusieurs réactions d'oxydoréduction consécutives, elle implique une accumulation transitoire de nitrite dans le biofiltre. Elle peut être dissociée en deux étapes:

$$NO_3^- \xrightarrow{(1)} NO_2^- \xrightarrow{(2)} N_2$$

Selon que l'on tient compte du phénomène de diffusion ou qu'on le néglige, le système d'EDP résultant de la modélisation du réacteur de dénitrification est parabolique ou hyperbolique. Le système d'EDP hyperbolique considère un terme de transport qui implique un opérateur différentiel spatial de premier ordre. Par ailleurs, le système d'EDP parabolique considère un terme de diffusion qui implique un opérateur différentiel spatial de deuxième ordre.

Associées aux équations dynamiques du procédé de dénitrification, nous considérons des conditions initiales et des conditions aux limites appropriées au biofiltre. Le système hyperbolique utilise généralement des conditions aux limites de Dirichlet à l'entrée du réacteur. Le système parabolique prend en compte des conditions aux limites de Robin en entrée et de Neumann en sortie du réacteur. Toutefois, des conditions aux limites dynamiques en sortie devraient plutôt être utilisées pour exprimer les phénomènes de transport à la frontière. Ces conditions dynamiques imitent le

modèle hyperbolique en ce point. Par ailleurs, une troisième condition a également été considérée qui se compose de conditions aux limites de Dirichlet + Robin (ou équivalente Dirichlet + Neumann) en entrée du réacteur. Cet ensemble de conditions nous permet de traiter le problème de la commande du biofiltre modelisé par un ensemble d'EDP paraboliques avec des stratégies différentes.

Une analyse de sensibilité effectuée sur le modèle parabolique nous permet de déterminer l'influence des paramètres les plus importants.

3. Simulation du procédé de dénitrification

La première étape du travail consiste à simuler le SPD. Cela implique qu'il faut résoudre numériquement les équations aux dérivées partielles d'un tel système. Les méthodes disponibles dépendent du type d'EDP à résoudre.

La méthode des lignes est une technique très générale pour résoudre numériquement différents types d'EDP. Cette méthode consiste à faire la discrétisation du domaine spatial et à approcher les dérivées spatiales afin d'obtenir un système d'equations differentielles ordinaires (EDO) [71]. Ce nouveau système d'EDO est intégré par rapport au temps pour pouvoir calculer la solution finale. Afin d'approcher les dérivées spatiales d'ordre N, nous considérons la méthode des éléments finis et la méthode aux différences finies. Ces deux méthodes peuvent être utilisées pour approcher le terme de diffusion et le terme de convection. La méthode des lignes peut ainsi être utilisée pour résoudre les deux systèmes d'EDP (hyperbolique et parabolique).

Par ailleurs, la méthode des caractéristiques est une méthode classique pour résoudre numériquement les équations aux dérivées partielles hyperboliques. Une EDP hyperbolique peut être séparée en une EDO qui varie dans le temps et en une autre EDO appelée caractéristique. Cette dernière EDO est résolue pour obtenir une courbe caractéristique afin de savoir comment la première EDO varie par rapport à l'espace [95].

Toutes les méthodes précédentes produisent des systèmes en espace d'état non linéaires d'ordre élevé qui pourraient ne pas convenir dans les futures stratégies de commande. La décomposition modale est une manière pratique et utile d'analyser les EDP en ne tenant compte que des modes du système les plus importants [95]. De cette façon, un système en espace d'état non linéaire d'ordre réduit est obtenu. Cette forme d'analyse est toujours possible lorsque les opérateurs spatiaux ont un spectre discret de valeurs propres réelles. Ce n'est pas le cas pour l'opérateur spatial de convection qui a, dans sa forme ordinaire, un spectre de valeurs propres complexes [60]. Par contre, c'est le cas de l'opérateur spatial de diffusion. Nous envisageons donc l'analyse modale du modèle parabolique du biofiltre. La décomposition Laplacienne est une technique très utile pour analyser les modes d'un système. Toutefois, cette décomposition n'est appropriée que s'il n'y a pas de terme de convection. Une autre technique classique pour analyser les modes d'un système est la méthode de la décomposition orthogonale propre qui a démontré son efficacité pour les systèmes d'EDP avec conditions aux limites non homogènes et terme de convection [85], tel que le système d'EDP paraboliques décrivant le réacteur de dénitrification.

La méthode des lignes est utilisée pour résoudre le modèle hyperbolique en approchant les dérivées spatiales par la méthode des différences finies (FDM). Le modèle parabolique est ensuite résolu par la même méthode, avec en revanche, les dérivés spatiales approchées par la méthode des éléments finis (FEM). Les matrices d'approximation spatiale résultant de la méthode des éléments finis seront utilisées plus tard, dans l'analyse modale, pour résoudre un problème de valeur propre, en approchant l'intégrale et les termes différentiels par des matrices FEM. Nous appliquons ensuite la méthode des caractéristiques sur le modèle hyperbolique et un ensemble d'équations aux différences est obtenu. Nous réalisons enfin une analyse modale sur le modèle parabolique afin de simuler le biofiltre de dénitrification en utilisant seulement les modes les plus importants.

4. Techniques basées sur l'approche *early lumping*

Suite aux approches de discrétisation spatiale, nous abordons le problème de la commande du procédé de dénitrification. La recherche en matière de la commande des bioprocédés a été principalement axée sur l'approche *early lumping* qui consiste à discrétiser spatialement le système d'EDP original avant de faire la synthèse du correcteur. La principale raison est que les stratégies de commande les plus importantes ont été développées pour les systèmes décrits par des modèles linéaires ou non linéaires représentés par des équations différentielles ordinaires (EDO).

Nous sommes intéressés par la régulation de la concentration de nitrate et de nitrite en sortie du réacteur à une valeur inférieure à la norme européenne. Du point de vue biologique, cela signifie qu'il faut que les micro-organismes consomment le nitrate pour produire du nitrite qui doit être lui-même consommée pour produire de l'azote gazeux. L'objectif est que les variations de charge en nitrate à l'entrée du réacteur se voient le moins possible en sortie du réacteur. Du point de vue de la commande, cela signifie qu'il faut atténuer l'énergie de la perturbation à l'entrée du réacteur ($S_{NO_3,in}$).

La norme H_2 permet de mesurer l'énergie d'un système [69], [93]. Dans ce contexte, nous choisissons la commande H_2 comme stratégie de commande afin de faire face au problème de l'atténuation des variations de la concentration de nitrate ($S_{NO_3,in}$) en entrée du biofiltre. L'objectif est donc de synthétiser des correcteurs par retour de sortie afin de minimiser l'énergie de la fonction de transfert définie entre la perturbation en entrée du réacteur et la sortie mesurée. Il faut donc que le problème de la commande du procédé de dénitrification soit exprimé sous la forme d'un problème de commande classique d'un système d'EDO linéaire après une discrétisation spatiale puis une linéarisation du système d'EDP original.

Nous nous intéressons aux méthodes de commande linéaire pour deux raisons principales:

- la première raison est que le système d'origine est simplifié lorsqu'il est décrit par des équations différentielles ordinaires. La transformation du système peut être poursuivie par une linéarisation autour d'un état stationnaire opérationnel, ce qui permet alors d'accéder au vaste monde de la commande linéaire, dans notre cas la commande H_2.

- la deuxième raison est liée à la facilité de comprendre et de manipuler les stratégies de commande linéaire. L'un des objectifs cachés de cette thèse est de renforcer l'interface entre la communauté de la commande et la communauté du génie des procédés. Les outils de commande linéaires sont plutôt des outils standards, indépendants de la forme du système d'origine et peuvent être décrits dans un cadre unifié qui pourrait être appliqué à d'autres classes de procédés biochimiques.

Puisque la commande H_2 a été développée pour les systèmes linéaires, il faut donc représenter le système d'EDP original sous forme linéaire en espace d'état en numérisant les dérivées spatiales puis en linéarisant autour d'un point d'opération. Ensuite, des lois de commande par retour d'état et des observateurs de Luenberger sont synthétisés. Des correcteurs robustes par retour de sortie basés sur observateur sont ansi obtenus à la fois dans leurs versions en temps discret et en temps continu en tenant compte du principe de séparation. Ces deux cas sont considérés car le système ODE concerné (en temps discret ou en temps continu) dépend de l'approche de discrétisation spatiale. Pour obtenir un modèle en espace d'état pour le système d'EDP hyperboliques nous considérons la méthode des caractéristiques. Pour le système d'EDP paraboliques, nous considérons la méthode de la décomposition orthogonale propre, ce qui permet de manipuler un modèle en espace d'état d'ordre réduit.

5. Techniques basées sur l'approche *late lumping*

D'autre part, dans les deux dernières décennies, plusieurs stratégies de commande ont été proposées en utilisant une approche dite *late lumping* basée sur la théorie de la

commande non-linéaire. Contrairement à l'approche *early lumping*, dans l'approche *late lumping* l'idée est de garder autant que possible la nature distribuée du modèle. En s'appuyant sur les travaux passés concernant la stabilité des systèmes décrits par des EDP [86] et la théorie de la commande non-linéaire [60] [35] [39], différents types de correcteurs non linéaires par retour de sortie ont été développés, selon que l'action de commande est distribuée dans l'espace [18], intervient dans les conditions aux limites [40] ou sur un terme dérivé [31]. Dans ce contexte, il est possible de synthétiser des correcteurs non-linéaires complétés par des observateurs non linéaires. Ils sont donc conçus directement sur les EDP non-linéaires. Afin de mettre en oeuvre le correcteur par retour de sortie basé sur observateur, les équations aux dérivées partielles obtenues sont résolues par des méthodes numériques, telles que celles présentées dans le chapitre 3.

Nous considérons donc des stratégies distribuées non linéaires en vue de synthétiser des correcteurs par retour de sortie basés sur observateur en linéarisant les dynamiques de sortie du biofiltre, d'abord pour le modèle d'EDP hyperboliques, puis pour celui d'EDP paraboliques. Il faut donc analyser le degré relatif du système afin de proposer un nouveau système de coordonnées [31]. Des stratégies de la commande linéarisante sont ensuite utilisées pour synthétiser une loi de commande pour linéariser les dynamiques de sortie, en assurant la stabilité asymptotique de la boucle fermée [35], [67]. Le correcteur à retour linéarisant est complété par un observateur à paramètres distribués [89], pour estimer l'ensemble des variables d'état réparties sur la longueur du réacteur. Cet observateur a ainsi le double rôle de montrer l'évolution de l'état le long du réacteur et de fournir au correcteur linéarisant les états dont il a besoin. Il est mis en oeuvre en résolvant les équations aux dérivées partielles par la méthode de lignes et en approchant les dérivées spatiales par des différences finies.

6. Conclusions

Dans cette thèse, la simulation et la commande d'un biofiltre de dénitrification décrit par un système d'EDP sont présentées. Un système d'EDP parabolique et un

système d'EDP hyperbolique ont été utilisés selon que l'on tient compte ou que l'on néglige la diffusion.

Une fois que le modèle du biofiltre de dénitrification a été défini, il est simulé afin de connaître ses dynamiques et de représenter le système sous forme d'espace d'état. Plusieurs méthodes sont disponibles pour résoudre numériquement un système d'EDP. La méthode des lignes est une technique générale qui peut être appliquée à toutes les classes d'EDP en rapprochant les dérivées spatiales, par des différences finies ou par des éléments finis. La méthode des différences finies est une technique très simple, basée sur une série de Taylor tronquée. Bien entendu, pour obtenir une approximation correcte des dérivées, il faut considérer un nombre suffisant de points de discrétisation dans l'espace. Une approximation des différences finies de quatrième ordre a démontré d'excellents résultats. D'autre part, la méthode des éléments finis est basée sur des séries de Fourier tronquée pour séparer les variables en une fonction du temps et une fonction de l'espace. Cette technique a pour résultat un ensemble de matrices qui approchent les termes dérivés et intégral. Toutefois, même si la synthèse des matrices FEM est plus complexe que la synthèse des matrices FDM, les résultats de simulation sont presque identiques. Les deux méthodes donnent un ensemble d'EDO à intégrer par rapport au temps.

Une autre technique utilisée pour résoudre numériquement le système d'EDP qui décrit le biofiltre est la méthode des caractéristiques. Toutefois, cette méthode ne peut être utilisée que pour le modèle hyperbolique, ce qui signifie qu'il faut négliger le terme de diffusion. La solution qui en résulte est un système d'équations aux différences à résoudre dans le temps. Les résultats de simulation sont très proches de ceux obtenus avec la méthode des lignes. Étant donné que cette méthode conduit à des équations en temps discret, la période de discrétisation utilisée pour calculer la solution finale est un point clé à considérer. Bien sûr, plus la période de temps est petite, plus la solution finale est précise.

L'opérateur spatial du modèle parabolique a des valeurs propres réelles, une analyse modale peut donc être effectuée en considérant une série de Fourier tronquée pour

séparer la variable d'état originale en une fonction de l'espace et en une fonction du temps. Les fonctions spatiales ont été calculées hors ligne en résolvant un problème de valeur propre avec les opérateurs intégraux et différentiels approximés par des matrices FEM. Elles ont également été utilisées pour définir un opérateur afin de projeter les variables d'état sur le domaine spatial. De cette façon, un système d'EDO pour calculer les modes du système (l'information temporelle) a été obtenu. Les résultats des simulations en tenant compte uniquement des modes les plus importants se sont avérés très proches de ceux obtenus en considérant la méthode des lignes.

Pour ce qui est de la commande du procédé, une approche *early lumping* basée sur la commande H_2 et le cadre des *LMI* a d'abord été considérée afin de réduire l'effet des variations de la concentration de nitrate en entrée du biofiltre et de maintenir la concentration d'azote en sortie sous une limite supérieure. Un système d'équations aux différences issu de la méthode des caractéristiques a été considéré pour synthétiser un correcteur par retour d'état en temps discret. Il a été complété par un observateur de Luenberger d'ordre plein ou d'ordre réduit. L'observateur d'ordre plein filtre mieux le bruit présent dans les mesures. Celui d'ordre réduit a l'avantage d'une plus petite dimension, ce qui est un aspect essentiel dans le cadre des *LMI*. Une stratégie très semblable a aussi été présentée pour commander le modèle parabolique. Cependant, on considère maintenant un ensemble d'EDO d'ordre réduit construit à partir des modes les plus importants du système et une version en temps continu de la stratégie de commande précédente. Un avantage important de cette stratégie est que le système décrit par les modes les plus importants et l'observateur associé sont d'un ordre beaucoup plus petit que ceux obtenus à partir des modèles issus de MOL ou de la méthode des caractéristiques. Ceci plaide pour l'utilisation du modèle parabolique du biofiltre, c'est-à-dire, tenant compte du phénomène de diffusion, plutôt que d'utiliser une a priori plus simple description du procédé, sans dérivées de second ordre. Les résultats, très similaires à ceux obtenus avec un modèle d'ordre supérieur du biofiltre, ont démontré que la loi de commande synthétisée en tenant compte des modes les plus importants atteint les objectifs de contrôle.

Le principal avantage de cette approche *early lumping* est qu'il en résulte une loi de commande facile à mettre en oeuvre (un système dynamique linéaire composé par une loi de commande par retour d'état + un observateur de l'état), mais au détriment de plusieurs manipulations (discrétisation, linéarisation, etc.) du système d'EDP original qui doivent être réalisées avant la synthèse du correcteur final. Il faut souligner que le principe de séparation n'est vérifié que dans la version qui ne tient pas compte des incertitudes sur le système linéarisé. Des stratégies plus complexes devront donc être considérées pour tenir compte des contraintes supplémentaires telles que les incertitudes du modèle. Les résultats obtenus ici ouvrent la voie, toutefois, pour l'utilisation des stratégies de commande linéaire pour ces systèmes d'EDP non linéaires.

Finalement, une approche *late lumping* basée sur la commande linéarisante a été considérée. L'objectif de commande, a été défini comme un problème de poursuite de référence (concentration d'azote en sortie) et d'atténuation d'une perturbation (concentration de nitrate en entrée). La stratégie suivie a été de synthétiser un correcteur qui linéarise les dynamiques du système en boucle fermée complété par un observateur à paramètres distribués. Il faut noter que la stabilité du système bouclé formé du correcteur linéarisant par retour de sortie basé sur observateur n'est pas garantie a priori car le principe de séparation ne s'applique pas aux systèmes non linéaires. Par ailleurs, cette stratégie de commande n'est pas très robuste aux incertitudes des paramètres du modèle. Son avantage est cependant qu'elle permet très simplement de proposer une stratégie directe sans beaucoup d'effort pour l'étape de synthèse. En particulier, seuls quelques paramètres doivent être calibrés.

Contents

List of Figures

List of Tables

Chapter 1

Introduction

Nitrate is a contaminant in groundwater aquifers and rivers which has been increasing in recent years mainly due to the extensive use of nitrogen fertilizers and improper treatment of wastewater from the industrial sites. Denitrification (reduction of nitrate nitrogen into nitrogen gas) is then an important step in biological wastewater treatment nutrient removal systems. It may be classically processed in full nitrification-denitrification activated sludge systems or by biofiltration. Biofiltration is a technology based on a biological reaction using micro-organisms which are immobilized forming biofilms or biolayers, where the bioreactions take place, around solid particles. These immobilized particles are packed in a column known as a biofilter [92]. The development of biofiltration has been promoted by its advantages over other alternative technologies. It is an environmentally, friendly and cost-effective method thanks to its compactness, efficiency and low energy consumption. With the advent of more and more stringent norms for water reject, reuse or for drinking water, the need for better understanding and improvement of reactor performance naturally comes to mind. This paves the way towards the development of efficient controllers to optimize the use of these processes.

Many mathematical models of biofilters have been proposed to understand and improve the reactor performance [20]. In order to model a biofilter, a system of differential equations based on the reaction variables (concentrations, biomass, etc.)

must be deduced to describe its dynamics. In addition, several parameters (porosity, kinetics of reaction, saturation constants, etc.) must be identified. The biofilter state variables may be distributed in both time and space. Therefore, they have to be described by means of partial differential equations (PDE). The set of PDEs from the mass balance of each component state variable constitutes a distributed parameter system (DPS).

Distributed parameter systems is a research area in control developed since the 1960s when the first works about the subject appeared, for example: in [14] the authors derived a general maximum principle for a class of DPS. In [87] the authors attempted to give precise mathematical description of DPS in term of a partial differential equation (PDE) set, the concepts of controllability and observabillity were also discussed. Another important work, [86], addressed the problem of stability of DPS with feedback controllers directly in the framework of PDEs, using Lyapunov techniques. More recently, several interesting works were developed. In [57], stability and stabilizability problems of infinite-dimensional systems were discussed. In [56], a Lyapunov stability analysis technique for DPS represented by hyperbolic or parabolic PDEs was presented. Controllability and observability issues were also considered and come up with a finite order feedback control formulation. However, the most important contributions in the DPS research area have been developed in the last two decades. Around the control strategies of interest in this thesis, we can mention several works: in [4], a decentralized control strategy based on linear matrix inequality theory for multi-dimensional but linear DPS is presented. In [61], a frequency domain input-output approach has been proposed for linear time invariant distributed parameter systems, based on a generalization of H_∞ control and the finite-dimensional approximation of LTI systems with distributed nature. In [19], [17] a robust finite distributed control design technique for DPS represented by hyperbolic and parabolic PDEs respectively are proposed. In the parabolic case, the Galerkin approach is used to come up with a suitable ODE system by keeping the lowest dynamics and by neglecting the fastest ones. In both cases, a nonlinear output

feedback control law that guarantees stability while making the system follows a desired reference is designed. Many of the innovative ideas about these robust control techniques are summarized in [18]. In [31], the problem of controlling a flow system described by a set of first-order PDEs with a single characteristic variable using the inverse system is addressed. In [15], the geometric theory of output regulation presented in [35], is extended for solving the state and output feedback regulation problems for infinite-dimensional linear control systems, assuming bounded control and observation operators. In [90], the output regulation of flow systems described by a class of two-time-scale nonlinear PDE system using the reduced-order slow model and geometric control is addressed. In [73], a feedback control method over the spatial interval that yields improved performance for DPS modelled by first-order hyperbolic PDEs has been designed. In [55], an optimal dynamic inversion strategy for DPS has been proposed by considering the combination of dynamic inversion principle and optimization theory for a class of one-dimensional nonlinear distributed parameter systems. In [75], a general procedure for parabolic PDEs with spatially continuous backstepping based boundary control is introduced. The backstepping method is formally proposed in [40] where the method is also applied to first-order hyperbolic PDEs.

In this thesis, we are interested in the reduction of nitrate and nitrite concentration throughout a denitrification reactor in spite of the external disturbances. The reactor under study is a biofilter modeled by a set of PDEs. The general model considers both a diffusion term (second-order spatial derivative) and a convection term (first-order spatial derivative), resulting in a parabolic PDE system. However, the diffusion term is sometimes neglected, resulting in an hyperbolic PDE system.

Hyperbolic PDE equations are sometimes called transport equations because they often describe the propagation of waves (for example into a reactor). They require initial conditions (where the waves start from) as well as boundary conditions (to describe how the wave and the boundary interact; for instance, the wave can be scattered or absorbed). The advection equation represents the hyperbolic PDE described

before:

$$\frac{\partial \zeta}{\partial t} = -v\frac{\partial \zeta}{\partial z}$$

It is easy to see that equation above is a first-order PDE, however it is called hyperbolic because the methods used to solve it are the same as the ones used to solve second-order hyperbolic PDEs.

Parabolic PDE equations are often called diffusion equations because they describe the diffusion and convection of some substance (such as water into a reactor). These equations require initial conditions (what the initial concentration of the substance is) as well as boundary conditions (to specify, for instance, whether the substance can cross the boundary or not). For example, the Fourier equation describes the diffusion phenomena in a parabolic PDE:

$$\frac{\partial \zeta}{\partial t} = k\frac{\partial^2 \zeta}{\partial z^2}$$

In order to know the dynamics of the DPS to control, it has to be simulated. This implies that the PDEs of such system must be numerically solved. The allowable methods depend of the type of the PDE system to solve. A general solution method is the method of lines, which consists in approximating the spatial derivative by using some approach like finite differences or finite elements and then integrate the resulting ODE system. On the other hand, there exist specific solution methods. The method of characteristics is a popular method useful for solving hyperbolic PDEs. The modal analysis is useful when the derivative operator has a set of real eigenvalues, which is normally the case for parabolic PDEs.

In order to control a DPS, two strategies are commonly used: early lumping approach and late lumping approach. In the first one, the partial differential equations are discretized to obtain an ordinary differential equation (ODE) system and then, ODE-based control strategies for nonlinear or linear systems may be applied (see for example [60]). On the other hand, in the second approach, control strategies have

been developed, based on the non-linear control theory, to design a controller for the PDE system so as to keep as much as possible its distributed nature (see for example [7], [19], [17]).

The research concerning control of bioprocesses was mainly focused on the early lumping approach. This is because the most important control strategies have been developed to control systems described by either linear or non-linear systems represented by ODEs. In this context, several works have been developed, for instance: [21] applied adaptive control schemes to nonlinear distributed parameter bioreactors by using an orthogonal collocation method to reduce the original PDE model to ODE equations. In [3] the authors dealt with the linear boundary control problem in an anaerobic digestion process by using the solution at steady state.

On the other hand, in the last two decades, several control strategies using a late lumping approach based on the non-linear control theory have been proposed. In [10], the authors have applied variable structure control to fixed bed reactors described by nonlinear hyperbolic PDEs. The authors of [2] have designed a nonlinear multivariable controller for an anaerobic digestion system described by a set of PDEs and consisting of an observer and two nonlinear control laws on the boundary conditions.

A DPS may be controlled either by a parameter in the derivative terms (see [31], [12], [2]), by a space distributed variable (see [19], [17]) or by the boundary conditions (see [12], [40]). Thus, state feedback controllers are synthesized by taking this constraint into account. However, due to their infinitely dimension nature, it is necessary to estimate also some of the states by using observation techniques. Observer-based output feedback controllers are therefore developed.

This thesis is then organized as follows: in chapter 2 the reactor under study is presented. First, the chemical equations inside the micro-organism metabolic path are described, then, the parabolic PDE model obtained by the mass balance is presented. By neglecting the diffusion term an hyperbolic PDE model is obtained; the difference between the two models is discussed. Next, the sensitivity of the parabolic PDE model

is analysed using the local sensitivity approach. At the end of the chapter, the problem to address is stated and the different control approaches to follow are presented. In chapter 3, the different strategies to numerically solve the PDE system are presented. Depending on the class of PDE is the method to use, but there also exist general methods that may be applied to both PDE systems. Normally, numerical solutions consist in discretizing the spatial derivative to transform the PDE into a high-order ODE. This is integrated to obtain the final solution. Modal analysis methods are further discussed to reduce the order of the ODE to integrate by keeping the most important modes of the original PDE system. At the end of each methodology, simulations will allow us to discuss the results obtained. In the following chapters, the control problem is addressed, first by an early lumping approach and then by a late lumping one. In chapter 4, the control problem is addressed by considering H_2 control techniques and the *LMI* framework as control strategy. Because H_2 control has been developed for linear systems, the original PDE system has to be represented in the classical state space form by discretizing the spatial derivative and linearizing the non-linear resulting ODE around an operating point. Following this early lumping approach, state feedback linear control laws and Luenberger observers are synthesized. By using the Separation Principle, they are complemented to obtain an observer-based feedback controller. In order to obtain a state space form for the hyperbolic PDE model the method of characteristics is used. On the other hand, for the parabolic PDE model the proper orthogonal decomposition method is used, and therefore, a reduced-order state space form is obtained. In chapter 5, the control problem is addressed by considering linearizing control in order to synthesize a feedback control law. This law is complemented by a distributed parameter observer to estimate the overall set of states needed. In this way, an observer-based feedback linearizing controller is obtained and it is implemented by solving the PDEs using the method of lines and approximating the spatial derivatives by finite differences. Finally, in chapter 6 some conclusions about the work developed and perspectives of future works not only in control engineering but also in human-machine interfaces, microcontroller architecture and data acquisition systems are presented.

Chapter 2

Denitrification biofilter

2.1 Introduction

Biofiltration has proven to be a promising reaction system for wastewater [24], [63] or drinking water treatment [58], [12], but also in aquaculture or for control of air pollution. Biofiltration is performed by a biofilter tubular reactor. Such a device is compact, fairly simple to build and operate, and has shown good efficiency for biological treatment associated to low energy consumption. Such biofiltration units are characterized by spatial distribution of micro-organisms which are fixed on a solid support [66]. They are mathematically described as distributed parameter systems (DPS) and represented by partial differential equations (PDE) to explain their distributed nature [22].

In this chapter the denitrification biofilter under study is presented. First, a brief description about the denitrification process and the variables involved in such process is presented. Following, the boundary conditions are deeply discussed and interpreted. The importance of the diffusion phenomenon is also pointed out because it determines the nature of the resulting PDE model, namely an hyperbolic or a parabolic one. Next, those two PDE models are described with the values of the parameters used in both models. Following, a sensitivity analysis is performed on the parabolic model to determine the influence of the most important parameters. Such

a study on the hyperbolic model would conclude exactly to the same results. Finally, the problems to be treated throughout this work are stated by describing the different control strategies to study.

2.2 Denitrification process

The denitrification process under study is a biofilter, shown in figure 2-1, filled with a porous pouzzolane material. Nitrate and nitrite nitrogen issued from some wastewater are considered at the reactor input. An additional ethanol supply source may be used as a control input action or at least to ensure a sufficiently high ratio C/N *(Carbon source per Nitrate)* such that carboneous component does not become the limiting source for the growth. Denitrification is performed in anaerobic conditions, it means, in absence of O_2 in gaseous form. The biological reaction is a two-stage reaction. The first stage is the denitration which transforms nitrate (NO_3) into nitrite (NO_2) while the second phase transforms nitrite into gaseous nitrogen (N_2). The same micro-organism population (bacteria) is involved in both stages, with ethanol as co-substrate. This biomass accumulates on the solid media surface due to filtration of bacteria present in the feeding water (if any) and to net growth. Thus, the biomass forms a biofilm around the filter particles, which thickens with time. One can then consider that all the biomass is fixed and does not move along the reactor. On the contrary, the soluble compounds (nitrate, nitrite and ethanol) are transported along the biofilter.

The objective is to eliminate the nitrate and the nitrite while going through the biofilter. The used bacteria take the organic carbon as source of energy. The denitrification metabolic path consists of several consecutive oxydoreduction reactions and it implies a transitory accumulation of nitrite into the biofilter [32]. It may be dissociated in two steps:

$$NO_3^- \xrightarrow{(1)} NO_2^- \xrightarrow{(2)} N_2$$

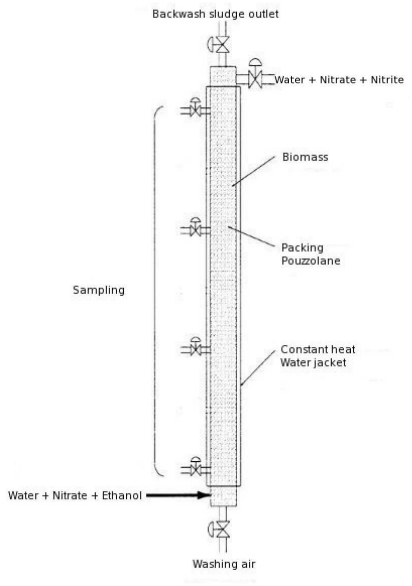

Figure 2-1: Denitrification biofilter.

The dynamics of the biofilter can be deduced from mass balance considerations for the four different components, considering the following assumptions:

- The detachment of biofilm and particles retained by filtration is neglected;
- Once the biofilm reaches a critical 'per unit' surface thickness, the deeper part of the biofilm is considered as inactivated, and a maximum active biomass concentration X_{amax} is reached [11]. Then, after some transition period, the growth of micro-organisms just balances the death and inactivation process;
- The decay of biomass is neglected, hidden in the notion of maximum active biomass concentration;
- Radial dispersion is negligible. Axial dispersion obeys Fick's diffusion law.

Remark 1 *The assumptions described above deserve a few comments. Theorically, the dynamical reactions inside the biofilm should be taken into account. Biological reactions would be the same like those ones along the biofilter, and the diffusion phenomenon would be the main cause of mouvement inside the biofilm [32, p.158]. In this study, such phenomenon has been however neglected inside the biofilm by considering*

a more overall description of a maximum active biomass. This simplification is supported by two considerations. First, it has been shown experimentally that, after the startup of the process, the activity converges to some sort of steady-state level since, after each washing out (necessary to avoid plugging due to the bacterial growth), it comes back to this level almost instantaneously [37]. This observation promoted the idea that the overall activity inside the biofilm was limited to a maximal capability, represented here as a maximal concentration of organisms. Second, the examination of biofilm models shows exactly the same behavior: growth is accompanied by an increase of the size of the biofilm but the internal loyers are limited by the nutritional elements (consumed in surface quicker than diffusion) [32, p.175]. Then, unless the subject of the study is the biofilm itself, it is reasonnable to neglect the internal activity of the biofilm in the description of the biofilter.

From a mathematical point of view, by taking into account the diffusion phenomenon, the model results in parabolic PDEs, while, on the other hand, by neglecting it the model results in hyperbolic PDEs. Both models have distinctive properties and derive in the difficulty to solve them numerically and the control strategies to consider. However, as will be shown in the following, simulation and control results by considering both PDE systems are very similar.

2.3 Denitrification reactor model

As above-mentioned, by considering or not the diffusion phenomenon the resulting PDE system of the denitrification reactor can be either a parabolic one or an hyperbolic one. In the hyperbolic PDE system a transport term implies a first-order spatial differential operator. In addition, in the parabolic PDE system, a diffusion term implies a second-order spatial differential operator. In this way, the initial boundary problem to solve is different [49].

Taking into account the diffusion phenomenon, the denitrification reactor is modeled by the following parabolic PDE system:

$$\frac{\partial S_{NO_3}(z,t)}{\partial t} = D_f \frac{\partial^2 S_{NO_3}(z,t)}{\partial z^2} - \frac{v}{\epsilon}\frac{\partial S_{NO_3}(z,t)}{\partial z} - \frac{1-Y_{h_1}}{1.14 Y_{h_1}\epsilon}\mu_1(S_{NO_3}(z,t), S_C(z,t))X_a(z,t) \tag{2.1}$$

$$\begin{aligned}\frac{\partial S_{NO_2}(z,t)}{\partial t} =& D_f \frac{\partial^2 S_{NO_2}(z,t)}{\partial z^2} - \frac{v}{\epsilon}\frac{\partial S_{NO_2}(z,t)}{\partial z} + \frac{1-Y_{h_1}}{1.14 Y_{h_1}\epsilon}\mu_1(S_{NO_3}(z,t), S_C(z,t))X_a(z,t) \\ & - \frac{1-Y_{h_2}}{1.71 Y_{h_2}\epsilon}\mu_2(S_{NO_2}(z,t), S_C(z,t))X_a(z,t)\end{aligned} \tag{2.2}$$

$$\begin{aligned}\frac{\partial S_C(z,t)}{\partial t} =& D_f \frac{\partial^2 S_C(z,t)}{\partial z^2} - \frac{v}{\epsilon}\frac{\partial S_C(z,t)}{\partial z} - \frac{1}{Y_{h_1}\epsilon}\mu_1(S_{NO_3}(z,t), S_C(z,t))X_a(z,t) \\ & - \frac{1}{Y_{h_2}\epsilon}\mu_2(S_{NO_2}(z,t), S_C(z,t))X_a(z,t)\end{aligned} \tag{2.3}$$

$$\begin{aligned}\frac{\partial X_a(z,t)}{\partial t} =& (\mu_1(S_{NO_3}(z,t), S_C(z,t))X_a(z,t) + \mu_2(S_{NO_2}(z,t), S_C(z,t))X_a(z,t)) \\ & \left(1 - \frac{X_a(z,t)}{X_{amax}}\right)\end{aligned} \tag{2.4}$$

In the equations above, z is the axial space variable, $S_{NO_3}(z,t)$, $S_{NO_2}(z,t)$, $S_C(z,t)$ and $X_a(z,t)$ represent the nitrate ($g[N]/m^3$), nitrite ($g[N]/m^3$), ethanol ($g[DCO]/m^3$) and active biomass concentrations. D_f, v, Y_{h_1}, Y_{h_2}, μ_1 and μ_2 represent the diffusion term m^2/h, the flow rate m/h (the ratio between the feeding rate (m^3/h) at the reactor input and the biofilter cross-section area (m^2)), micro-organisms yield coefficients and population specific rates which transform nitrate into nitrite, then nitrite into gas nitrogen ($1/h$) respectively.

The nitrate and nitrite specific growth rates μ_1 and μ_2 depend both on the microorganism used and on environmental parameters of the culture like composition, temperature, pH, Eh, thermodynamic activity of the water, etc. These parameters are however often neglected and the growth rates are typically described by the model

of Monod, in this application represented as [11]:

$$\mu_1(S_{NO_3}(z,t), S_C(z,t)) = \eta_g \mu_{1_{max}} \frac{S_{NO_3}}{S_{NO_3}+K_{NO_3}} \frac{S_C}{S_C+K_C}$$

$$\mu_2(S_{NO_2}(z,t), S_C(z,t)) = \eta_g \mu_{2_{max}} \frac{S_{NO_2}}{S_{NO_2}+K_{NO_2}} \frac{S_C}{S_C+K_C}$$

where η_g, $\mu_{1_{max}}$, $\mu_{2_{max}}$, K_{NO_3}, K_{NO_2} and K_C are the correction factor for the anaerobic growth, the maximum specific growth rates of biomass on nitrate and nitrite and the affinity constants with respect to nitrate, nitrite and ethanol, respectively. However, it must be pointed out that this model does not always represent the data suitably, especially when the culture media is complex and contain several carbon and nitrogen sources [1].

Associated to the dynamical equations for the denitrification process, appropriate initial spatial profile at $t = 0$ for $0 \leq z \leq L$ expresses that the biomass and the substrate are homogeneously distributed along the biofilter:

$$S_{NO_3}(z,0) = S_{NO_3,0}(z) \tag{2.5}$$

$$S_{NO_2}(z,0) = S_{NO_2,0}(z) \tag{2.6}$$

$$S_C(z,0) = S_{C,0}(z) \tag{2.7}$$

$$X_a(z,0) = X_{a,0}(z) \tag{2.8}$$

Remark 2 *Such an initial profile is considered, without loss of generality, only to simplify the numerical initialization of the simulations. Any other initial profiles could be considered with only slight transient differences in the forthcoming simulations, but without changing any of the conclusions drawn from the simulations.*

In the numerous literature on biofilter modelling including diffusion phenomenon [23], [44], [92], boundary conditions have been considered both at the input and the

output of the biofilter. Most generally, the literature suggests:

- Robin boundary conditions for S_{NO_3}, S_{NO_2} and S_C at $z = 0$ (input) for $t > 0$:

$$\frac{\partial S_{NO_3}(0,t)}{\partial z} = \frac{v}{\epsilon D_f}\left(S_{NO_3}(0,t) - S_{NO_3,in}(t)\right) \tag{2.9}$$

$$\frac{\partial S_{NO_2}(0,t)}{\partial z} = \frac{v}{\epsilon D_f}\left(S_{NO_2}(0,t) - S_{NO_2,in}(t)\right) \tag{2.10}$$

$$\frac{\partial S_C(0,t)}{\partial z} = \frac{v}{\epsilon D_f}\left(S_C(0,t) - S_{C,in}(t)\right) \tag{2.11}$$

- Neumann boundary conditions at $z = L$ (output) for $t > 0$:

$$\frac{\partial S_{NO_3}(L,t)}{\partial z} = 0 \tag{2.12}$$

$$\frac{\partial S_{NO_2}(L,t)}{\partial z} = 0 \tag{2.13}$$

$$\frac{\partial S_C(L,t)}{\partial z} = 0 \tag{2.14}$$

where $S_{NO_3,in}(t)$, $S_{NO_2,in}(t)$ and $S_{C,in}(t)$ represent the nitrate, the nitrite and the ethanol at the biofilter input respectively.

However, in this thesis, we would like to discuss those boundary conditions. Neumann boundary conditions had been originally proposed for the heat equation to stress that the temperature profile becomes flat at the outlet (in the heat equation, it corresponds to an insulated beam). Even if the diffusion phenomenon which takes place in the biofilter model assimilates to the heat diffusion, such boundary conditions are in fact not well adapted to the biofilter. As a matter of fact, considering that the concentration is asymptotically constant at the output limit of the biofilter (or, more exactly, at the limit of the packed material colonized by the microorganisms) is

no sense. This is true only if limitations by the nutriments occur before the output of the biofilter such as the reaction rates converge toward 0. A dynamic boundary condition, similar to that one proposed by Schiesser in [72], would then be more appropriate to take into account the transport and reaction phenomena at the output frontier of the biofilter. This leads, instead of using Neumann boundary conditions (2.12)-(2.14), to consider:

- Dynamic boundary conditions at $z = L$ (output) for $t > 0$:

$$\frac{\partial S_{NO_3}(L,t)}{\partial t} = -\frac{v}{\epsilon}\frac{\partial S_{NO_3}(L,t)}{\partial z} - \frac{1-Y_{h_1}}{1.14Y_{h_1}\epsilon}\mu_1(S_{NO_3}(L,t), S_C(L,t))X_a(L,t) \tag{2.15}$$

$$\begin{aligned}\frac{\partial S_{NO_2}(L,t)}{\partial t} = &-\frac{v}{\epsilon}\frac{\partial S_{NO_2}(L,t)}{\partial z} + \frac{1-Y_{h_1}}{1.14Y_{h_1}\epsilon}\mu_1(S_{NO_3}(L,t), S_C(L,t))X_a(L,t) \\ &- \frac{1-Y_{h_2}}{1.71Y_{h_2}\epsilon}\mu_2(S_{NO_2}(L,t), S_C(L,t))X_a(L,t)\end{aligned} \tag{2.16}$$

$$\begin{aligned}\frac{\partial S_C(L,t)}{\partial t} = &-\frac{v}{\epsilon}\frac{\partial S_C(L,t)}{\partial z} - \frac{1}{Y_{h_1}\epsilon}\mu_1(S_{NO_3}(L,t), S_C(L,t))X_a(L,t) \\ &- \frac{1}{Y_{h_2}\epsilon}\mu_2(S_{NO_2}(L,t), S_C(L,t))X_a(L,t)\end{aligned} \tag{2.17}$$

Remark 3 *Such a dynamic boundary condition signifies that, at the boundary, the parabolic biofilter problem mimics that one of the hyperbolic biofilter problem where diffusion is neglected.*

Moreover, to go further, one can also conceive of transforming such two-point boundary-value problems into an initial-value problem, where space boundary conditions are all set at the input of the biofilter. Historically, classical boundary conditions have been proposed at the two extremal points to evaluate analytical solutions of PDEs problems. However, even if it is not Hadamard-correctly posed [34], it is legitimate and relevant for the applications to consider initial-boundary conditions formed

with Dirichlet boundary conditions associated with the Robin boundary conditions described above.

- Dirichlet boundary conditions at $z = 0$ (input) for $t > 0$:

$$S_{NO_3}(0,t) = S_{NO_3,in}(t) \tag{2.18}$$

$$S_{NO_2}(0,t) = S_{NO_2,in}(t) \tag{2.19}$$

$$S_C(0,t) = S_{C,in}(t) \tag{2.20}$$

Remark 4 *The idea behind the terminology of Hadamard-correctly posed stresses that the Cauchy problem (existence and unicity of a solution to a PDEs problem) may be weakened, especially from a numerical simulation point of view [34]. In that sense, the wave equation problem in two variables with boundary conditions all set at the same point is correctly posed in the sense of Hadamard [34], [62]. Moreover, it has been recently shown that, using ideas issued from flatness, the heat equation problem may also be associated to boundary conditions at the same point [41].*

In the sequel, any of those combinations of boundary conditions may be used to numerically simulate the parabolic PDEs biofilter (Chapter 3). They all give the same results (especially since a Neumann condition at $z = 0$ is hidden in the initialization of the Robin condition). On the other hand, we will see in Chapter 5 that, in order to build linearizing controllers, it is preferable to consider the case with Dirichlet + Robin conditions at $z = 0$.

For simulation, the parameters are set to the values given in table 2.1, issued from [11] and [68].

Figure 2-2 shows the time evolution at several locations for the parabolic PDE system (2.1)-(2.4). The PDE system was solved using the method of lines using 151

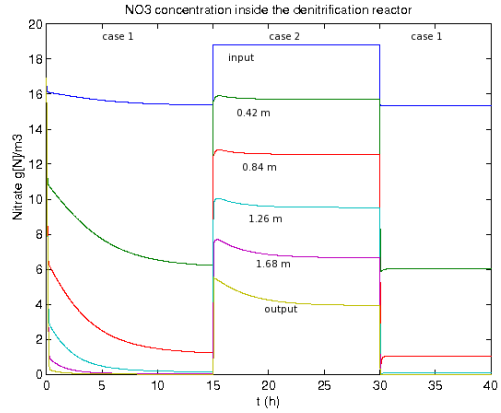

(a) NO_3 solution.

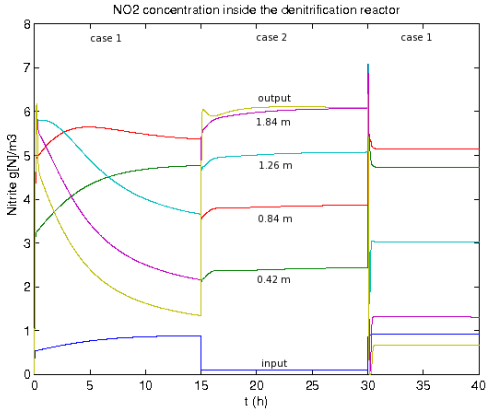

(b) NO_2 solution.

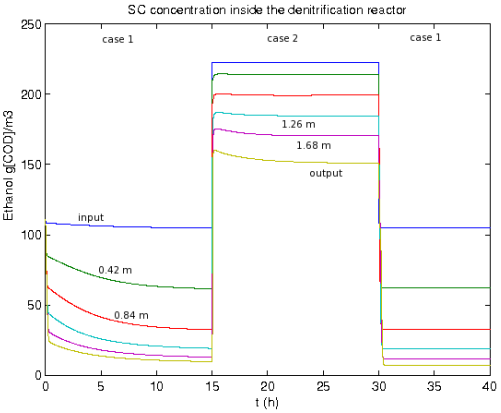

(c) S_C solution.

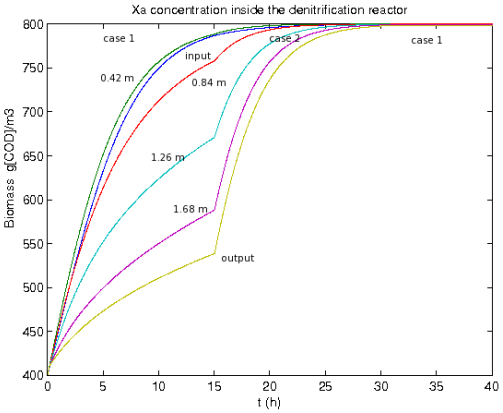

(d) X_a solution.

Figure 2-2: Time and space (at six locations) evolution of the parabolic PDE system by using MOL-FDM.

Parameter	Value	Parameter	Value
Y_{h_1}	0.56	Y_{h_2}	0.54
$\mu_{1_{max}}$	0.36 $1/h$	$\mu_{2_{max}}$	0.32 $1/h$
K_{NO_3}	1.5 $g[N]/m^3$	K_{NO_2}	1.0 $g[N]/m^3$
K_C	40 $g[COD]/m^3$	X_{amax}	800 $g[COD]/m^3$
n_g	0.8	ϵ	0.52
D_f	0.4756 m^2/h	L	2.1 m

Table 2.1: Physical and biological parameters of the denitrification biofilter, issued from [11] and [68].

Condition	Value	Condition	Value
$S_{NO_3,in}(t)$	16.93 $g[N]/m^3$	$S_{NO_2,in}(t)$	0 $g[N]/m^3$
$S_{C,in}(t)$	111.5 $g[COD]/m^3$	v	4 m/h

Table 2.2: Influent conditions (case 1).

discretization points uniformly distributed along the reactor. The derivative terms were approximated by considering the finite difference method. In Chapter 3 we will discuss in detail this methodology to numerically solve PDE systems. For the sake of clarity, the solution is shown only at six points along the reactor.

Two different operating conditions are succesively applied. During the first 15 hours and from 30 hours to the end of the simulation, the influent operating conditions are those of Table 2.2. Between 15 hours and 30 hours, the influent operating conditions are those of Table 2.3. The simulation is initialized with homogeneous values for the state variables along the reactor given in Table 2.4.

Let us now consider the case when the diffusion phenomenon is neglected. In that case, the denitrification reactor model results in an hyperbolic PDE system, which is different from a parabolic one because the second derivative term in equations (2.1)-(2.4) disappears and therefore there exist only (Dirichlet) boundary conditions at $z = 0$ (input) for $t > 0$.

Condition	Value	Condition	Value
$S_{NO_3,in}(t)$	18.93 $g[N]/m^3$	$S_{NO_2,in}(t)$	0 $g[N]/m^3$
$S_{C,in}(t)$	203 $g[COD]/m^3$	v	16 m/h

Table 2.3: Influent conditions (case 2).

Condition	Value	Condition	Value
$S_{NO_3,0}(z)$	16.93 $g[N]/m^3$	$S_{NO_2,0}(z)$	0 $g[N]/m^3$
$S_{C,0}(z)$	111.5 $g[COD]/m^3$	$X_{a,0}(z)$	$X_{amax}/2$ $g[COD]/m^3$

Table 2.4: Initial homogeneous conditions in the biofilter.

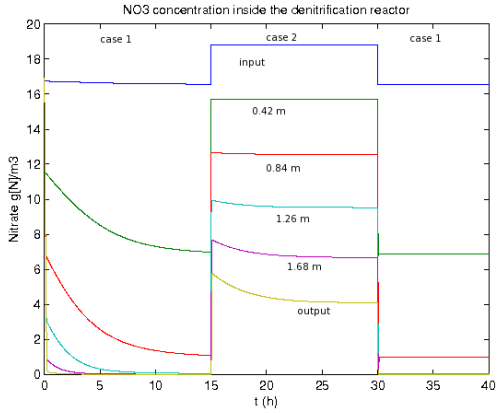

(a) NO_3 solution.

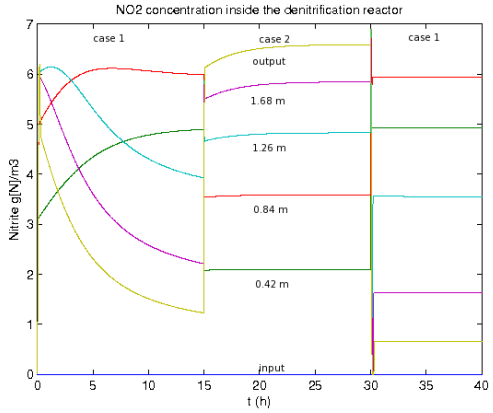

(b) NO_2 solution.

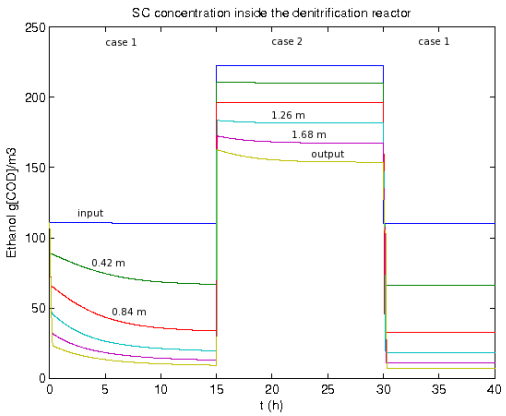

(c) S_C solution.

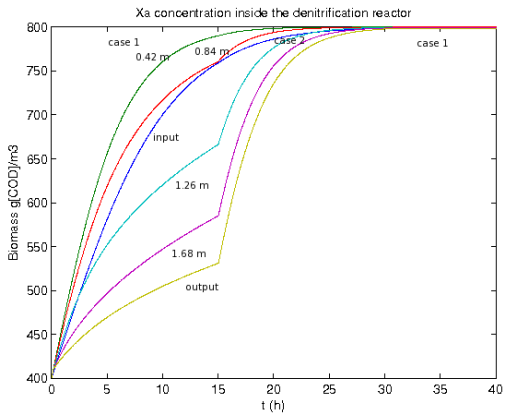

(d) X_a solution.

Figure 2-3: Time and space (at six locations) evolution of the hyperbolic PDE system by using MOL-FDM.

Figure 2-3 shows the time evolution at several locations for the resulting hyperbolic PDE system. Again, the PDE system was solved using the method of lines using 151 discretization points uniformly distributed along the reactor. The derivative terms were approximated by considering the finite difference method. For sake of clarity, the solution is shown only at six points along the reactor. The simulation conditions are those ones used for the parabolic model.

A few comments can be made about those simulations (the parabolic PDE and the hyperbolic PDE systems). Considering the first set of influent conditions, with a concentration of biomass initially present in the reactor corresponding to a partial colonization of the biofilter ($X_{a,0}(z) = X_{amax}/2$), it may be seen that the biomass concentration evolves towards the limit X_{amax}. However, the influent concentrations are not high enough to ensure a sufficient concentration of nutriments until the top locations of the biofilter. It results that the concentration of biomass in the upper locations evolves slowly and cannot converge to its maximal value. On the other hand, if non limiting influent conditions are provided, the biomass concentration converges to its maximum value all along the reactor (between 15h and 30h). Then, even if the influent conditions are reduced to their first values, the biomass concentration remains at its maximum value and the system becomes independent of this variable. The idea is therefore to apply non-limiting conditions to the system from the beginning (Table 2.3) such as to *saturate* the concentration of biomass. Variations of influent conditions will be then easier to absorb in more standard operating conditions (Table 2.2). From this discussion, as soon as $X_a(z,t) = X_{amax}$, it has no more influence on the reactions and may be neglected. In accordance to the conclusion of [11], the dynamical evolution of X_a is then neglected and, without loss of generality, only the three first equations of the original parabolic PDE system will be consider in the remainder of the document.

Finally, the system (2.1)-(2.3) may be rewritten in matrix form as:

$$\frac{\partial S}{\partial t} = A_1 \frac{\partial^2 S}{\partial z^2} + A_2 \frac{\partial S}{\partial z} + h(S) \tag{2.21}$$

where $S = [S_{NO_3}\ S_{NO_2}\ S_C]^T$ is the state vector, defined on the domain $\mathcal{D} = \mathcal{V} \times \mathcal{B} \times \mathcal{T}$ where $\mathcal{V} \subset \mathbb{R}$ is the spatial domain with boundary $\mathcal{B}$ and $\mathcal{T}$ is the semiopen time interval $[0, \infty)$. Matrices $A_1, A_2 \in \mathbb{R}^{3\times3}$ are diagonal square matrices whose diagonal elements are D_f and v/ϵ respectively, and $h(S) \in \mathbb{R}^3$ is a vector of non-linear functions. Note that the hyperbolic case corresponds to $D_f = 0$, and that the associated boundary conditions are different.

Considering now the biofilter PDE system of dimension 3, with $X_a(z,t) = X_{amax}$ for all z and t, the simulations of both parabolic and hyperbolic cases using the same numerical method (method of lines using 151 discretization points uniformly distributed along the reactor and derivative terms approximated by the finite difference method) are plotted in figure 2-4. Parameters are taken from Table 2.1, influent conditions from Table 2.2 and initial condition of the three soluble components from Table 2.4. It illustrates the similarity on both solutions. Even if the evolution of every state variable is not exactly the same for both models, the systems at steady state are very close, considering the diffusion or not. The main difference between both simulations comes from the different boundary condition at $z = 0$, visible mainly at the vicinity of the input of the biofilter.

2.4 Sensitivity analysis of the denitrification biofilter model

Sensitivity analysis allows to evaluate how the variation in the output of a dynamic system model can be apportioned to different sources of variation, but also, how the given model depends upon the information fed into it. Indeed, sensitivity analysis was created to deal with uncertainties in the input variables and model parameters. As a whole, sensitivity analysis is used to increase the confidence in the model and its predictions, by providing an understanding of how the model variables respond to changes in the inputs, be the data used to calibrate it, model structures or factors, i.e. the model-independent variables. The sensitivity analysis is thus closely linked

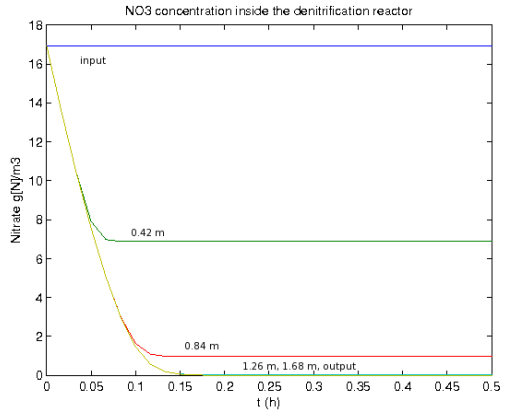

(a) NO_3 solution of the hyperbolic PDE.

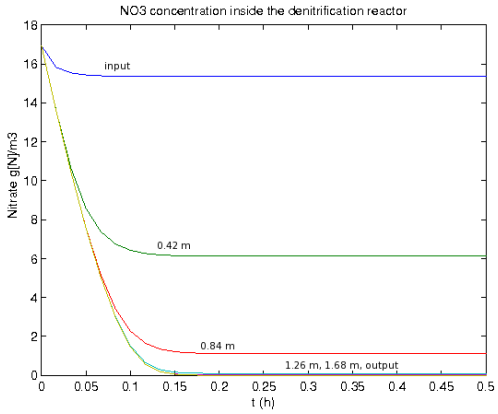

(b) NO_3 solution of the parabolic PDE.

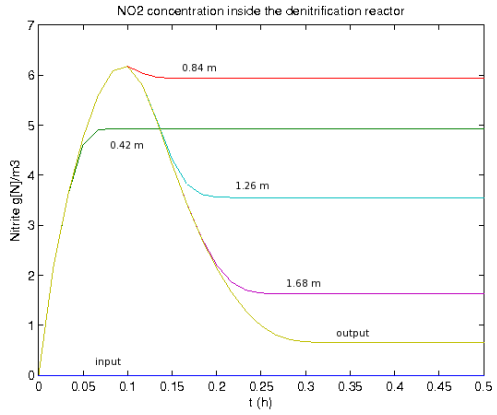

(c) NO_2 solution of the hyperbolic PDE.

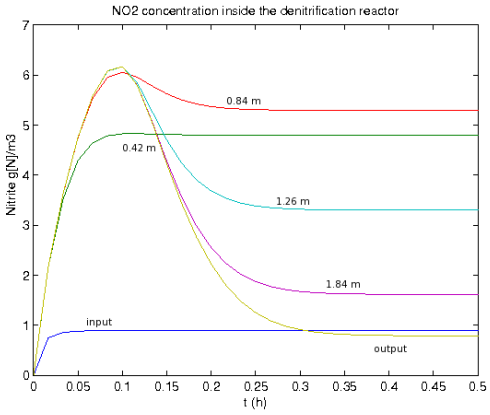

(d) NO_2 solution of the parabolic PDE.

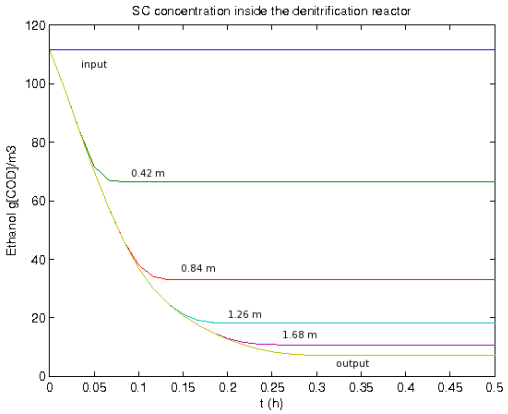

(e) S_C solution of the hyperbolic PDE.

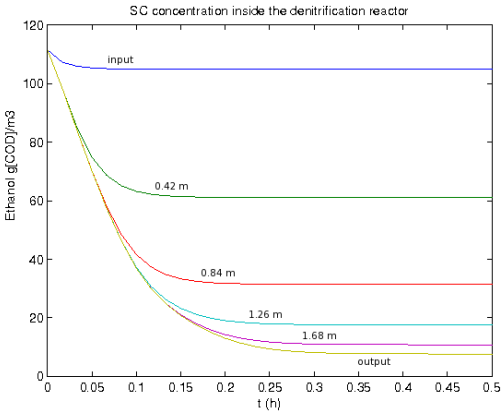

(f) S_C solution of the parabolic PDE.

Figure 2-4: Time and space (at six locations) comparison of both PDE models by using MOL-FDM.

to uncertainty analysis which aims at quantifying the overall uncertainty associated with the response as a result of uncertainties in the original model [65], [78].

Different sensitivity analysis strategies may be applied, depending on the setting:

- *Factor screening*, where the task is to identify influencial factors in a system with many factors. It may be useful as a first step when dealing with a model containing a large number of factors. Often, only a few of the parameters have a significant effect on the model output.

- *Local sensitivity analysis*, where the emphasis is on the local (point) impact of the factors on the model. It is usually carried out by computing the variation of the state variables of the original system with respect to the input factors. The local sensitivity approach is practicable when the variation around the midpoint of the input factors is small; in general, the input - output relationship is assumed to be linear.

- *Global sensitivity analysis*, where the emphasis is on apportioning the output uncertainty to the uncertainty in the input factors. Global sensitivity analysis typically considers a sampling approach, and the uncertainty range given in the inputs reflects our imperfect knowledge of the model factors. Distributions for each factor provide the input for the analysis.

Equations (2.1)-(2.3), representing the denitrification reactor dynamics, depend on several parameters (factors) which are generally not easy to estimate and which may vary in real applications. It is therefore desirable to determine the sensitivity of the system with respect to the most important model parameters. Such sensitivity information can be used to estimate which parameters are the most influential in affecting the simulation behavior, to evaluate robustness in control design or to investigate their estimation for model calibration [59]. Local sensitivities provide the slope of the calculated model output in the parameter space at a given set of values. Moreover, local sensitivity analysis is a computationally efficient technique that al-

lows a rapid preliminary exploration of the model. This strategy, and in particular the direct method, is then selected in this work [65].

Let us consider the distributed parameter system:

$$\frac{\partial S}{\partial t} = A_1 \frac{\partial^2 S}{\partial z^2} + A_2 \frac{\partial S}{\partial z} + h(S, p) \tag{2.22}$$

where S is a n-vector of state variables and p is the m-vector of system parameters. Note that $n = 3$ in the case of the system (2.1)-(2.3).

Differentiation of equation (2.22) with respect to p_k gives the following system of sensitivity differential equations:

$$\frac{\partial}{\partial t}\frac{\partial S}{\partial p_k} = A_1 \frac{\partial^2}{\partial z^2}\frac{\partial S}{\partial p_k} + A_2 \frac{\partial}{\partial z}\frac{\partial S}{\partial p_k} + \frac{\partial h}{\partial S}\frac{\partial S}{\partial p_k} + \frac{\partial h}{\partial p_k}\ ; \quad k = 1, \ldots, m \tag{2.23}$$

The sensitivity matrix with respect to the model parameters is then defined as the Jacobian matrix:

$$s(t) = J_S(p) = \frac{\partial S}{\partial p}$$

In the denitrification biofilter system, Monod laws involving the nitrate and nitrite are the main terms which may affect the model's sensibility. In this way, the influence of the parameters, $\eta_g \mu_{1_{max}}$, $\eta_g \mu_{2_{max}}$, K_{NO_3}, mainly, K_{NO_2} and K_C, has to be analyzed in order to evaluate the confidence in the models which are manipulated in the following chapters. Note however that a similar sensitivity analysis could be conducted for the other parameters.

Let $p = [\eta_g \mu_{1_{max}}\ \eta_g \mu_{2_{max}}\ K_{NO_3}\ K_{NO_2}\ K_C]^T = [p_1\ p_2\ p_3\ p_4\ p_5]^T$ be the vector of parameters to analyze. The elements of the sensitivity matrix with respect to the model parameters satisfy the following sensitivity equation:

$$\frac{\partial s_{ik}}{\partial t} = D_f \frac{\partial^2 s_{ik}}{\partial z^2} - \frac{v}{\epsilon}\frac{\partial s_{ik}}{\partial z} + \sum_{j=1}^{n} \frac{\partial h_i(S)}{\partial S_j} s_{jk} + \frac{\partial h_i(S)}{\partial p_k} \tag{2.24}$$

for $i = 1, 2, 3$ and $k = 1, 2, 3, 4, 5$.

The sensitivity differential equations for each state variable are summarized in the appendix A. They are solved using the method of lines considering 151 discretization points uniformly distributed along the reactor. The derivative terms were approximated by considering the finite difference method. Parameters used in the simulations are taken from Table 2.1. Operating conditions are taken from Table 2.2, with initial conditions along the reactor given in Table 2.4. Recall that $X_a(z,t) = X_{amax}$.

2.4.1 Parametric sensitivity analysis of the nitrate concentration

Figure 2-5 shows the sensitivity normalized time evolution of nitrate with respect to the vector p defined above. For the sake of clarity, the figures show the time evolution of the nitrate sensitivity at six positions along the reactor only.

As expected, the nitrate concentration is not sensitive to parameters $\eta_g\mu_{2_{max}}$ and K_{NO_2} because these parameters do not appear in equation (2.1). On the other hand the nitrate concentration is very sensitive to parameters $\eta_g\mu_{1_{max}}$ and K_C, while sensitivity to K_{NO_3} is rather small.

2.4.2 Parametric sensitivity analysis of the nitrite concentration

Figure 2-6 shows the sensitivity normalized time evolution of nitrite with respect to the vector p defined above at the same six positions along the reactor as in the section 2.4.1.

It can be observed that nitrite concentration is really sensitive to both parameters $\eta_g\mu_{1_{max}}$ and $\eta_g\mu_{2_{max}}$ (sensitivity value over the unity). The sensitivity to the parameter K_{NO_3} is important too. On the other hand, the sensitivity to the parameters K_{NO_2} and K_C is less important.

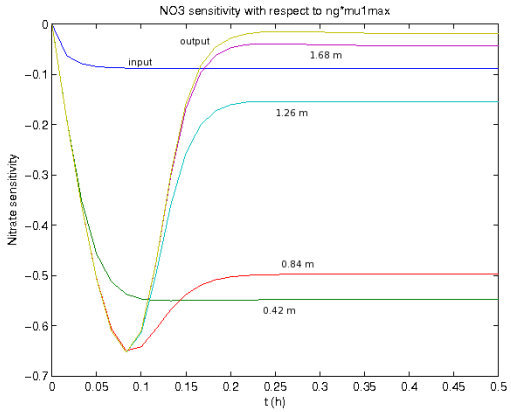

(a) Sensitivity of NO_3 with respect to $\eta_g \mu_{1_{max}}$.

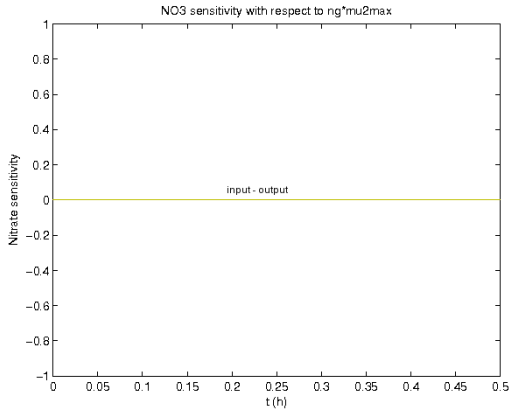

(b) Sensitivity of NO_3 with respect to $\eta_g \mu_{2_{max}}$.

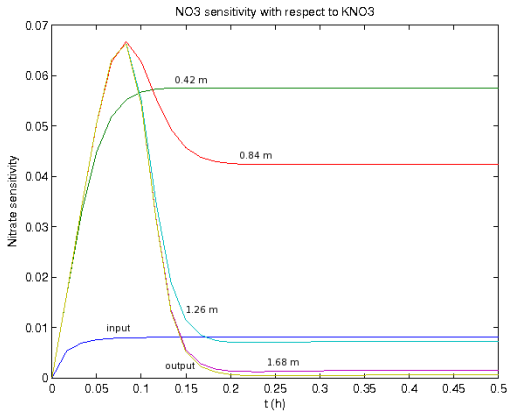

(c) Sensitivity of NO_3 with respect to K_{NO_3}.

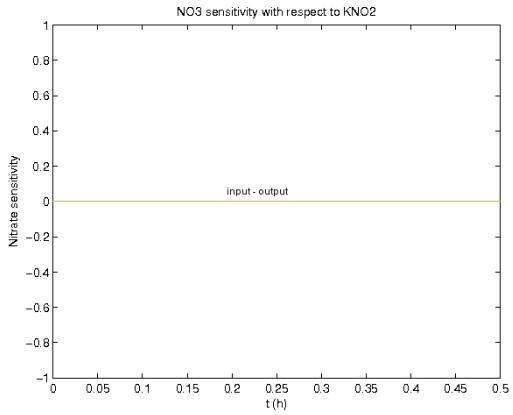

(d) Sensitivity of NO_3 with respect to K_{NO_2}.

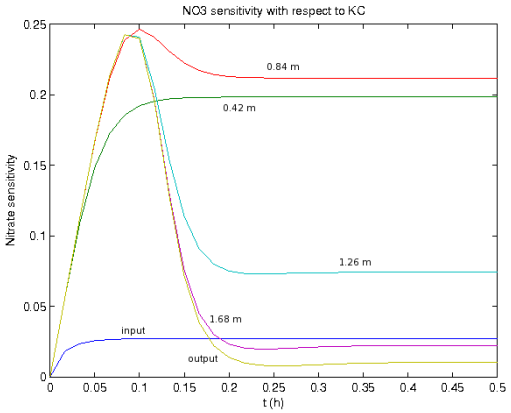

(e) Sensitivity of NO_3 with respect to K_C.

Figure 2-5: Sensitivity of the nitrate concentration for the parabolic PDE system. Time evolution at six location points with respect to the different parameters (figures 2-5a to 2-5e).

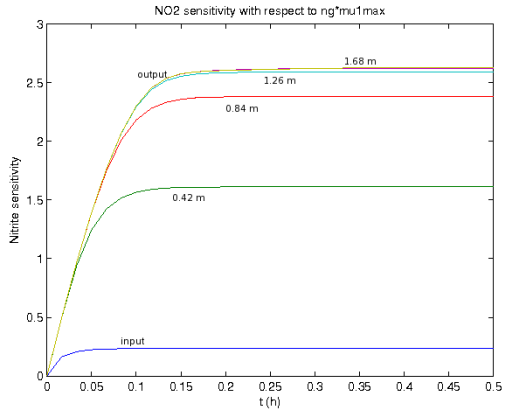

(a) Sensitivity of NO_2 with respect to $\eta_g \mu_{1_{max}}$.

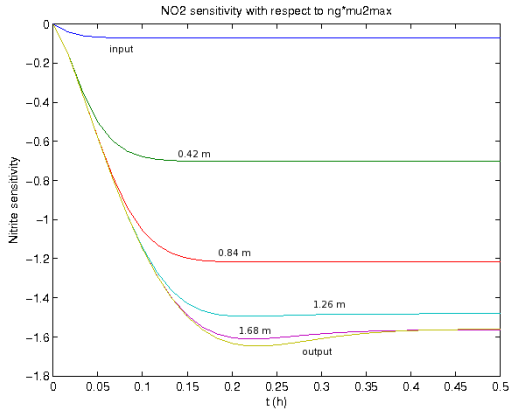

(b) Sensitivity of NO_2 with respect to $\eta_g \mu_{2_{max}}$.

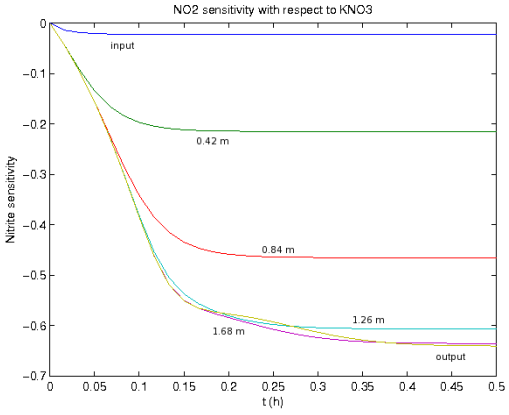

(c) Sensitivity of NO_2 with respect to K_{NO_3}.

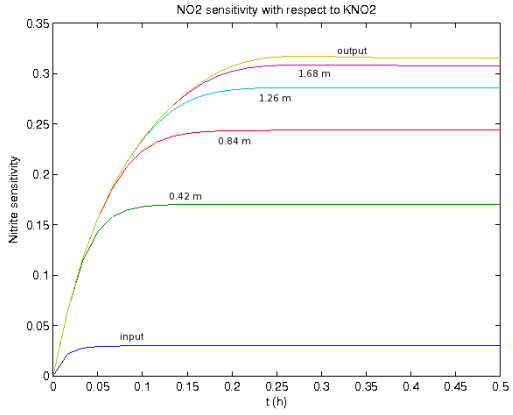

(d) Sensitivity of NO_2 with respect to K_{NO_2}.

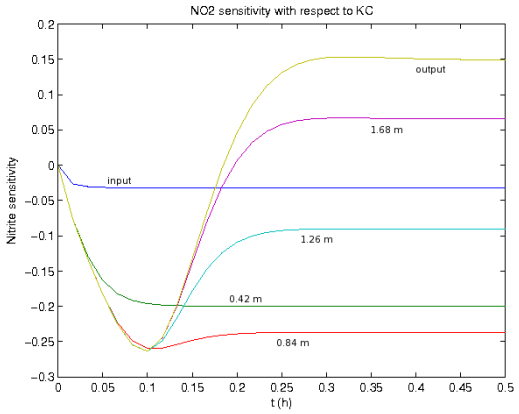

(e) Sensitivity of NO_2 with respect to K_C.

Figure 2-6: Sensitivity of the nitrite concentration for the parabolic PDE system. Time evolution at six location points with respect to the different parameters (figures 2-6a to 2-6e).

2.4.3 Parametric sensitivity analysis of the ethanol concentration

Figure 2-7 shows the sensitivity normalized time evolution of ethanol with respect to the vector p defined above at the same six positions along the reactor as in section 2.4.1.

The ethanol sensitivity is not important with respect to the overall set of parameters. It can be observed that the maximum sensitivity value is -0.27 with respect to $\eta_g \mu_{1_{max}}$.

2.5 Statement of problem

The control strategies for nonlinear distributed parameter systems may be divided into two main classes: the late lumping approaches and the early lumping approaches. In the late lumping approaches, the idea is to keep as much as possible the distributed nature of the process. In this way, the design of the controller is done directly on the nonlinear PDEs. Then, the discretization only occurs at the implementation (or simulation) step [60], [18], [89].

On the other hand, in the early lumping approach the nonlinear PDEs are simplified by discretizing the space operators in order to obtain a high-order semi-discrete time-depending ODE set. Alternatively and if the PDE system is well posed, modal analysis may be used to obtain a reduced-order semi-discrete time-depending ODE set. Then, by using any nonlinear control strategy, the design of the controller may be done [60], [89], [53]. Since many classical control strategies have been developed for linear systems, it is also possible to linearize the nonlinear ODE system around an operating point to obtain its linear state space representation. Linear control strategies may then be applied [60].

Once the approach has been selected and by considering several features of the system such as its dynamics, its controlabillity and the states measured, different

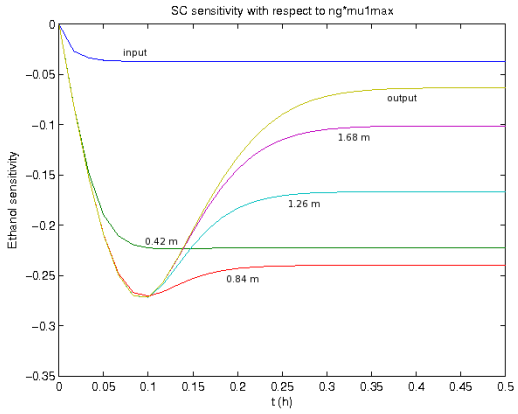

(a) Sensitivity of S_C with respect to $\eta_g \mu_{1_{max}}$.

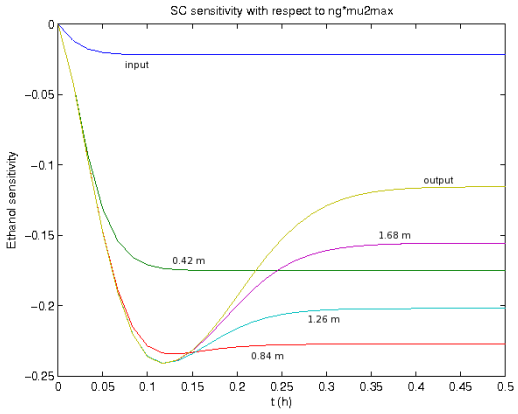

(b) Sensitivity of S_C with respect to $\eta_g \mu_{2_{max}}$.

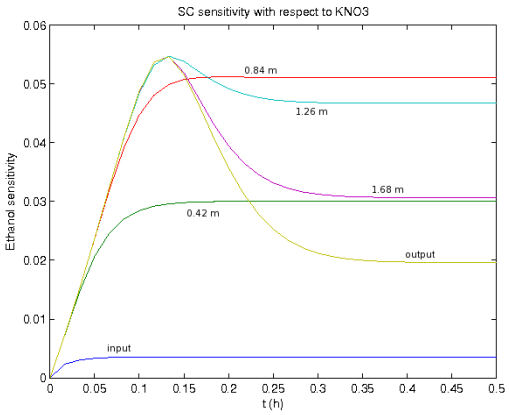

(c) Sensitivity of S_C with respect to K_{NO_3}.

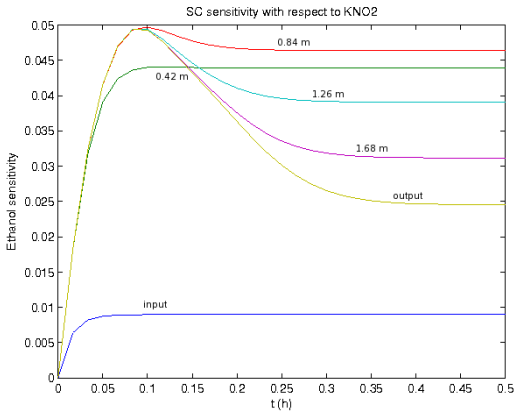

(d) Sensitivity of S_C with respect to K_{NO_2}.

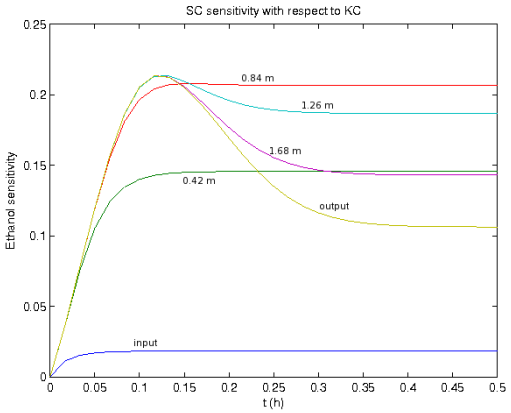

(e) Sensitivity of S_C with respect to K_C.

Figure 2-7: Sensitivity of the ethanol concentration for the parabolic PDE system. Time evolution at six location points with respect to the different parameters (figures 2-7a to 2-7e).

controller design strategies can be investigated:

- Static state feedback;
- Static output feedback;
- Dynamic output feedback;
- Dynamic observer-based output feedback.

In this work we are interested in simulating distributed parameter systems and designing state feedback controllers for them. However, in real applications it is very difficult to access all the states of the system. This is especially the case for biotechnological systems where either the sensors are expensive or some of them are not available but also for PDE systems where their distributed nature forces to take a large number of states into account. Therefore, the problem of state estimation is also addressed in this thesis in order to complement the state feedback control strategies and to design observer-based output feedback controllers.

The objective of the denitrification reactor is to transform the nitrate from the input wastewater stream into gaseous nitrogen to maintain the nitrogen concentration at the output water stream lower than some norm. In this context, the denitrification process may be controlled either by the flow rate $F(t)/A$ or by the ethanol concentration at the reactor input $S_{C,in}(t)$, that is, by a parameter in a derivative term or by a boundary condition, respectively [11]. In those contexts, several control strategies have been developed by using either early lumping or late lumping approaches [60], [89], [53]. This work considers the flow rate as the control input and the nitrate concentration at reactor input $S_{NO_3,in}$ as an external disturbance to be rejected.

2.6 Conclusion

In this chapter, the denitrification process under study has been presented. Several aspects have been brought to the fore:

- The biofilter process, preliminary described by four state variables, has been reduced to a model with only the three soluble concentrations. This is justified by the fact that there are no more significant variations of the active biomass concentration as soon as the filter is fully colonized by the microbial population.

- It has been shown that, according to the negligence of the diffusion phenomenon or not, the PDE system which describes the biofilter dynamics is an hyperbolic or a parabolic PDE system. Even if it does not change much the space and time evolutions of the process variables, we will see in the sequel that it allows to use (or not) different strategies for simulation and control.

- The boundary conditions classically considered in the literature of biofilter simulation through parabolic PDEs are the combination of Robin at the input and Neumann at the output conditions. It has been shown that this choice is questionable and that an admissible and more relevant choice in the context of the application is to consider Robin + Dirichlet conditions at the input.

- The sensitivity analysis has shown the importance of the growth rate parameters, and, in particular, to $\eta_g \mu_{1_{max}}$, to simulate the biofilter dynamics. This analysis will be useful in the sequel to analyze the performance of nonlinear controllers and observers.

Finally, this chapter has ended stating the different problems which will be addressed in this work:

- simulation of the denitrification biofilter;

- design of state feedback controllers following both early lumping and late lumping approaches;

- design of state observers to bypass the lack of measurements (especially in the late lumping context).

Chapter 3

Simulation of the denitrification process

3.1 Introduction

In order to design and to implement control strategies for distributed parameter systems, the first task to perform is to simulate the PDE system. By considering the class of PDE system and their characteristics, there exist several methods to numerically solve them. In this thesis, the denitrification reactor described by a parabolic PDE system taking the diffusion phenomenon into account or by an hyperbolic one neglecting it, is considered.

The method of lines is a very general technique to numerically solve several types of PDEs. This method consists in descretizing the spatial domain and then approximating the spatial derivatives to obtain a system of ordinary differential equations (ODE) [71]. This ODE system is integrated to compute the PDE final solution. In order to approximate the *N-order* spatial derivatives, finite element method and finite difference method may be considered. Both of them can be used therefore to approximate diffusion and convection terms. In this way, the method of lines may be used to solve both hyperbolic and parabolic PDE systems.

On the other hand, the method of characteristics is a classical method to nu-

merycally solve hyperbolic PDEs. They may be separated in a time-varing ODE and a charateristic ODE. This last ODE is solved to obtain a characteristic curve to know how the first ODE varies with respect to the space [95].

All these methods produce high-order nonlinear state space systems that may be unsuitable to future control strategies. Modal decomposition is a convenient and useful form of analysis for simulating PDEs by considering the most important system modes [95]. In this way, a reduced-order nonlinear state space system may be obtained. This form of analysis is possible when spatial operators have a real discrete spectrum of eigenvalues. It is not the case for the convection term spatial operator which has, in its regular form, a complex spectrum of eigenvalues [60]. On the other hand, this is the case for the diffusion term spatial operator. Modal analysis of the parabolic PDE biofilter model may therefore be considered. The Laplacian decomposition is a very useful technique to analyse the system modes. However, this decomposition is only suitable if there is no convection term. Another classical technique to analyse the system modes is the proper orthogonal decomposition method which has shown to be efficient for PDE systems with non-homogeneous boundary conditions and convection term [85], such as the parabolic PDE system describing the denitrification reactor.

In this chapter, the method of lines, the method of characteristics and the modal analysis are investigated and their application to simulate the denitrification reactor is presented. First, the method of lines is used to solve the hyperbolic model approximating the spatial derivatives by the finite difference method. Then, the parabolic model is solved by the same method but now, the spatial derivatives are approximated by the finite element method. The spatial approximation matrices resulting from the finite element method will be used later to solve an eigenproblem, by approximating both the integral and the differential terms by FEM matrices in the modal analysis. Following, the method of characteristics is used to solve the hyperbolic model, resulting in a set of difference equations. Finally, a modal analysis of the parabolic model is performed to simulate the denitrification biofilter using only the most important

modes.

3.2 Method of lines

The method of lines (MOL) is a general technique to numerically solve PDEs. The idea behind this method is the substitution of derivatives with respect to the space variable by an approximation using either finite difference or finite element relationships and numerical integration with respect to time of the resulting semi-discrete ODE system (discrete in space - continuous in time). In this way, the method of lines may be applied both to hyperbolic and to parabolic PDEs [95].

In order to exemplify the method of lines, the finite difference approach is used to numerically solve the hyperbolic PDE system and the finite element approach is used to numerically solve the parabolic one. The spatial approximation matrices resulting from the finite element method will be used later to compute the eigenvectors associated to the PDE system in order to derive its modes and then, to reduce the order of the ODE system to integrate.

3.2.1 The finite difference approximation

The finite difference technique consists in replacing the spatial derivatives appearing in the PDE by finite difference approximations. The most basic approach uses a finite difference based only on values of each state variable at a number of points close to the discretization points and the standard definition of the derivative. Further, Taylor series may also be used to derive an appropriate finite difference formula, using the method of *undetermined coefficients*. For example, the spatial variation of the nitrate concentration ($S_{NO_3}(z)$), may be approximated by a Taylor series [42] with respect to z as:

$$S_{NO_3}(z) = a_0 + a_1(z - z_i) + a_2(z - z_i)^2 + a_3(z - z_i)^3 + \dots \tag{3.1}$$

where z_i is a value of z to be specified and a_0, a_1, a_2, a_3, ... are constants to be

determined.

To determine the first constant, let $z = z_i$ and immediately it is obtained $a_0 = S_{NO_3}(z_i)$. Next, by differentiating equation (3.1) with respect to z:

$$\frac{dS_{NO_3}(z)}{dz} = a_1 + 2a_2(z - z_i) + 3a_3(z - z_i)^2 + \dots$$

from which, with $z = z_i$, it is obtained the second constant $a_1 = \frac{dS_{NO_3}(z_i)}{dz}$. Successive differentiations, followed by setting $z = z_i$, give $a_2 = \frac{1}{2!}\frac{d^2S_{NO_3}(z_i)}{dz^2}$, $a_3 = \frac{1}{3!}\frac{d^3S_{NO_3}(z_i)}{dz^3}$, etc. In general:

$$a_n = \frac{1}{n!}\frac{d^nS_{NO_3}(z_i)}{dz^n} \tag{3.2}$$

By replacing (3.2) into (3.1) it is obtained the following Taylor series:

$$S_{NO_3}(z) = \sum_{n=0}^{\infty}\frac{1}{n!}\frac{d^nS_{NO_3}(z_i)}{dz^n}(z - z_i)^n \tag{3.3}$$

The spatial first derivative of $S_{NO_3}(z_i, t)$ is then approximated by an algebraic formula of $dS_{NO_3}(z_i)/dz$:

The most basic spatial approximation uses two points, for example:

$$\frac{dS_{NO_3}(z_i)}{dz} = \frac{S_{NO_3}(z_i) - S_{NO_3}(z_{i-1})}{\Delta z}$$

However, in order to obtain a good approximation of the state variables, a larger number of points on the spatial grid are generally used to build the spatial first derivative. In particular, four-order finite difference approximation is classically used, in which the values of $S_{NO_3}(z, t)$ at five points z_{i-2}, z_{i-1}, z_i, z_{i+1} and z_{i+2} into the spatial grid are used. By considering the same interval Δz between any two succesive points, Taylor series (3.3) for grid points $i-2$, $i-1$, $i+1$ and $i+2$ are then rewritten as [71]:

$$S_{NO_3}(z_{i-2}) = S_{NO_3}(z_i) + \left(\frac{dS_{NO_3}(z_i)}{dz}\right)(-2\Delta z) + \frac{1}{2!}\left(\frac{d^2S_{NO_3}(z_i)}{dz^2}\right)(-2\Delta z)^2 + \ldots \tag{3.4}$$

$$S_{NO_3}(z_{i-1}) = S_{NO_3}(z_i) + \left(\frac{dS_{NO_3}(z_i)}{dz}\right)(-\Delta z) + \frac{1}{2!}\left(\frac{d^2S_{NO_3}(z_i)}{dz^2}\right)(-\Delta z)^2 + \ldots \tag{3.5}$$

$$S_{NO_3}(z_{i+1}) = S_{NO_3}(z_i) + \left(\frac{dS_{NO_3}(z_i)}{dz}\right)(\Delta z) + \frac{1}{2!}\left(\frac{d^2S_{NO_3}(z_i)}{dz^2}\right)(\Delta z)^2 + \ldots \tag{3.6}$$

$$S_{NO_3}(z_{i+2}) = S_{NO_3}(z_i) + \left(\frac{dS_{NO_3}(z_i)}{dz}\right)(2\Delta z) + \frac{1}{2!}\left(\frac{d^2S_{NO_3}(z_i)}{dz^2}\right)(2\Delta z)^2 + \ldots \tag{3.7}$$

Now, a linear combination of equations (3.4)-(3.7) is taken so as to keep the derivative of interest, $dS_{NO_3}(z_i)/dz$, and drop as many of the higher derivative terms as possible.

If equation (3.4) is multiplied by a constant a, equation (3.5) by a constant b, equation (3.6) by a constant c and equation (3.7) by a constant d, and using the sum of the resulting equations, the first derivative term, $dS_{NO_3}(z_i)/dz$, may be retained by imposing the condition:

$$-2a - b + c + 2d = 1 \tag{3.8}$$

The equality of equation (3.8) ensures that when equations (3.4)-(3.7) are added with the values a, b, c and d, still to be determined, the first derivative term remains. Similary, in order to eliminate the second derivative term, $d^2S_{NO_3}(z_i)/dz^2$, the following condition may be imposed:

$$4a + b + c + 4d = 0 \tag{3.9}$$

The equality of equation (3.9) ensures that when equations (3.4)-(3.7) are added with the values a, b, c and d, still to be determined, the second derivative term is eliminated.

In the same way, to eliminate the third- and fourth-order derivative terms the following conditions may be imposed:

$$-8a - b + c + 8d = 0 \tag{3.10}$$

$$16a + b + c + 16d = 0 \tag{3.11}$$

The set of equations (3.8)-(3.11) gives a unique solution for a, b, c and d. The sum of equations (3.4)-(3.7) with their respective coefficients $a - d$, allows to finally compute:

$$\begin{aligned}\frac{dS_{NO_3}(z_i)}{dz} = \left(\frac{1}{12\Delta z}\right) &(S_{NO_3}(z_{i-2}) - 8S_{NO_3}(z_{i-1}) + 0S_{NO_3}(z_i) + 8S_{NO_3}(z_{i+1}) \\ &- S_{NO_3}(z_{i+2})) + O(\Delta z^4)\end{aligned} \tag{3.12}$$

Equation (3.12) is a central difference approximation since values of $S_{NO_3}(z)$ located symmetrically around $S_{NO_3}(z_i)$ are used to calculate $dS_{NO_3}(z_i)/dz$. However, equation (3.12) cannot be applied at grid points $i = 1, 2$ because $S_{NO_3}(z_{-1})$ and $S_{NO_3}(z_0)$ would be required; similary, equation (3.12) cannot be applied at grid points $i = N - 1, N$ because $S_{NO_3}(z_{N+1})$ and $S_{NO_3}(z_{N+2})$ would be required.

To obtain an approximation for $dS_{NO_3}(z_1)/dz$ Taylor series for $S_{NO_3}(z_2)$, $S_{NO_3}(z_3)$, $S_{NO_3}(z_4)$ and $S_{NO_3}(z_5)$ are used, with respective multiplicative coefficients a, b, c and d.

A similar procedure is applied to calculate the new coefficients a, b, c and d

which will allow to compute $dS_{NO_3}(z_1)/dz$. They are solution of the following set of equations:

$$\begin{aligned} a + 2b + 3c + 4d &= 1 \\ a + 4b + 9c + 16d &= 0 \\ a + 8b + 27c + 64d &= 0 \\ a + 16b + 81c + 256d &= 0 \end{aligned} \tag{3.13}$$

The first derivative term $dS_{NO_3}(z_1)/dz$ is then computed as:

$$\begin{aligned} \frac{dS_{NO_3}(z_1)}{dz} = \left(\frac{1}{12\Delta z}\right) (&-25S_{NO_3}(z_1) + 48S_{NO_3}(z_2) - 36S_{NO_3}(z_3) + 16S_{NO_3}(z_4) \\ &-3S_{NO_3}(z_5)) + O(\Delta z^4) \end{aligned} \tag{3.14}$$

Similarly, for an approximation of $dS_{NO_3}(z_2)/dz$, four Taylor series for $S_{NO_3}(z_1)$, $S_{NO_3}(z_3)$, $S_{NO_3}(z_4)$ and $S_{NO_3}(z_5)$ are used, resulting in parameters a, b, c and d solution to:

$$\begin{aligned} -a + b + 2c + 3d &= 1 \\ a + b + 4c + 9d &= 0 \\ -a + b + 8c + 27d &= 0 \\ a + b + 16c + 81d &= 0 \end{aligned} \tag{3.15}$$

which are used to compute the first derivative term $dS_{NO_3}(z_2)/dz$ as:

$$\begin{aligned} \frac{dS_{NO_3}(z_2)}{dz} = \left(\frac{1}{12\Delta z}\right) (&-3S_{NO_3}(z_1) - 10S_{NO_3}(z_2) + 18S_{NO_3}(z_3) - 6S_{NO_3}(z_4) \\ &+S_{NO_3}(z_5)) + O(\Delta z^4) \end{aligned} \tag{3.16}$$

For an approximation of $dS_{NO_3}(z_{N-1})/dz$, four Taylor series for $S_{NO_3}(z_{N-4})$, $S_{NO_3}(z_{N-3})$, $S_{NO_3}(z_{N-2})$ and $S_{NO_3}(z_N)$ are used and, with the respective multiplicative coefficients a, b, c and d solution to:

$$\begin{aligned} -3a - 2b - c + d &= 1 \\ 9a + 4b + c + d &= 0 \\ -27a - 8b - c + d &= 0 \\ 81a + 16b + c + d &= 0 \end{aligned} \tag{3.17}$$

the first derivative term $dS_{NO_3}(z_{N-1})/dz$ is computed as:

$$\begin{aligned} \frac{dS_{NO_3}(z_{N-1})}{dz} = \left(\frac{1}{12\Delta z}\right) (&-S_{NO_3}(z_{N-4}) + 6S_{NO_3}(z_{N-3}) - 18S_{NO_3}(z_{N-2}) + 10S_{NO_3}(z_{N-1}) \\ &+3S_{NO_3}(z_N)) + O(\Delta z^4) \end{aligned} \tag{3.18}$$

Finally, for an approximation of $dS_{NO_3}(z_N)/dz$, four Taylor series for $S_{NO_3}(z_{N-4})$, $S_{NO_3}(z_{N-3})$, $S_{NO_3}(z_{N-2})$ and $S_{NO_3}(z_{N-1})$ are used and, with the respective multiplicative coefficients a, b, c and d solution to:

$$\begin{aligned} -4a - 3b - 2c - d &= 1 \\ 16a + 9b + 4c + d &= 0 \\ -64a - 27b - 8c - d &= 0 \\ 256a + 81b + 16c + d &= 0 \end{aligned} \tag{3.19}$$

the first derivative term $dS_{NO_3}(z_N)/dz$ is computed as:

$$\begin{aligned} \frac{dS_{NO_3}(z_N)}{dz} = \left(\frac{1}{12\Delta z}\right) (&3S_{NO_3}(z_{N-4}) - 16S_{NO_3}(z_{N-3}) + 36S_{NO_3}(z_{N-2}) - 48S_{NO_3}(z_{N-1}) \\ &+25S_{NO_3}(z_N)) + O(\Delta z^4) \end{aligned} \tag{3.20}$$

Equations (3.12), (3.14), (3.16), (3.18) and (3.20) may be summarized in terms of a differentiation matrix as:

$$\frac{dx_1}{dz} = D_z x_1 \tag{3.21}$$

where $D_z \in \mathbb{R}^{N \times N}$ is a matrix with the coefficients resulting from the application of

the fourth-order finite differences method (FDM). The vector $x_1 \in \mathbb{R}^N$ is the space discretized nitrate concentration. The same discretization is performed for the nitrite and the ethanol to obtain spatial derivative approximations as:

$$\frac{dx_2}{dz} = D_z x_2 \tag{3.22}$$

$$\frac{dx_3}{dz} = D_z x_3 \tag{3.23}$$

where x_2 is the space discretized nitrite concentration and x_3 is the space discretized ethanol concentration.

These spatial discretizations are then used to numerically solve the hyperbolic PDE model, with N points uniformly distributed throughout the reactor. The resulting system, with space discretized state variable $x_i \in \mathbb{R}^N$ $(i = 1, 2, 3)$, can be solved by a finite procedure [1]:

$$\frac{dx_1(t)}{dt} = -\frac{v}{\epsilon} D_z x_1(t) - \frac{1 - Y_{h_1}}{1.14 Y_{h_1} \epsilon} \mu_1(x_1, x_3) X_{amax} \tag{3.24}$$

$$\frac{dx_2(t)}{dt} = -\frac{v}{\epsilon} D_z x_2(t) + \frac{1 - Y_{h_1}}{1.14 Y_{h_1} \epsilon} \mu_1(x_1, x_3) X_{amax} - \frac{1 - Y_{h_2}}{1.71 Y_{h_2} \epsilon} \mu_2(x_2, x_3) X_{amax} \tag{3.25}$$

$$\frac{dx_3(t)}{dt} = -\frac{v}{\epsilon} D_z x_3(t) - \frac{1}{Y_{h_1} \epsilon} \mu_1(x_1, x_3) X_{amax} - \frac{1}{Y_{h_2} \epsilon} \mu_2(x_2, x_3) X_{amax} \tag{3.26}$$

Figure 3-1 shows the time evolution of the concentrations of nitrate (2-4a), nitrite (2-4c) and ethanol (2-4e) at only six positions along the reactor (*input*, $42cm.$, $84cm.$, $126cm.$, $168cm.$ and *output*) to improve clarity. The hyperbolic model is spatially discretized with 50 intervals ($N = 51$ in solid blue), with 100 intervals ($N = 101$ in dashed red), with 150 intervals ($N = 151$ in pointed black) and with 200 inter-

[1] $\mu_1(x_1, x_3)$ and $\mu_2(x_2, x_3)$ now represent a vector of dimension N.

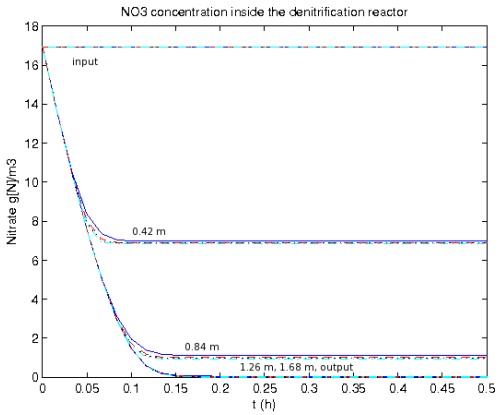

(a) NO_3 solution.

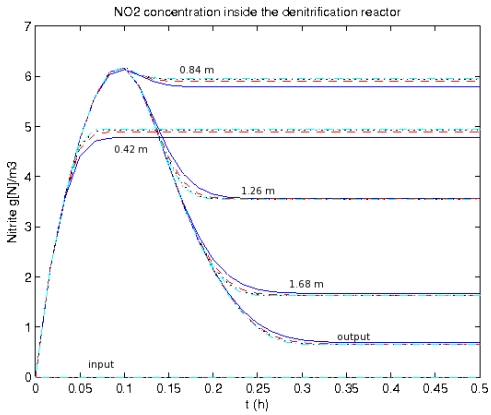

(b) NO_2 solution.

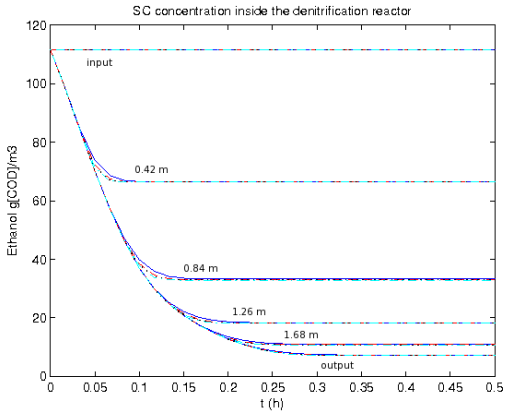

(c) S_C solution.

Figure 3-1: Time and space (at six positions) evolution of the hyperbolic PDE system using MOL-FDM.

vals ($N = 201$ in pointed-dashed cyan) using the method of lines and derivatives approximated by the four-order finite difference method described above.

It can be observed in figure 3-1 that the time and space evolution of the state variables depends on the number of discretization points. However, it is observed that the time and space evolution are so close with 150 and 200 intervals, that is, $N = 151$ may be considered as a sufficient number of discretization points to simulate the PDE system describing the denitrification biofilter. Such a behavior has also been observed in other simulation conditions and with the Finite Element Method (see section 3.2.2). It explains why the simulations presented in chapter 2 considered

150 intervals, and why the remaining of this document considers 150 intervals for the simulations.

It must be pointed out that this strategy may be used on the parabolic PDE model of the denitrification reactor (as shown in chapter 2). In that case, the second derivative term $\partial^2 S_{NO_3}(z,t)/\partial z^2$ must also be approximated, in a similar way, by new algebraic formulas computed from Taylor series.

3.2.2 The finite element approximation

Another technique to approximate spatial derivatives is the finite element method (FEM), which allows, in addition, to approximate spatial integrals by matrix operations. It is presented and illustrated in this section with the parabolic PDE model of the denitrification biofilter.

Let us consider the vector $S = [S_{NO_3}\ S_{NO_2}\ S_C]^T = [S_1\ S_2\ S_3]^T$. Each state variable $S_i(z,t)$ may be expanded in a Fourier series of the form:

$$S_i(z,t) = \sum_{j=1}^{\infty} r_i^j(t)\varphi_i^j(z) \tag{3.27}$$

where $\Phi_i = \left\{\varphi_i^j(z)\right\}_{j=1}^{\infty}$ forms an orthonormal basis on a Hilbert space $\mathcal{L}_2$ [85].

The state variable $S_i(z,t)$ is then approximated by truncating the series (3.27) as:

$$\tilde{S}_i(z,t) = \sum_{j=1}^{N} r_i^j(t)\varphi_i^j(z) \tag{3.28}$$

Because $\tilde{S}_i$ is an approximation, by replacing it into (2.21) a residual is obtained as:

$$R_i(z,t) = \frac{\partial \tilde{S}_i}{\partial t} - D_f \frac{\partial^2 \tilde{S}_i}{\partial z^2} + \frac{v}{\epsilon}\frac{\partial \tilde{S}_i}{\partial z} - h_i(\tilde{S}) \tag{3.29}$$

In FEM, such as in other methods of weighted residuals (MWR), $R_i(z,t)$ must be made zero, thus:

$$\int_{\mathcal{V}} R_i(z,t)\psi_i^j(z)dz = 0 \tag{3.30}$$

where $\Psi_i = \left\{\psi_i^j(z)\right\}_{j=1}^{N}$ are the weighting functions to be chosen [60].

The choice of the weighting functions leads to several criteria. In this work the Galerkin's method is considered, in which, the weighting functions ψ_i^j coincide with the basis functions φ_i^j which form a complete set for the N dimensional subspace where the approximated solution is found. This has the advantage that the residual is made orthogonal to each basis function and is, therefore, the best solution possible in the space made up of the N functions $\varphi_i^j(z)$ [85].

The finite element formulation of a PDE problem is obtained through a number of steps (see [94] for details). Firstly, the spatial domain of (2.21) must be divided into N finite discrete elements (finite element mesh), so as to define a basis set. Secondly, the system (2.21) is represented in a new mathematical representation called *the weak form* derived by multiplying it by an arbitrary test function ψ_i and integrating the result over the spatial domain. Thus, from (3.29) and (3.30):

$$\int_{\mathcal{V}} \psi_i \frac{\partial S_i}{\partial t}dz + \frac{v}{\epsilon}\int_{\mathcal{V}} \psi_i \frac{\partial S_i}{\partial z}dz = D_f \int_{\mathcal{V}} \psi_i \frac{\partial^2 S_i}{\partial z^2}dz + \int_{\mathcal{V}} \psi_i h_i(S)dz \tag{3.31}$$

By using the Green's first identity, the first term of the right hand size of equation (3.31) may be expressed as:

$$D_f \int_{\mathcal{V}} \psi_i \frac{\partial^2 S_i}{\partial z^2}dz = D_f \int_{\mathcal{B}} \psi_i \frac{\partial S_i}{\partial z}dz - D_f \int_{\mathcal{V}} \frac{\partial \psi_i}{\partial z}\frac{\partial S_i}{\partial z}dz \tag{3.32}$$

where $\mathcal{B}$ is the boundary of the spatial domain $\mathcal{V}$. By sustituting the last equation into (3.31) it is obtained:

$$\int_{\mathcal{V}} \psi_i \frac{\partial S_i}{\partial t}dz + \frac{v}{\epsilon}\int_{\mathcal{V}} \psi_i \frac{\partial S_i}{\partial z}dz + D_f \int_{\mathcal{V}} \frac{\partial \psi_i}{\partial z}\frac{\partial S_i}{\partial z}dz = D_f \int_{\mathcal{B}} \psi_i \frac{\partial S_i}{\partial z}dz + \int_{\mathcal{V}} \psi_i h_i(S)dz \tag{3.33}$$

and by introducing the boundary conditions (2.9)-(2.11) into the previous equation, it is obtained:

$$\begin{aligned}&\int_{\mathcal{V}} \psi_i \frac{\partial S_i}{\partial t} dz + \frac{v}{\epsilon} \int_{\mathcal{V}} \psi_i \frac{\partial S_i}{\partial z} dz + D_f \int_{\mathcal{V}} \frac{\partial \psi_i}{\partial z} \frac{\partial S_i}{\partial z} dz + \frac{v}{\epsilon} \int_{\mathcal{B}} \psi_i S_i dz \\ &= \frac{v}{\epsilon} \int_{\mathcal{B}} \psi_i S_{in} dz + \int_{\mathcal{V}} \psi_i h_i(S) dz\end{aligned} \tag{3.34}$$

Thirdly, $S_i(z,t)$ is approximated using (3.28) and because the FEM is based on the Galerkin approach the test functions ψ_i are choosen so as to coincide with the basis functions φ_i. In this way, the following set of N equations is obtained:

$$\begin{aligned}&\int_{\mathcal{V}} \varphi_i^k(z) \frac{\partial \sum_{j=1}^N r_i^j(t) \varphi_i^j(z)}{\partial t} dz + \frac{v}{\epsilon} \int_{\mathcal{V}} \varphi_i^k(z) \frac{\partial \sum_{j=1}^N r_i^j(t) \varphi_i^j(z)}{\partial z} dz \\ &+ D_f \int_{\mathcal{V}} \frac{\partial \varphi_i^k(z)}{\partial z} \frac{\partial \sum_{j=1}^N r_i^j(t) \varphi_i^j(z)}{\partial z} dz + \frac{v}{\epsilon} \int_{\mathcal{B}} \varphi_i^k(z) \sum_{j=1}^N r_i^j(t) \varphi_i^j(z) dz \\ &= \frac{v}{\epsilon} \int_{\mathcal{B}} \varphi_i^k(z) S_{in} dz + \int_{\mathcal{V}} \varphi_i^k(z) h_i(S) dz\end{aligned} \tag{3.35}$$

for $k = 1, 2, \ldots, N$. In a more compact form, the last equation may be rewritten as:

$$\sum_{j=1}^N M_{Mi}^{kj} \frac{\partial r_i^j(t)}{\partial t} + \sum_{j=1}^N \left(\frac{v}{\epsilon} M_{Ci}^{kj} + D_f M_{Di}^{kj} + \frac{v}{\epsilon} M_{Bi}^{kj} \right) r_i^j(t) = \frac{v}{\epsilon} G_i^k + H_i^k \tag{3.36}$$

where the matrices in the former expression are:

$$M_{Mi}^{kj} = \int_{\mathcal{V}} \varphi_i^k(z) \varphi_i^j(z) dz \tag{3.37}$$

$$M_{Ci}^{kj} = \int_{\mathcal{V}} \varphi_i^k(z) \frac{\partial \varphi_i^j(z)}{\partial z} dz \tag{3.38}$$

$$M_{Di}^{kj} = \int_{\mathcal{V}} \frac{\partial \varphi_i^k(z)}{\partial z} \frac{\partial \varphi_i^j(z)}{\partial z} dz \tag{3.39}$$

$$M_{Bi}^{kj} = \int_{\mathcal{B}} \varphi_i^k(z)\varphi_i^j(z)dz \tag{3.40}$$

$$G_i^k = \int_{\mathcal{B}} \varphi_i^k(z)S_{in}dz \tag{3.41}$$

$$H_i^k = \int_{\mathcal{V}} \varphi_i^k(z)h_i(S)dz \tag{3.42}$$

In the FEM, the basis functions φ_i are selected to be algebraic polynomials. In general the higher is the order of the polynomial, the better is the approximation. However, it also produces a larger number of equations. For simplicity, the value of φ is often taken as the unity on one node of an element $\mathcal{V}$ and zero on the others (see figure 3-2) [85].

$$\varphi_i^k(\xi_j) = \begin{cases} 1 & if \quad k = j \\ 0 & if \quad k \neq j \end{cases} \tag{3.43}$$

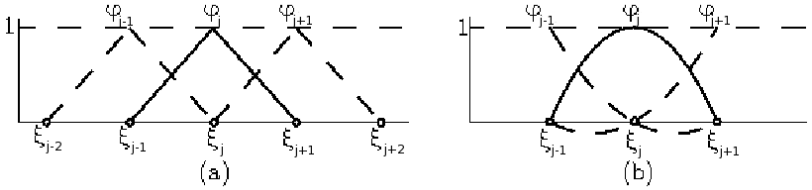

Figure 3-2: Typical basis function of the FEM. The white circles represent the element nodes. (a) 1D domains and first order polynomials and (b) 1D domains and second order polynomials.

Thus, with the application of the finite element method, the following matrices are obtained: the mass matrix $M_{Mi} \in \mathbb{R}^{N\times N}$, the convection matrix $M_{Ci} \in \mathbb{R}^{N\times N}$, the diffusion matrix $M_{Di} \in \mathbb{R}^{N\times N}$ and the boundary conditions matrix $M_{Bi} \in \mathbb{R}^{N\times N}$ to approximate the spatial derivatives like:

$$\frac{v}{\epsilon}\frac{\partial}{\partial z} = \frac{v}{\epsilon}M_{Mi}^{-1}M_{Ci}$$

$$D_f\frac{\partial^2}{\partial z^2} = -M_{Mi}^{-1}\left(D_f M_{Di} + \frac{v}{\epsilon}M_{Bi}\right)$$

Therefore, the following semi-discrete ODE system is obtained for each spatially discretized state variable $x_i \in \mathbb{R}^N$, defined as in subsection 3.2.1:

$$\frac{dx_i(t)}{dt} = -M_{Mi}^{-1}(D_f M_{Di} + \frac{v}{\epsilon}(M_{Ci} + M_{Bi}))x_i + \frac{v}{\epsilon}M_{Mi}^{-1}G_i(x_{i,in}) + h_i(x) \tag{3.44}$$

for $i = 1, 2, 3$. The resulting system of semi-discrete ODEs is then integrated in time to compute the final solution.

Remark 5 *M_{Bi} involves information about the homogeneous part of the Robin boundary conditions (2.9)-(2.11) and the $G_i(x_{i,in})$ vector contains information about the non-homogeneous part, specifically in its first element (the element at the boundary $z = 0$).*

Figure 3-3 shows the time evolution of the concentration of nitrate (3-3a), nitrite (3-3b) and ethanol (3-3c) issued from (2.1)-(2.3). The finite element method described above is applied with $N = 151$ discretization points uniformly distributed along the reactor. For greater clarity, the figures show only the time evolution at the same six positions along the reactor as in the section 3.2.1.

It can be observed when comparing figure 2-4 (simulations using MOL-FDM) and figure 3-3 (simulations using MOL-FEM) that the time and space evolution of the parabolic PDE system is exactly the same for both discretization approaches.

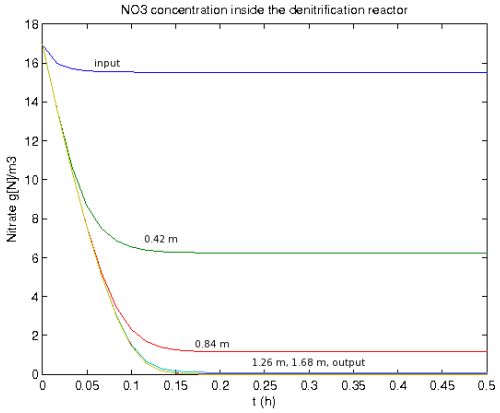

(a) NO_3 solution.

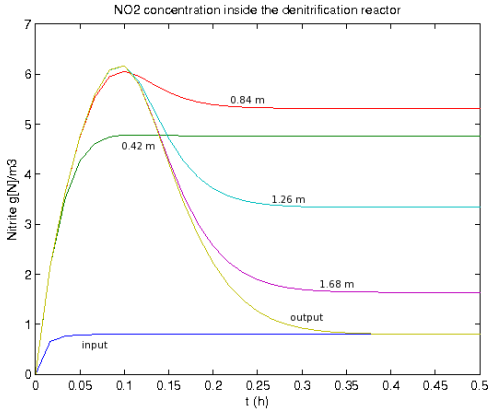

(b) NO_2 solution.

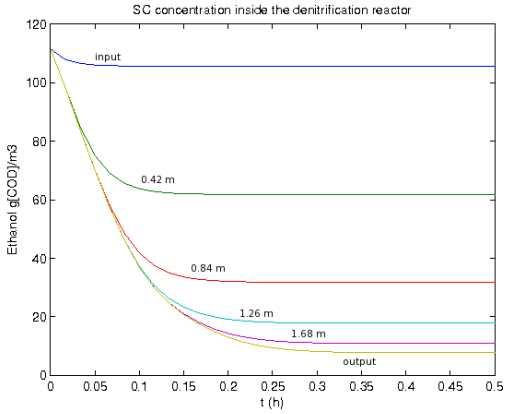

(c) S_C solution.

Figure 3-3: Time and space (at six positions) evolution of the parabolic PDE system using MOL-FEM.

3.3 Method of characteristics

The hyperbolic model is a quasilinear PDE system. It can then be transformed, through the method of characteristics (MOC), into a set of ODEs that defines the characteristics and a set of ODEs describing how the solution changes along any specific characteristic [95].

The nitrate hyperbolic equation has been previously given by:

$$\frac{\partial S_{NO_3}(z,t)}{\partial t} + \frac{v}{\epsilon}\frac{\partial S_{NO_3}(z,t)}{\partial z} = -\frac{1-Y_{h_1}}{1.14Y_{h_1}\epsilon}\mu_1(S_{NO_3}(z,t), S_C(z,t))X_{amax} \tag{3.45}$$

If $S_{NO_3}(z,t)$ is differentiated with respect to the variable r, then one obtains:

$$\frac{dS_{NO_3}}{dr} = \frac{\partial S_{NO_3}}{\partial z}\frac{dz}{dr} + \frac{\partial S_{NO_3}}{\partial t}\frac{dt}{dr} = \frac{dt}{dr}\frac{\partial S_{NO_3}}{\partial t} + \frac{dz}{dr}\frac{\partial S_{NO_3}}{\partial z} \tag{3.46}$$

By comparing (3.45) and (3.46), it can be observed that:

$$\frac{dt}{dr} = 1 \tag{3.47}$$

$$\frac{dz}{dr} = \frac{v}{\epsilon} \tag{3.48}$$

By solving (3.47) and (3.48), with $r = t$, it may be concluded that:

$$z = \frac{1}{\epsilon}\int_0^t v(\tau)d\tau + z_0 \tag{3.49}$$

$$\frac{dS_{NO_3}(z,t)}{dt} = -\frac{1-Y_{h_1}}{1.14Y_{h_1}\epsilon}\mu_1(S_{NO_3}(z,t), S_C(z,t))X_{amax} \tag{3.50}$$

Therefore, the solution to (3.50) along a characteristic curve defined by (3.49) may be found. The repeated solution of (3.50) at different values of z_0 will give the entire solution for the original PDE equation [60].

In the same way, one can express for the nitrite and the ethanol their time evolution

as:

$$\begin{aligned}\frac{dS_{NO_2}(z,t)}{dt} =& \frac{1-Y_{h_1}}{1.14Y_{h_1}\epsilon}\mu_1(S_{NO_3}(z,t),S_C(z,t))X_{amax} \\ &- \frac{1-Y_{h_2}}{1.71Y_{h_2}\epsilon}\mu_2(S_{NO_2}(z,t),S_C(z,t))X_{amax}\end{aligned} \tag{3.51}$$

$$\begin{aligned}\frac{dS_C(z,t)}{dt} =& -\frac{1}{Y_{h_1}\epsilon}\mu_1(S_{NO_3}(z,t),S_C(z,t))X_{amax} \\ &- \frac{1}{Y_{h_2}\epsilon}\mu_2(S_{NO_2}(z,t),S_C(z,t))X_{amax}\end{aligned} \tag{3.52}$$

along the characteristic curve (3.49).

Equations (3.50)-(3.52) can also be written in the state-space representation form, which is suitable for the simulation and application of a broad variety of control algorithms.

First, let us define the constants:

$$a = \frac{(1-Y_{h_1})n_g\mu_{NO_{3max}}}{1.14Y_{h_1}\epsilon}$$

$$b = \frac{(1-Y_{h_2})n_g\mu_{NO_{2max}}}{1.71Y_{h_2}\epsilon}$$

$$c = -\frac{n_g\mu_{NO_{3max}}}{Y_{h_1}\epsilon}$$

$$d = -\frac{n_g\mu_{NO_{2max}}}{Y_{h_2}\epsilon}$$

$$e = n_g\mu_{NO_{3max}}$$

$$f = n_g\mu_{NO_{2max}}$$

and the functions:

$$f_{S_1}(S_{NO_3}) = \frac{S_{NO_3}}{S_{NO_3} + K_{NO_3}}$$

$$f_{S_2}(S_{NO_2}) = \frac{S_{NO_2}}{S_{NO_2} + K_{NO_2}}$$

$$f_{S_3}(S_C) = \frac{S_C}{S_C + K_C}$$

Therefore, equations (3.50), (3.51) and (3.52) are rewritten as:

$$\dot{S}_{NO_3} = -a f_{S_1} f_{S_3} X_{amax} \tag{3.53}$$

$$\dot{S}_{NO_2} = a f_{S_1} f_{S_3} X_{amax} - b f_{S_2} f_{S_3} X_{amax} \tag{3.54}$$

$$\dot{S}_C = c f_{S_1} f_{S_3} X_a + d f_{S_2} f_{S_3} X_{amax} \tag{3.55}$$

The system (3.53)-(3.55) is numerically solved by approximating the differentials by finite differences to obtain [52]:

$$\Delta S_{NO_3} = -aT f_{S_1} f_{S_3} X_{amax} \tag{3.56}$$

$$\Delta S_{NO_2} = aT f_{S_1} f_{S_3} X_{amax} - bT f_{S_2} f_{S_3} X_{amax} \tag{3.57}$$

$$\Delta S_C = cT f_{S_1} f_{S_3} X_{amax} + dT f_{S_2} f_{S_3} X_{amax} \tag{3.58}$$

where T is the sample period.

In general, the solution of (3.49) is not a linear equation and steps in space are not the same as those ones in time, as shown in figure 3-4. For sufficiently small T, the characteristic curve C can be approximated by line segments between kT and

$(k+1)T$ as shown in figure 3-4. It is then easy to see that [2]:

$$S_{NO_3}(j,k+1) - S_{NO_3}(j-\psi,k) = -aTf_{S_1}(j-\psi,k)f_{S_3}(j-\psi,k)X_{amax} \tag{3.59}$$

$$\begin{aligned} S_{NO_2}(j,k+1) - S_{NO_2}(j-\psi,k) =& aTf_{S_1}(j-\psi,k)f_{S_3}(j-\psi,k)X_{amax} \\ & - bTf_{S_2}(j-\psi,k)f_{S_3}(j-\psi,k)X_{amax} \end{aligned} \tag{3.60}$$

$$\begin{aligned} S_C(j,k+1) - S_C(j-\psi,k) =& cTf_{S_1}(j-\psi,k)f_{S_3}(j-\psi,k)X_{amax} \\ & + dTf_{S_2}(j-\psi,k)f_{S_3}(j-\psi,k)X_{amax} \end{aligned} \tag{3.61}$$

for $k \geq 0$ and $0 \leq j \leq N-1$.

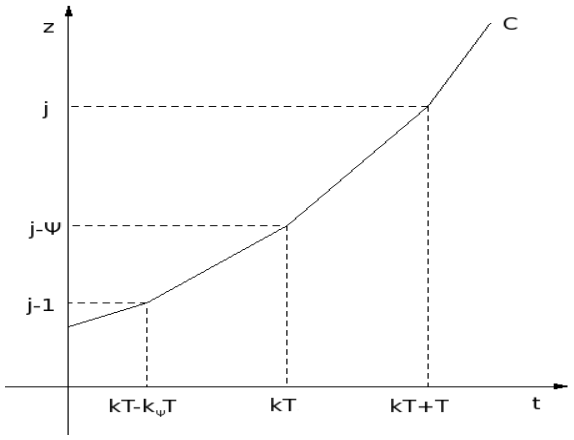

Figure 3-4: Illustration of the characteristic curve.

By linear interpolation [48], S_{NO_3} can be calculated as:

[2]The classical abusive notation $S_{NO_3}(j,k)$ is used instead of $S_{NO_3}(j\Delta z, kT)$ to simplify the equations which follow.

$$S_{NO_3}(z,k) - S_{NO_3}(j,k) = \left(\frac{S_{NO_3}(j-1,k) - S_{NO_3}(j,k)}{(j-1)\Delta z - j\Delta z}\right)(z - z_j) = \frac{(S_{NO_3}(j-1,k) - S_{NO_3}(j,k))(z - z_j)}{-\Delta z} \tag{3.62}$$

If T is sufficiently small, $v(t)$ may be considered to remain constant between kT and $(k+1)T$. A solution to (3.49) for each segment between kT and $(k+1)T$ is then obtained as:

$$z - j\Delta z = \frac{v(k)}{\epsilon}(t - kT - T)$$

If $z = (j - \psi)\Delta z$, then:

$$(j-\psi)\Delta z - j\Delta z = \frac{v(k)}{\epsilon}(kT - kT - T) = -\frac{v(k)}{\epsilon}T$$

Therefore, from (3.62), relation above and by replacing $S_{NO_3}(z,k) = S_{NO_3}(j - \psi, k)$, we have:

$$S_{NO_3}(j-\psi,k) = S_{NO_3}(j,k) + \left(\frac{v(k)T}{\Delta z\epsilon}\right)(S_{NO_3}(j-1,k) - S_{NO_3}(j,k))$$

Let us consider $\gamma(k) = \frac{v(k)T}{\Delta z\epsilon}$. By developing the equation above, it is obtained:

$$S_{NO_3}(j-\psi,k) = \gamma(k)S_{NO_3}(j-1,k) + (1-\gamma(k))S_{NO_3}(j,k) \tag{3.63}$$

In the same way, similar expresions to compute $S_{NO_2}(j-\psi,k)$, $S_C(j-\psi,k)$, $f_{S_1}(j-\psi,k)$, $f_{S_2}(j-\psi,k)$ and $f_{S_3}(j-\psi,k)$ may be obtained.

Let us define the space discretized state variable $x_i \in \mathbb{R}^N$ $(i = 1,2,3)$ as in subsection 3.2.1. By using (3.63) and the others similar expresions into (3.59)-(3.61), it is obtained:

$$
\begin{aligned}
x_1(j,k+1) =& [\gamma(k)x_1(j-1,k) + (1-\gamma(k))x_1(j,k)] \\
& - aT[\gamma(k)f_{S_1}(j-1,k) + (1-\gamma(k))f_{S_1}(j,k)] \\
& [\gamma(k)f_{S_3}(j-1,k) + (1-\gamma(k))f_{S_3}(j,k)]X_{amax}
\end{aligned} \tag{3.64}
$$

$$
\begin{aligned}
x_2(j,k+1) =& [\gamma(k)x_2(j-1,k) + (1-\gamma(k))x_2(j,k)] \\
& + aT[\gamma(k)f_{S_1}(j-1,k) + (1-\gamma(k))f_{S_1}(j,k)] \\
& [\gamma(k)f_{S_3}(j-1,k) + (1-\gamma(k))f_{S_3}(j,k)]X_{amax} \\
& - bT[\gamma(k)f_{S_2}(j-1,k) + (1-\gamma(k))f_{S_2}(j,k)] \\
& [\gamma(k)f_{S_3}(j-1,k) + (1-\gamma(k))f_{S_3}(j,k)]X_{amax}
\end{aligned} \tag{3.65}
$$

$$
\begin{aligned}
x_3(j,k+1) =& [\gamma(k)x_3(j-1,k) + (1-\gamma(k))x_3(j,k)] \\
& + cT[\gamma(k)f_{S_1}(j-1,k) + (1-\gamma(k))f_{S_1}(j,k)] \\
& [\gamma(k)f_{S_3}(j-1,k) + (1-\gamma(k))f_{S_3}(j,k)]X_{amax} \\
& + dT[\gamma(k)f_{S_2}(j-1,k) + (1-\gamma(k))f_{S_2}(j,k)] \\
& [\gamma(k)f_{S_3}(j-1,k) + (1-\gamma(k))f_{S_3}(j,k)]X_{amax}
\end{aligned} \tag{3.66}
$$

for $2 \leq j \leq N$.

Furthermore, by considering boundary conditions, it is obtained:

$$
\begin{aligned}
x_1(1,k+1) =& [\gamma(k)x_{1,in}(k) + (1-\gamma(k))x_1(1,k)] \\
& - aT[\gamma(k)f_{S_1,in}(k) + (1-\gamma(k))f_{S_1}(1,k)] \\
& [\gamma(k)f_{S_3,in}(k) + (1-\gamma(k))f_{S_3}(1,k)][(1-\gamma(k))X_{amax}]
\end{aligned} \tag{3.67}
$$

$$
\begin{aligned}
x_2(1,k+1) =& [\gamma(k)x_{2,in}(k) + (1-\gamma(k))x_2(1,k)] \\
&+ aT[\gamma(k)f_{S_1,in}(k) + (1-\gamma(k))f_{S_1}(1,k)] \\
&[\gamma(k)f_{S_3,in}(k) + (1-\gamma(k))f_{S_3}(1,k)][(1-\gamma(k))X_{amax}] \\
&- bT[\gamma(k)f_{S_2,in}(k) + (1-\gamma(k))f_{S_2}(1,k)] \\
&[\gamma(k)f_{S_3,in}(k) + (1-\gamma(k))f_{S_3}(1,k)][(1-\gamma(k))X_{amax}]
\end{aligned} \tag{3.68}
$$

$$
\begin{aligned}
x_3(1,k+1) =& [\gamma(k)x_{3,in}(k) + (1-\gamma(k))x_3(1,k)] \\
&+ cT[\gamma(k)f_{S_1,in}(k) + (1-\gamma(k))f_{S_1}(1,k)] \\
&[\gamma(k)f_{S_3,in}(k) + (1-\gamma(k))f_{S_3}(1,k)][(1-\gamma(k))X_{amax}] \\
&+ dT[\gamma(k)f_{S_2,in}(k) + (1-\gamma(k))f_{S_2}(1,k)] \\
&[\gamma(k)f_{S_3,in}(k) + (1-\gamma(k))f_{S_3}(1,k)][(1-\gamma(k))X_{amax}]
\end{aligned} \tag{3.69}
$$

Figure 3-5 shows the time evolution of the concentration of nitrate (3-5a), nitrite (3-5b) and ethanol (3-5c), solution to the hyperbolic PDE system describing the biofilter, for $N = 151$ by using the method of characteristics. For greater clarity, the figures show only the solution at the same six positions along the reactor as in section 3.2.1.

When the same hyperbolic PDE biofilter model is considered, the space and time evolution of the system dynamics simulated with the method of characteristics shows, as expected, the same behavior like that one obtained using the method of lines (figure 3-1). Note however that, by using the method of lines an ODE system to integrate is obtained and by using the method of characteristics a difference equation system is obtained. Unfortunately, this method cannot be applied to parabolic PDEs because their form is not suitable for separating them in a new ODE and its characteristic curve.

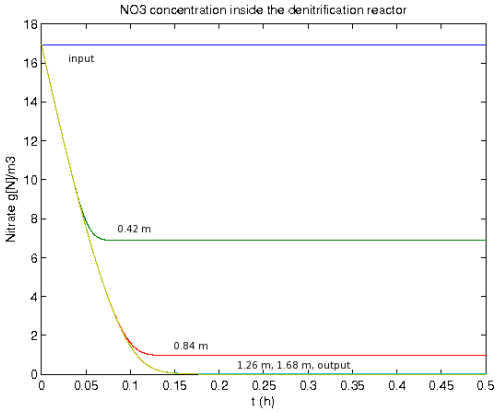

(a) NO_3 solution.

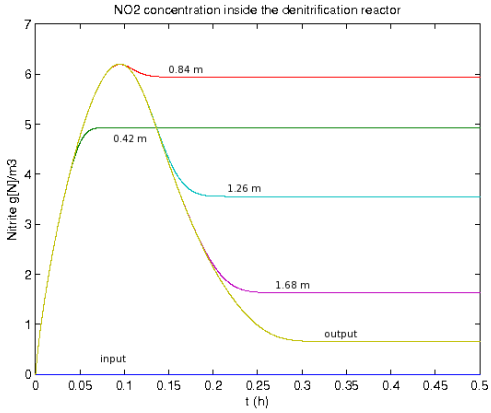

(b) NO_2 solution.

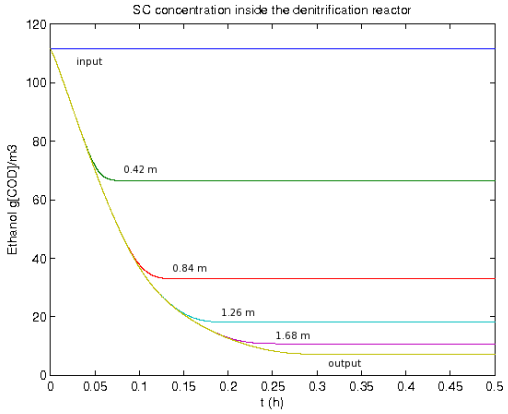

(c) S_C solution.

Figure 3-5: Time and space (at six locations) evolution of the hyperbolic PDE system using MOC.

3.4 Proper orthogonal decomposition method

In many cases, especially in highly nonlinear systems, in order to obtain a good precision of the simulation, the method of lines induces a high order semi-discrete ODE system, which may be unsuitable for future use in control design strategies [85]. Modal decomposition is then a convenient and useful form of analysis for solving PDEs. This form of analysis is however possible only when PDEs have a spatial operator which can be made self-adjoint and which have a real discrete spectrum of eigenvalues [60]. This is generally the case for parabolic PDE systems.

Again, let us consider the vector $S = [S_{NO_3}\ S_{NO_2}\ S_C]^T = [S_1\ S_2\ S_3]^T$. The state variable $S_{\xi i}(\xi, t) : \mathbb{R}^N \times \mathcal{T} \to \mathbb{R}$, where $\mathcal{T}$ being the semiopen time interval $[0, \infty)$, may be expanded in a truncated Fourier series (as in FEM, but now the basis functions will be different), thus:

$$S_{\xi i}(\xi, t) \approx \sum_{j=1}^{N_m} \phi_i^j(\xi) m_i^j(t)\ ;\quad i = 1, 2, 3 \tag{3.70}$$

where $\{\phi_i^j(\xi)\}_{j=1}^{N_m}$ is a set of functions to be determined off-line and $\{m_i^j(t)\}_{j=1}^{N_m}$ is a set of functions to be computed from a reduced order ODE system.

In this section a modal analysis is used in order to transform the PDEs (2.1)-(2.3) into a reduced order ODE system using the proper orthogonal decomposition (POD) method [74], [8]. The method was first proposed both in [38] and in [46] independently, this is why this technique is also called as Karhunen-Loeve (K-L) expansion. It has shown to be efficient in PDE systems with non-homogeneous boundary conditions and convection term [85]. The power of POD method lies in the fact that it creates problem oriented basis funtions, which leads to a very low dimensional representation of the PDE systems with high accuracy [53].

In the POD method, a set of basis functions are computed as those which minimize the distance between a set of measurements of the system (snapshots) and the subspace built with such basis. The solution of this optimization leads to the following

eigenvalue problem [74]:

$$\phi_i(\xi) = \lambda_i \int_{\mathcal{V}} \mathcal{K}_i(\xi, \xi^T)\phi_i(\xi^T)d\xi^T \tag{3.71}$$

where the kernel $\mathcal{K}_i$ is defined, in its discrete version, as:

$$\mathcal{K}_i = \frac{1}{k_f}\sum_{k=1}^{k_f} \mathcal{X}_i(k)\mathcal{X}_i(k)^T \tag{3.72}$$

$\mathcal{X}_i \in \mathbb{R}^N$ are measurements of the original state variable $S_i(z,t)$ at a finite number $N > N_m$ of spatial points and at a specific time t_k [85].

The FEM mass matrix M_{Mi} (defined and used in section 3.2.2) can be also employed for approximating spatial integrals by algebraic operations (see [94] for details). In this way, the eigenproblem (3.71) may be approximated to compute a matrix $\Phi_i = [\phi_i^1\ \phi_i^2\ \dots\ \phi_i^{N_m}] \in \mathbb{R}^{N\times N_m}$ as:

$$\Phi_i = \Lambda_i \mathcal{K}_i M_{Mi} \Phi_i \tag{3.73}$$

with $\mathcal{K}_i$ constructed as in (3.72). The eigenvectors contain the spatial information of the solution (3.70). In order to be able to reconstruct the solution, the modes m_i (time information) have to be computed. To that purpose, the spatially discretized state variable $x_i \in \mathbb{R}^N$, defined as in subsection 3.2.1, are approximated by using Fourier series (3.70), the matrix of eigenvectors Φ_i and the modes m_i as:

$$x_i(t) = \Phi_i(\xi)m_i(t) \tag{3.74}$$

In addition, let us define a spatial projection operator as $P_i = \Phi_i^T M_{Mi}$. Applying this operator to (3.44) and because the set of eigenvectors forms a complete orthonormal basis set [85], the following equation system is obtained:

$$\frac{dm_i(t)}{dt} = -\Phi_i^T(D_f M_{Di} + \frac{v}{\epsilon}(M_{Ti} + M_{Bi}))\Phi_i m_i(t) + P_i\left(\frac{v}{\epsilon}M_{Mi}^{-1}G_i(x_{i,in}) + h_i(x)\right) \tag{3.75}$$

where $m_i = [m_i^1 \ m_i^2 \ \dots \ m_i^{N_m}] \in \mathbb{R}^{N_M}$ are the time dependent modes of x_i, for $i = 1, 2, 3$.

It is important to point out that the number of discretization points N has no significant influence both on the number of modes (N_m) which will be kept after reduction and on their values. Thus, a state space model may be obtained using only a small number N of discretization points and it will allow to build an almost identical modal system as that one (more realistic) which would be obtained by using a higher number of discretization points.

Figure 3-6 shows the modes related to nitrate, nitrite and ethanol, computed for $N = 151$ discretization points by using the proper orthogonal decomposition described above. The first six modes are the most important because the remaining ones evolve so fast to zero that their contribution to the solution may be neglected.

Figure 3-7 shows the time and space (at six location points) of the original parabolic PDEs (2.1)-(2.3) computed by (3.74) using the first six modes $N_m = 6$. As expected, the solution is very similar to that one obtained by using FEM (see figure 3-3). It must be pointed out that the FEM simulation of section 3.2.2 imposed the integration of a $3N = 3 \times 151$ vector field when the POD one only needs the integration of a $3N_m = 3 \times 6$ vector field.

3.5 Conclusion

This chapter was devoted to the simulation of the denitrification reactor. As mentioned in chapter 2, the PDEs describing the reactor may be either parabolic if the diffusion phenomenon is considered or hyperbolic if it is neglected.

From the PDE characteristics, the numerical solution method may be selected. Table 3.1 shows a comparative issue about the different methods used here to simulate the reactor model. As previously mentioned, the method of lines is a very general

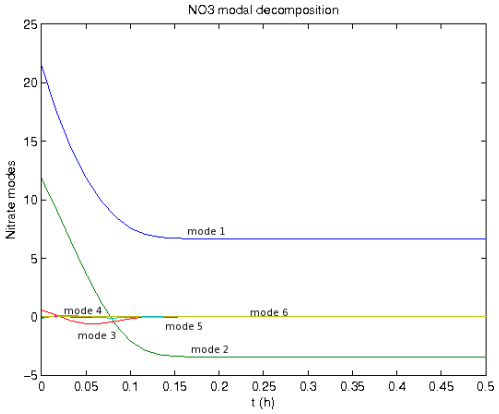

(a) NO_3 modes.

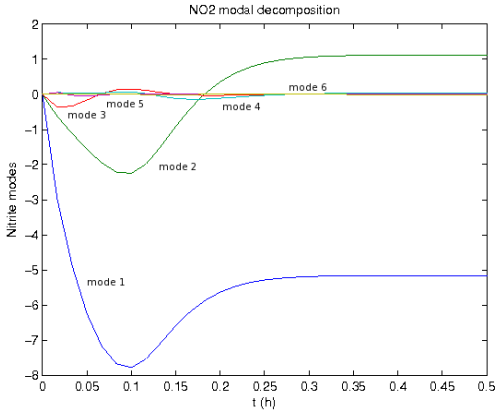

(b) NO_2 modes.

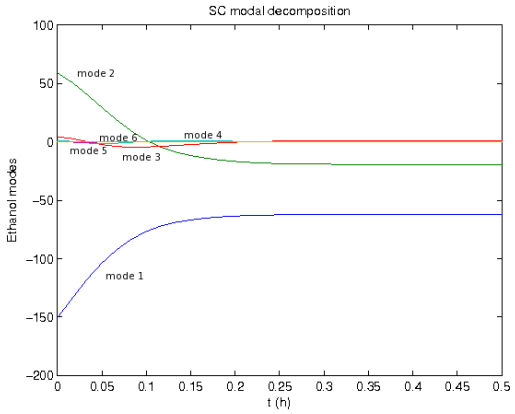

(c) S_C modes.

Figure 3-6: Modes of the parabolic system computed using POD.

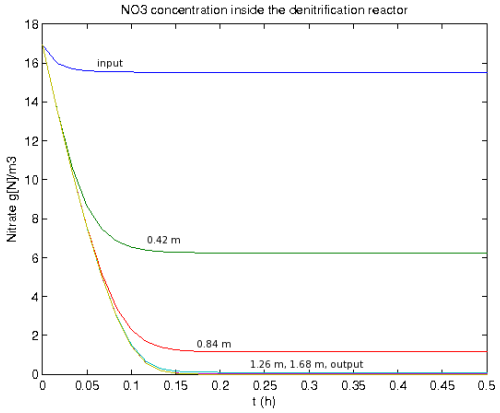

(a) NO_3 solution.

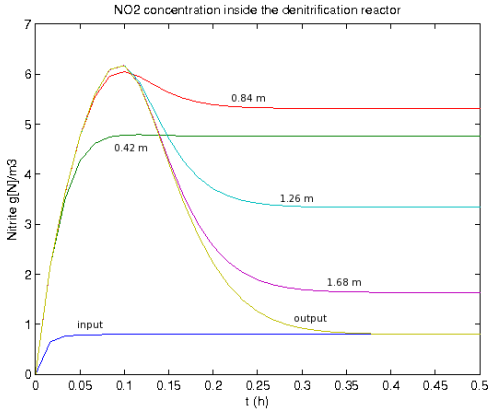

(b) NO_2 solution.

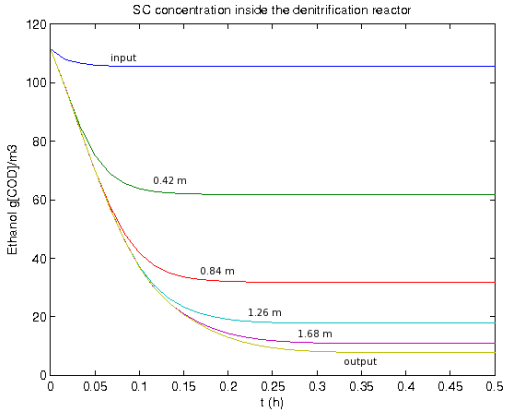

(c) S_C solution.

Figure 3-7: Time and space (at six locations) evolution of the parabolic PDE system using POD.

Method	Parabolic PDEs	Hyperbolic PDEs
Method of lines-FDM	Yes	Yes
Method of lines-FEM	Yes	Yes
Method of characteristics	No	Yes
Proper orthogonal decomposition	Yes	If real eigenvalues

Table 3.1: Comparative table about the methods to numerically solve PDEs.

method to solve PDEs. Indeed, one can discretize the space variable and then, use finite differences or finite elements to approximate the *n-order* spatial derivative terms.

On the other hand, the method of characteristics is a specific approach to solve hyperbolic PDEs because they may be represented by a time-dependent ODE and a *characteristic curve* which determines how the solution of the first ODE changes with respect to the space.

Finally, the proper orthogonal decomposition may be used to simulate the parabolic PDE model because it has a real discrete spectrum of eigenvalues. In this way, the semi-discrete high-order ODE system obtained by the method of lines can be reduced by considering only the most important modes of the system. This pleads for the use of parabolics PDE description of the biofilter (i.e. including diffusion phenomenon) instead of hyperbolic PDE description (which from a mathematical point of view, looks simpler), since a low order description of the system may then be used in future control strategies.

The boundary conditions affect the simulations, since they are not the same for the parabolic and the hyperbolic models. Results are not the same even if the simulation conditions are equal. As expected, in the hyperbolic model simulation, at the input it is observed the value $x_{i,in}$. On the other hand, in the parabolic model, at the input it is observed the solution of the differential equation representing the boundary condition at this position. This condition affects the results along the reactor in both models.

Next chapters will be devoted to the control and estimation of the denitrification reactor. In the next chapter, we will use early lumping approaches to design state feedback controllers and Luenberger observers, both for the hyperbolic and for the

parabolic models. Then, in the last chapter, late lumping control strategies will be investigated.

Chapter 4

Early lumping approach techniques

4.1 Introduction

Following the spatial discretization approaches proposed in the previous chapter to simulate a distributed parameter system, the control problem of the denitrification process can be addressed. As mentioned in the problem statement, we are interested in regulating the nitrate and the nitrite concentrations at the reactor output lower than the european norm. From a biological point of view, it means that the nitrate has to be consumed by the micro-organisms to produce nitrite and then, the nitrite has to be consumed to produce gaseous nitrogen as much as possible, according to a specific micro-organism metabolic path. From a control point of view, it means that the energy of the perturbation at the reactor input $S_{NO_3,in}$ has to be attenuated along the reactor.

The H_2 norm allows to measure the energy of a system [69], [93]. In this context, H_2 control techniques may be chosen as the control strategy to cope with the attenuation problem of the variations of influent nitrate ($S_{NO_3,in}$). The objective in this chapter is therefore to synthesize feedback controllers in order to minimize the energy of the transfer function defined between the perturbation at the reactor input and the measured output. The control problem of the denitrification process has then to be cast as a classical control problem of an ODE system after a preliminary spatial

discretization of the original PDE system. Such control strategies are named early lumping approaches.

In general, once a PDE system is described as a set of ODEs, any control strategy may be applied. In this chapter we are interested with linear control approaches for two main reasons:

- the first reason is that the original system is simplified when described by ODEs. The transformation of the system may be continued through a linearization around an operational steady state, which then allows to access the wide world of linear control, in our case the H_2 control.

- the second reason is yet related to the facility to understand and manipulate linear control strategies. One hidden objective of this thesis is to reinforce the interface between the control community and the process engineering community. Linear control tools are rather standard tools, independent of the original system form and may be described in a unified framework which could be applied to many other classes of biochemical process.

In this chapter, robust observer-based output feedback controllers are synthesized both in their digital and in their continuous time versions by using the separation principle. Those two cases are considered since the class (discrete-time or continuous-time) of the ODE system depends on the spatial discretization approach.

The chapter is organized as follows. First, a preliminary background about H_2 control techniques with main focus on Linear Matrix Inequalities *(LMI)* constraints is presented. Next, a discrete-time form of the control law is employed to control the denitrification process for the case where the hyperbolic PDE system is numerically solved by the method of characteristics. Since we are interested in observer-based output feedback controllers, the separation principle is then stated. The continuous-time form of the control law follows from a modal analysis made over the parabolic PDE system. A discusion about both case studies is provided in the conclusion of the chapter.

4.2 Background on H_2 control and the *LMI* framework

Linear Matrix Inequalities (*LMI*) have been developed as a tool for control analysis and synthesis based on the determination of Lyapunov funtionals. Such *LMIs*, associated with convex optimization algorithms, benefit from powerful numerical tools [50], [27], [76], and friendly interfaces [27], [47]. A brief summary of the concepts used in the sequel for the control of the biofilter are presented in this section.

The use of matrix inequalities to demonstrate certain properties of dynamical systems takes its origin from the initial work on stability by Lyapunov who established the well-known stability method and its direct representation in the linear case. By taking advantages from quadratic Lyapunov stability and stabilization approaches, later followed in the eigthies, with the apparition of associated numerical tools [9], [13], several *LMI*-based optimization problems have been proposed. They deal with additive disturbances [26], [36], parametric uncertainties [30], [51], but also non-linear isolated elements [77], [33] or new classes of pseudo-linear systems (bilinear, hybrid, etc.). The results are generally established for state feedback control, but many extensions have been proposed for output feedback control [25], [54], observer-based output feedback [70], [45], both in continuous-time and in dicrete-time context.

This brief summary only gives a very partial view of the numerous results produced in this research area. In the sequel, we will be concerned with observer-based output feedback control strategies, both for continuous-time and discrete-time systems.

4.2.1 Linear state space representation

Consider the non-linear system of the form:

$$\delta[\chi(\tau)] = F(\chi(\tau), u(\tau), w(\tau)) \; ; \;\; \chi(0) = \chi_0 \tag{4.1}$$

with $\delta[\chi(\tau)] \equiv d\chi(t)/dt$, $\tau \equiv t$, for continuous-time systems, and $\delta[\chi(\tau)] \equiv \chi(k+1)$,

$\tau \equiv k$, for dicrete-time systems. $F(\chi, u, w) \in \mathbb{R}^n$ is a vector of nonlinear functions, $\chi(\tau) \in \mathbb{R}^n$ is a vector of state variables, $u(\tau) \in \mathbb{R}^m$ is a vector of control inputs and $w(\tau) \in \mathbb{R}^q$ is a vector of disturbances.

System (4.1) is classicaly linearized by Taylor series developed around an operating point formed by the vectors $\chi^* \in \mathbb{R}^n$, $u^* \in \mathbb{R}^m$, $w^* \in \mathbb{R}^q$ such that, for the discrete-time case $F(\chi^*, u^*, w^*) = \chi^*$ and, for the continuous-time case $F(\chi^*, u^*, w^*) = 0$ [64].

After linearization, system (4.1) may be rewritten in the classic state space form as:

$$\delta[\bar{\chi}(\tau)] = A\bar{\chi}(\tau) + B_u\bar{u}(\tau) + B_w\bar{w}(\tau)\ ;\ \ \chi(0) = \chi_0 \tag{4.2}$$

where $A \in \mathbb{R}^{n\times n}$ is the Jacobian matrix $J_{F(\chi,u,w)}(\chi)$, $B_u \in \mathbb{R}^{n\times m}$ is the Jacobian matrix $J_{F(\chi,u,w)}(u)$ and $B_w \in \mathbb{R}^{n\times q}$ is the Jacobian matrix $J_{F(\chi,u,w)}(w)$. Furthermore, $\bar{\chi} = \chi - \chi^*$, $\bar{u} = u - u^*$ and $\bar{w} = w - w^*$.

In order to complete the linear state space representation of the system, the controlled output $z(\tau) \in \mathbb{R}^p$ is defined as:

$$z(\tau) = C_z\bar{\chi}(\tau) + D_z\bar{u}(\tau) \tag{4.3}$$

where $C_z \in \mathbb{R}^{p\times n}$ and $D_z \in \mathbb{R}^{p\times m}$. On the other hand, the measured output $\bar{y}(\tau) \in \mathbb{R}^l$ is defined as:

$$\bar{y}(\tau) = C_y\bar{\chi}(\tau) \tag{4.4}$$

where $C_y \in \mathbb{R}^{l\times n}$.

4.2.2 Nominal stability of linear systems

Let us first consider the linear autonomous system:

$$\delta[\bar{\chi}(\tau)] = \mathcal{A}\bar{\chi}(\tau) \tag{4.5}$$

where $\mathcal{A} \in \mathbb{R}^{n\times n}$. We are interested in investigating the stability of (4.5) at the operating point χ^*. The positive definite quadratic function $V : \mathbb{R}^n \to \mathbb{R}$ defined by:

$$V(\bar{\chi}) = \bar{\chi}^T P \bar{\chi} \tag{4.6}$$

for $P = P^T \in \mathbb{R}^{n\times n}$, serves as a quadratic Lyapunov function.

For the continuous-time case, the derivative of $V(\bar{\chi})$ with respect to time, given by:

$$\dot{V}(\bar{\chi}) = \bar{\chi}^T [\mathcal{A}^T P + P\mathcal{A}]\bar{\chi} \tag{4.7}$$

and for the discrete-time case, the difference $V_{k+1}(\chi) - V_k(\chi)$ given by:

$$V_{k+1}(\bar{\chi}) - V_k(\bar{\chi}) = \bar{\chi}^T [\mathcal{A}^T P \mathcal{A} - P]\bar{\chi} \tag{4.8}$$

have to be negative to guarantee that χ^* is an asymptotically stable operating point of (4.5) in the continuous-time and in the discrete-time cases, respectively.

Moreover, if the following *LMIs*:

$$\begin{aligned} P &> 0 \\ \mathcal{A}^T P + P\mathcal{A} &< 0 \end{aligned} \tag{4.9}$$

for the continuous-time case, or:

$$\begin{aligned} P &> 0 \\ \mathcal{A}^T P \mathcal{A} - P &< 0 \end{aligned} \tag{4.10}$$

for the discrete-time case, are feasible, then the operating point χ^* of the nonlinear system (4.1) is locally asymptotically stable [69]. By denoting $W = P^{-1}$, conditions (4.9) and (4.10) are equivalently written as:

$$\begin{aligned} W &> 0 \\ W\mathcal{A}^T + \mathcal{A}W &< 0 \end{aligned} \tag{4.11}$$

for the continuous-time case, and:

$$\begin{aligned} W &> 0 \\ \begin{bmatrix} -W & \mathcal{A}W \\ W\mathcal{A}^T & -W \end{bmatrix} &< 0 \end{aligned} \tag{4.12}$$

for the discrete-time case.

4.2.3 Stability regions for LTI systems

As well known, the autonomous linear system (4.5) is asymptotically stable if and only if all the eigenvalues of $\mathcal{A}$ lie in the open left half complex plane for continuous-time systems and inside the origin centered unit circle in the complex plane for discrete-time systems. However, the system dynamics may be improved, in synthesis problems, by placing the closed-loop poles into specific complex plane regions. In this context, we are also interested in particular stability regions, often defined as $\mathcal{D}$-stable regions [16], [28].

Let us define a stability region as a subset $\mathcal{D} \subseteq \mathbb{C}$ with the following two properties [69]:

- $\lambda \in \mathcal{D} \Longrightarrow \bar{\lambda} \in \mathcal{D}$;
- $\mathcal{D}$ is convex.

In addition to the general stability regions for continuous-time and discrete-time systems described above, we are interested in three particular stability regions and their *LMI* representation described by [16], [28]:

- The vertical strip $\mathcal{D}_1 = \{s \in \mathbb{C} \mid Re(s) < -d\}$, with $d \in \mathbb{R}$, represented by the *LMI*:

$$\mathcal{A}W + W\mathcal{A}^T + 2dW < 0 \tag{4.13}$$

- The disk centered at origin $\mathcal{D}_2 = \{s \in \mathbb{C} \mid |s| < r\}$, with $r \in \mathbb{R}$, represented by the *LMI*:

$$\begin{bmatrix} -rW & \mathcal{A}W \\ W\mathcal{A}^T & -rW \end{bmatrix} < 0 \tag{4.14}$$

- The intersection between the vertical strip and the disk centered at origin $\mathcal{D}_3 = \mathcal{D}_1 \cap \mathcal{D}_2$ shown in figure 4-1.

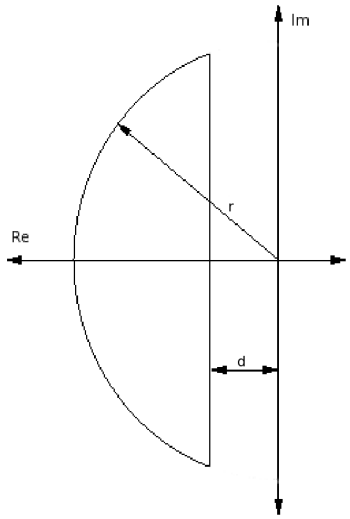

Figure 4-1: Stability region $\mathcal{D}_3$

4.2.4 H_2 nominal performance

Let us now consider the system:

$$\begin{aligned} \delta[\bar{\chi}(\tau)] &= \mathcal{A}\bar{\chi}(\tau) + B_w\bar{w}(\tau) \\ \zeta &= \mathcal{C}_\zeta\bar{\chi}(\tau) \end{aligned} \tag{4.15}$$

where $\zeta \in \mathbb{R}^{n_\zeta}$ and $C_\zeta \in \mathbb{R}^{n_\zeta \times n}$. In addition, its transfer function is defined as $T(\varsigma) = \mathcal{C}_\zeta(I\varsigma - \mathcal{A})^{-1}B_w$, with $\varsigma \equiv s$ for the continuous-time case and $\varsigma \equiv z$ for the discrete-time case. We wish to minimize the effect of the disturbance w on the error indicator ζ. To do this, we consider the H_2 norm of $T(\varsigma)$, which allows indeed

to compute the total 'output energy' in the impulse response of the system denoted $||T(\varsigma)||_2$.

Proposition 1 *[69] Suppose that the system (4.1) is asymptotically stable in* χ^* *and let* $T(\varsigma) = \mathcal{C}_\zeta(I\varsigma - \mathcal{A})^{-1}B_w$ *denote its transfer function, then the following statements are equivalent:*

- $||T(\varsigma)||_2 < \rho$, *with* $\rho \in \mathbb{R}$.
- *There exists* $W > 0$ *such that* $trace(\mathcal{C}_\zeta W \mathcal{C}_\zeta^T) < \rho^2$ *and the following LMI:*

$$\mathcal{A}W + W\mathcal{A}^T + B_w B_w^T < 0 \tag{4.16}$$

for the continuous-time case, or:

$$\begin{bmatrix} -W & \mathcal{A}W \\ W\mathcal{A}^T & -W + B_w B_w^T \end{bmatrix} < 0 \tag{4.17}$$

for the discrete-time case, is feasible.

4.3 Digital observer-based output feedback linear control

In this section, an observer-based dynamic output feedback controller for the denitrification reactor described by an hyperbolic PDE system is synthesized. First, a state feedback control law is designed. Following, both a full-order observer and a reduced-order observer are designed. Finally, by using the separation principle, the state feedback controller is complemented with any of the observers. Different results about the topics developed are presented in each subsection. The results presented in this section were published in [79] and [80].

In chapter 3 the method of characteristics was used to solve the hyperbolic PDE

system. The resulting equation system (3.64)-(3.66) represents a nonlinear state space system of the form:

$$x(k+1) = F_\xi(x(k), \bar{u}(k), \bar{w}(k)) \; ; \;\; x(0) = x_0 \tag{4.18}$$

where $F_\xi \in \mathbb{R}^{3N}$ is a vector of nonlinear functions constructed as:

$$F_\xi(x(k), \bar{u}(k), \bar{w}(k)) = \left[f_{\xi 1}^1 \; f_{\xi 2}^1 \; f_{\xi 3}^1 \; \ldots \; f_{\xi 1}^N \; f_{\xi 2}^N \; f_{\xi 3}^N \; \right]^T$$

$x \in \mathbb{R}^{3N}$ is the vector of state variables constructed as:

$$x = \left[x_1^1 \; x_2^1 \; x_3^1 \; \ldots \; x_1^N \; x_2^N \; x_3^N \; \right]^T$$

$u \in \mathbb{R}^m$ is the vector of control inputs and $w \in \mathbb{R}^q$ is the vector of external disturbances. After linearization around the operating point (x^*, u^*, w^*), (4.18) may be rewritten in the classic state space form as:

$$\bar{x}(k+1) = A\bar{x}(k) + B_u\bar{u}(k) + B_w\bar{w}(k) \tag{4.19}$$

In all the numerical applications provided in this section, the linear state space model (4.19) is built with eleven discretization points ($N = 11$). It means that one considers only a rough description of the original model to apply control and observation strategies.

The control objective is to maintain the nitrogen concentration (nitrate + nitrite) at the reactor output around a constraint lower than the European norm ($5.65g[N]/m^3$) while limiting as much as possible the activity of the controlled input. In this study, the flow rate $v(k) = F(k)/A$ is considered as the controlled input. It means $\bar{u}(k) = v(k)$ around a nominal regime determined by $v = 4m/h$ with $m = 1$.

Remark 6 *The controlled input could be either the flow rate v or the ethanol concentration at the reactor input $S_{C,in}$ [11]. The fundamental difference between these two potential control inputs is that $S_{C,in}$ is present in the system through the boundary*

condition only. However, as soon as an early lumping approach is addressed, this does not change the definition of the control problem, but only the elements involved in the matrix B_u.

On the other hand, the nitrate concentration at the reactor input $S_{NO_3,in}$ is considered as a disturbance, it means $\bar{w}(k) = S_{NO_3,in}(k)$ which values may vary between $14.93g[N]/m^3$ and $18.93g[N]/m^3$ around a nominal regime determined by $S_{NO_3,in} = 16.93g[N]/m^3$ with $q = 1$.

4.3.1 Digital state feedback H_2 controller

The linear state space equation (4.19) is complemented by a controlled output equation of the form (4.3), to obtain the system:

$$\begin{aligned} \bar{x}(k+1) &= A\bar{x}(k) + B_u\bar{u}(k) + B_w\bar{w}(k) \\ z(k) &= C_z\bar{x}(k) + D_z\bar{u}(k) \end{aligned} \tag{4.20}$$

According to the control objective related to the nitrogen concentration at the reactor output, C_z is defined as:

$$C_z = [0 \ \ldots \ 0 \ 1 \ 1 \ 0]$$

and therefore, $p = 1$.

On the other hand, D_z is used as a degree of freedom to calibrate the compromise between the energy of the permissible control and the quality of the regulation. The idea behind the choice of D_z is to take it as small as possible to reach a good closed-loop performance, but large enough to avoid saturation problems which could be expected if the energy of the controlled output is not limited. In this section, a preliminary choice is $D_z = 0.15$.

A feedback control law $\bar{u}(k) = K\bar{x}(k)$ is then proposed to decrease the influence of the disturbance w on the controlled output z. By replacing it in (4.20), the following system is obtained:

$$\begin{aligned} \bar{x}(k+1) &= (A + B_u K)\bar{x}(k) + B_w \bar{w}(k) \\ z(k) &= (C_z + D_z K)\bar{x}(k) \end{aligned} \tag{4.21}$$

The transfer function of the closed loop system (4.21) from w to z is given by:

$$T_{wz} = \frac{Z(z)}{W(z)} = (C_z + D_z K)(zI - (A + B_u K))^{-1} B_w \tag{4.22}$$

Proposition 1 with (4.17) is then used to state the following convex optimal H_2 problem to compute a static feedback controller $K \in \mathbb{R}^{m \times 3N}$ for stabilizing the closed-loop dynamics:

$$\begin{aligned} &\min_{W_1, W_2, W_3} trace(W_3) \\ &under \\ &W_1 > 0 \\ &\begin{bmatrix} -W_1 & AW_1 + B_u W_2 \\ W_1 A^T + W_2^T B_u^T & -W_1 + B_w B_w^T \end{bmatrix} \leq 0 \\ &\begin{bmatrix} W_1 & W_1 C_z^T + W_2^T D_z^T \\ C_z W_1 + D_z W_2 & W_3 \end{bmatrix} \geq 0 \end{aligned} \tag{4.23}$$

where $W_1 \in \mathbb{R}^{3N \times 3N}$, $W_2 \in \mathbb{R}^{m \times 3N}$ and $W_3 \in \mathbb{R}^{p \times p}$. The controller gain, solution of the optimization problem (4.23), may then be calculated as $K = W_2 W_1^{-1}$ and $\|T_{wz}\|_2 = trace(W_3)$ [6], [69].

In order to simulate the closed-loop system, the PDEs are solved yet by the method of characteristics using 151 discretization points. The flow rate $v(k) = K\bar{x}(k)$ is then computed at each sampling instant considering the values of the state vector x at the space locations corresponding to the $N = 11$ discretization points used for the control synthesis.

Figure 4-2b shows the open-loop response of the system according to the disturbance input $\bar{w}(k)$ evolution shown in figure 4-2a. A composed sine signal to simulate nitrate inlet variations has been used. It was above mentioned that the control ob-

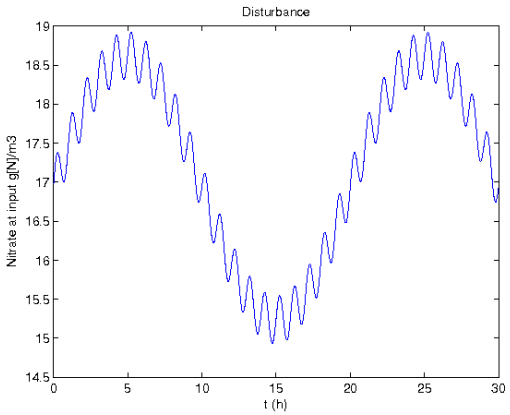

(a) Time-evolution of $S_{NO_3,in}(t)$.

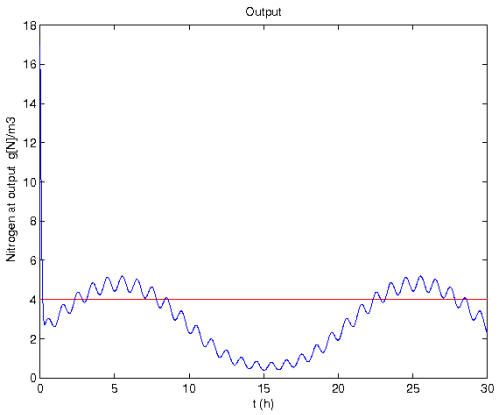

(b) Time-evolution of the nitrogen concentration at the output of the biofilter. In red the output reference and in blue the real nitrogen concentration.

Figure 4-2: Open-loop time-evolution of the system.

jective is to maintain the nitrogen concentration at reactor output below than the European norm. However, it is suggested here as the objective to remain below $4mg[N]/m^3$. It is clear that the nitrogen concentration at the reactor output in open-loop does not remain below the allowable limit.

After solving the optimization problem (4.23) using the YALMIP matlab interface with the SDPA solver [47], a gain $K \in \mathbb{R}^{1\times 3N}$ was computed. The system was then simulated in closed-loop. The state feedback control strategy intends to maintain the state of the nonlinear system close to its nominal state, which implicitly corresponds to maintain the output of the system below $4mg[N]/m^3$. Figures 4-3a and 4-3b respectively show the time evolution of the nitrogen concentration at the output of the biofilter and the time evolution of the flow rate. It can be seen that the constraint is well respected. However, when the disturbance is maximal, the control input $\bar{u}(k)$ comes near to zero and the nitrogen concentration at the reactor output is not well regulated around a constant value. A higher control gain would perhaps improve this performance, but to the detriment of input saturation, which, being not considered in the control problem, should preferably be avoided.

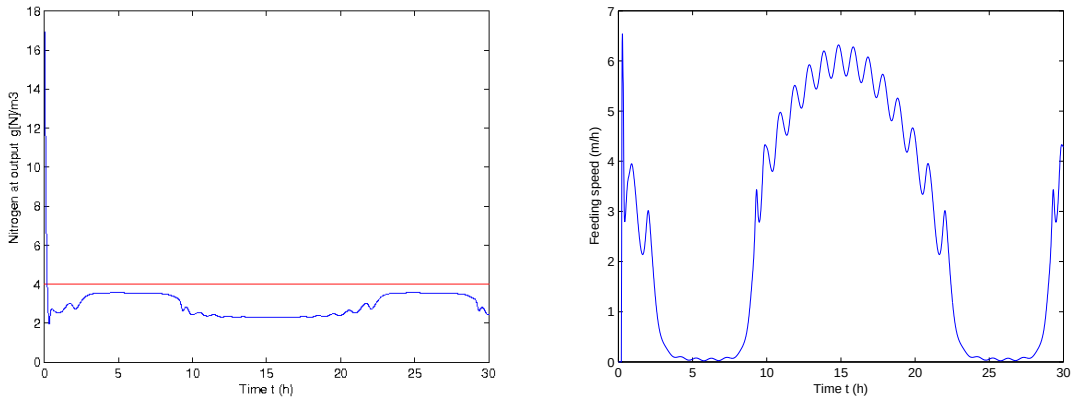

(a) Time-evolution of the nitrogen concentration at the biofilter output. In red the output reference and in blue the real nitrogen concentration.

(b) Time-evolution of the flow rate.

Figure 4-3: Closed-loop time-evolution by considering the state feedback controller.

4.3.2 Digital H_2 full-order observer

In real applications, unfortunately, the overall set of states is not available, especially in biotechnological applications where the sensors would have to be distributed at several locations of the biofilter. Therefore, unless output feedback strategies are investigated, the state vector has to be estimated.

By using the linear representation (4.19) of the denitrification reactor, let the linear Luenberger observer be defined as:

$$\hat{x}(k+1) = A\hat{x}(k) + B_u\bar{u}(k) + \Gamma(\bar{y}(k) - \hat{y}(k)) \tag{4.24}$$

where $\hat{x} \in \mathbb{R}^{3N}$ is the vector of estimated state variables constructed as:

$$\hat{x} = \left[\hat{x}_1^1\ \hat{x}_2^1\ \hat{x}_3^1\ \ldots\ \hat{x}_1^N\ \hat{x}_2^N\ \hat{x}_3^N\ \right]^T$$

$u \in \mathbb{R}^m$ is the vector of control inputs, $y \in \mathbb{R}^l$ is the vector of measured outputs defined in its discrete version as:

$$\bar{y}(k) = C_y\bar{x}(k) \tag{4.25}$$

and the estimated measured output $\hat{y} \in \mathbb{R}^l$ defined as:

$$\hat{y}(k) = C_y \hat{x}(k) \tag{4.26}$$

By replacing (4.25) and (4.26) in (4.24) the estimated state vector may be calculated by [5]:

$$\hat{x}(k+1) = (A - \Gamma C_y)\hat{x}(k) + B_u \bar{u}(k) + \Gamma C_y \bar{x}(k) \tag{4.27}$$

Let $e = \bar{x} - \hat{x}$ be the error between the real state vector and the estimated state vector, then from (4.20) and (4.27):

$$e(k+1) = \bar{x}(k+1) - \hat{x}(k+1) = (A - \Gamma C_y)e(k) + B_w \bar{w}(k) \tag{4.28}$$

The transfer function from w to e is given by:

$$T_{we} = \frac{E(z)}{W(z)} = (zI - (A - \Gamma C_y))^{-1} B_w \tag{4.29}$$

An observer gain Γ with the objective to decrease the influence of the disturbance w on the estimation error e is then searched. In addition, we can accelerate its dynamics by placing the poles of the observer into a stability region defined by a disk, smaller than the unit circle, centered at origin. Proposition 1 with (4.17), and (4.14) are then used to state the following convex optimal H_2 problem for the observation problem, dual of the control problem, to compute the gain Γ:

$$
\begin{aligned}
&\min_{W_1,W_2,W_3} trace(W_3) \\
&under \\
&\begin{bmatrix} -W_1 & A^TW_1 - C_y^TW_2^T & 0 \\ W_1A - W_2C_y & -W_1 & W_1B_w \\ 0 & B_w^TW_1 & -I \end{bmatrix} \leq 0 \\
&\begin{bmatrix} -rW_1 & W_1A - W_2C_y \\ A^TW_1 - C_y^TW_2^T & -rW_1 \end{bmatrix} \leq 0 \\
&\begin{bmatrix} W_1 & I \\ I & W_3 \end{bmatrix} \geq 0
\end{aligned}
\tag{4.30}
$$

where r is the radius of the disk, $W_1 \in \mathbb{R}^{3N\times 3N}$, $W_2 \in \mathbb{R}^{3N\times l}$ and $W_3 \in \mathbb{R}^{3N\times 3N}$. The observer gain, solution of the optimal solution of (4.30), can be calculated as $\Gamma = W_1^{-1}W_2$ and $\|T_{we}\|_2 = trace(W_3)$ [16], [69].

To solve the optimization problem (4.30), the matrix C_y is constructed according to the observability test described in appendix B. Considering that only nitrate and nitrite concentrations are accesible to measurements, an observability test has shown that at least six measurement points have to be considered for those two variables to achieve complete observability of the state vector (of dimension $3N$). The pole placement constraint is a disk of radius $r = 0.8$ centered at the origin. Using the YALMIP matlab interface with the SEDUMI solver [47], a gain Γ was computed. Figure 4-4 shows the nitrate, the nitrite and the ethanol estimations. Only five locations between the eleven locations used to built the linear state space model are plotted to increase the readability of the figure. These locations are those ones where the variables were not measured. In blue the true values and in black the estimated ones. The real values of the original state variables are obtained by simulating the hyperbolic PDE system using the method of characteristics with $\bar{u}(k) = u^*$ and $\bar{w}(k)$ as shown in figure 4-2a. Noise level upon 2% on the measured output $y(k)$ was correctly filtered.

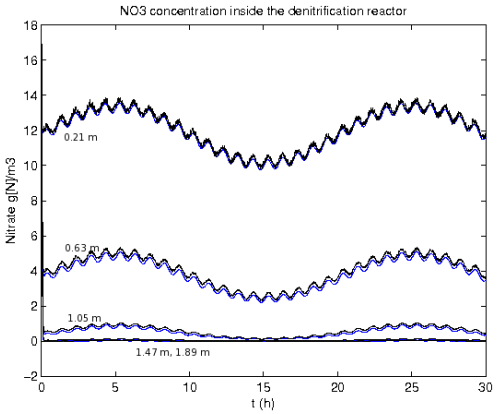

(a) NO_3 estimated.

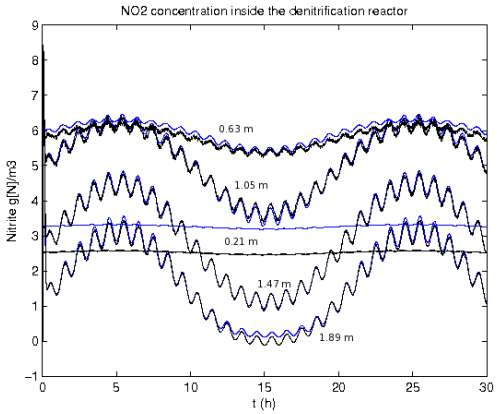

(b) NO_2 estimated.

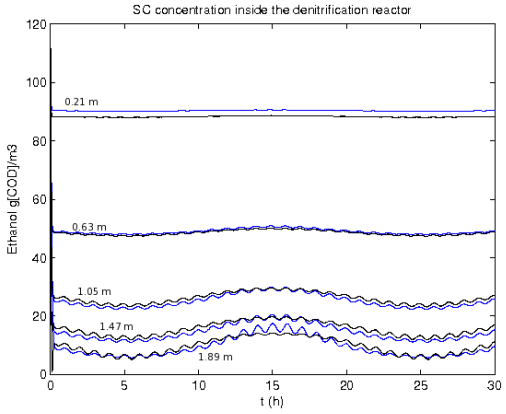

(c) S_C estimated.

Figure 4-4: State variables estimated by considering the full-order observer. In blue the simulated states and in black the estimated ones. Only five locations among the eleven locations used to built the linear state space model are plotted to increase the readability of the figure. These locations are those ones where the variables were not measured.

As shown in the figure 4-4, nitrate and nitrite are correctly estimated almost in all measurement points, however, as closer to the biofilter input, they are more sensitive to noise. On the other hand, ethanol is correctly estimated and is less sensitive to noise. In addition, it can be seen that the observer rejects appropriately the disturbance by following the state variables measurements.

4.3.3 Digital H_2 reduced-order observer

Because some states are measured, the size of the observation problem may be reduced. Therefore, only a subset of the system states of dimension $\nu = 3N - l$ is to be estimated. The strategy presented in the sequel is issued from [5].

In order to design a reduced-order observer, the part of the state vector that is available by direct measurements is used. First, the state vector is separated in a first part which is measured (x'_1) and a second part which is not measured (x'_2). One considers then, a new matrix $C'_y = [I_l \; 0_\nu]$.

Let R be defined as:

$$R = \begin{bmatrix} C_y \\ \hat{C}_y \end{bmatrix}$$

where $\hat{C}_y$ is such that R is nonsingular. Then, $\bar{y}(k) = C_y R^{-1} R\bar{x}(k)$. Therefore, the measured output (4.4) may be re-defined as:

$$\bar{y}(k) = C'_y \bar{x}'(k) \tag{4.31}$$

where $C'_y = C_y R^{-1} = [I_l \; 0_\nu]$ and $\bar{x}'(k) = R\bar{x}(k)$.

In the same way, from (4.20):

$$R\bar{x}(k+1) = RAR^{-1}R\bar{x}(k) + RB_u\bar{u}(k) + RB_w\bar{w}(k)$$

Equation above may be rewritten as:

$$\bar{x}'(k+1) = A'\bar{x}'(k) + B'_u\bar{u}(k) + B'_w\bar{w}(k) \tag{4.32}$$

where $A' = RAR^{-1}$, $B'_u = RB_u$ and $B'_w = RB_w$.

Equations (4.31) and (4.32) form a new system used to design a *ν-order* observer [5].

The new system can be divided in two parts:

$$\begin{bmatrix} \bar{x}'_1(k+1) \\ \bar{x}'_2(k+1) \end{bmatrix} = \begin{bmatrix} A'_{11} & A'_{12} \\ A'_{21} & A'_{22} \end{bmatrix} \begin{bmatrix} \bar{x}'_1(k) \\ \bar{x}'_2(k) \end{bmatrix} + \begin{bmatrix} B'_{u_1} \\ B'_{u_2} \end{bmatrix} \bar{u}(k) + \begin{bmatrix} B'_{w_1} \\ B'_{w_2} \end{bmatrix} \bar{w}(k)$$

$$\bar{y}(k) = \begin{bmatrix} I_l & 0_\nu \end{bmatrix} \begin{bmatrix} \bar{x}'_1(k) \\ \bar{x}'_2(k) \end{bmatrix}$$

It is easy to see that $\bar{y}(k) = \bar{x}'_1(k) \in \mathbb{R}^l$ represents the l measured states. It means that the first part may be obtained directly. Then, only $\bar{x}'_2 \in \mathbb{R}^\nu$ is to be estimated. Therefore, the part of the state vector to be estimated is now given by:

$$\bar{x}'_2(k+1) = A'_{21}\bar{x}'_1(k) + A'_{22}\bar{x}'_2(k) + B'_{u_2}\bar{u}(k) + B'_{w_2}\bar{w}(k)$$

$$\bar{x}'_2(k+1) = A'_{22}\bar{x}'_2(k) + \begin{bmatrix} A'_{21} & B'_{u_2} \end{bmatrix} \begin{bmatrix} \bar{x}'_1(k) \\ \bar{u}(k) \end{bmatrix} + B'_{w_2}\bar{w}(k)$$

Equation above can be rewritten as:

$$\bar{x}'_2(k+1) = A'_{22}\bar{x}'_2(k) + \tilde{B}_u\tilde{u}(k) + B'_{w_2}\bar{w}(k) \tag{4.33}$$

where:

$$\tilde{B}_u = \begin{bmatrix} A'_{21} & B'_{u_2} \end{bmatrix}$$

$$\tilde{u}(k) = \begin{bmatrix} \bar{x}'_1(k) \\ \bar{u}(k) \end{bmatrix} = \begin{bmatrix} \bar{y}(k) \\ \bar{u}(k) \end{bmatrix}$$

Furthermore, it is defined:

$$\tilde{y}(k) = \bar{x}'_1(k+1) - A'_{11}\bar{x}'_1(k) - B'_{u_1}\bar{u}(k) = A'_{12}\bar{x}'_2(k) + B'_{w_1}\bar{w}(k)$$

$\tilde{y}$ is calculated as:

$$\tilde{y}(k) = \bar{y}(k+1) - A'_{11}\bar{y}(k) - B'_{u_1}\bar{u}(k) \tag{4.34}$$

It can be observed that $\tilde{y}$ is known since it depends on the controlled input $\bar{u}$ and measured output $\bar{y}$ only.

An observer for $\bar{x}'_2$ can now be constructed in the form:

$$\hat{x}'_2(k+1) = A'_{22}\hat{x}'_2(k) + \tilde{B}_u\tilde{u}(k) + \tilde{\Gamma}(\tilde{y}(k) - \hat{\tilde{y}}(k)) \tag{4.35}$$

with estimated output:

$$\hat{\tilde{y}}(k) = A'_{12}\hat{x}'_2(k) + B'_{w_1}\bar{w}(k) \tag{4.36}$$

Let $e = x'_2 - \hat{x}'_2$ be the error between the real state vector and the estimated state vector. From (4.33), (4.35) and (4.36), it is obtained:

$$e(k+1) = (A'_{22} - \tilde{\Gamma}A'_{12})e(k) + B'_{w_2}\bar{w}(k) \tag{4.37}$$

The transfer function from w to e is given by:

$$T_{we} = \frac{E(z)}{W(z)} = (zI - (A'_{22} - \tilde{\Gamma}A'_{12}))^{-1}B'_{w_2} \tag{4.38}$$

An observer gain $\tilde{\Gamma}$ to decrease the influence of the disturbance w on the estimation error e is then searched. In addition, we can accelerate its dynamics by placing the poles of the observer into a stability region defined by a disk, smaller than the unit circle, centered at origin. Proposition 1 with (4.17), and (4.14) are then used to state the following convex optimal H_2 problem to compute the gain $\tilde{\Gamma}$:

$$\begin{aligned}
&\min_{W_1,W_2,W_3} trace(W_3) \\
&under \\
&\begin{bmatrix} -W_1 & {A'_{22}}^T W_1 - {A'_{12}}^T W_2^T & 0 \\ W_1 A'_{22} - W_2 A'_{12} & -W_1 & W_1 B'_{w2} \\ 0 & {B'_{w2}}^T W_1 & -I \end{bmatrix} \leq 0 \\
&\begin{bmatrix} -rW_1 & W_1 A'_{22} - W_2 A'_{12} \\ {A'_{22}}^T W_1 - {A'_{12}}^T W_2^T & -rW_1 \end{bmatrix} \leq 0 \\
&\begin{bmatrix} W_1 & I \\ I & W_3 \end{bmatrix} \geq 0
\end{aligned} \tag{4.39}$$

where r is the radius of the origin centered disk, $W_1 \in \mathbb{R}^{\nu\times\nu}$, $W_2 \in \mathbb{R}^{\nu\times l}$ and $W_3 \in \mathbb{R}^{\nu\times\nu}$. The observer gain, solution of the optimization problem (4.39), can be then calculated as $\tilde{\Gamma} = W_1^{-1}W_2$ and $\|T_{we}\|_2 = trace(W_3)$ [16], [69].

In order to build and simulate the reduced-order observer, the same conditions like in the complete-order observer implementation are used. In addition, the matrix $\hat{C}_y$ is defined such that matrix R is a square matrix of dimension $3N \times 3N$ and is non-singular.

Figure 4-5 shows the nitrate, the nitrite and the ethanol estimations. In blue the true values and in black the estimated ones. The position of the state variables estimated are those ones that are not directly measured. As before, nitrate and nitrite

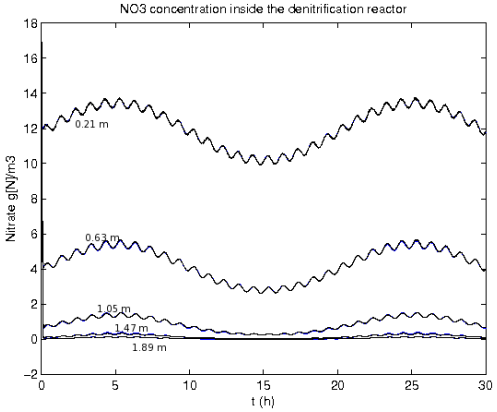

(a) NO_3 estimated.

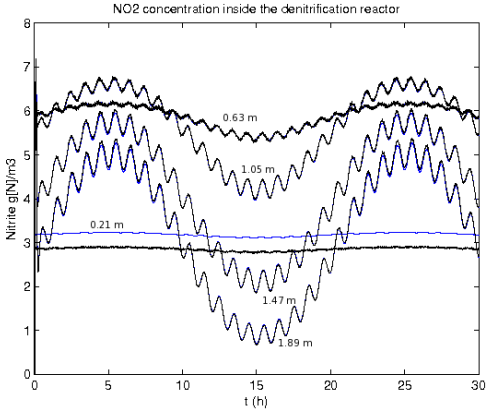

(b) NO_2 estimated.

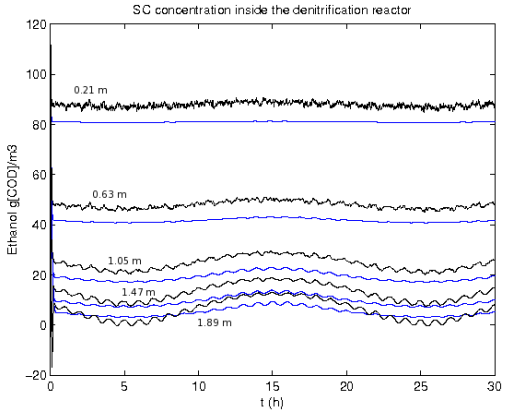

(c) S_C estimated.

Figure 4-5: State variables estimated by considering the reduced-order observer. In blue the simulated states and in black the estimated ones. The concentrations are plotted only at five locations. They correspond to the locations where nothing was measured.

are correctly estimated almost in all measurement points, however, as closer to the biofilter input, they are more sensitive to noise. On the other hand, ethanol estimation is more sensitive to noise and in this case, the estimation is poor. Therefore, we have reduced the order of the observer but its filter properties have been degraded by using real measurements. Again, noise level upon 2% on the measured output $y(k)$ was correctly filtered.

4.3.4 Digital observer-based output feedback H_2 controller

In section 4.3.1 a linear state feedback control law was synthesized. It was implicitly assumed that the state vector $\bar{x}(k)$ is available for measurement. The values of the states $\bar{x}(k)$ for $k > 0$ were fed back and used to generate a control input according to the relation $\bar{u}(k) = K\bar{x}(k)$. In the denitrification process, however, it is not practical to measure the nitrate, the nitrite and the ethanol along the reactor. This has provided the motivation to estimate the overall set of state variables by measuring only a subset of them. In this way, the state feedback controller may be complemented by a Luenberger state observer. A natural topic is therefore to investigate the resulting closed-loop system performance.

The hyperbolic PDE original system is compensated by state feedback using the control law:

$$\bar{u}(k) = K\hat{x}(k) \tag{4.40}$$

where $\hat{x}(k)$ is the output of the Luenberger observer:

$$\hat{x}(k+1) = (A + B_u K - \Gamma C_y)\hat{x}(k) + \Gamma\bar{y}(k) \tag{4.41}$$

We wish to analyze the behavior of the compensated system. By replacing (4.40) in (4.20) and (4.24), we obtain:

$$\bar{x}(k+1) = A\bar{x}(k) + B_u K\hat{x}(k) + B_w\bar{w}(k)$$

and

$$\hat{x}(k+1) = \Gamma C_y \bar{x}(k) + (A - \Gamma C_y + B_u K)\hat{x}(k)$$

By rewriting the two expressions above in matrix form:

$$\begin{bmatrix} \bar{x}(k+1) \\ \hat{x}(k+1) \end{bmatrix} = \begin{bmatrix} A & B_u K \\ \Gamma C_y & A - \Gamma C_y + B_u K \end{bmatrix} \begin{bmatrix} \bar{x}(k) \\ \hat{x}(k) \end{bmatrix} + \begin{bmatrix} B_w \\ 0 \end{bmatrix} \bar{w}(k) \tag{4.42}$$

a representation of the compensated closed-loop system is obtained. Its properties are more easily studied if an appropriate similarity transformation is used to simplify the representation, given by:

$$\begin{bmatrix} I & 0 \\ I & -I \end{bmatrix} \begin{bmatrix} \bar{x}(k) \\ \hat{x}(k) \end{bmatrix} = \begin{bmatrix} \bar{x}(k) \\ e(k) \end{bmatrix} \tag{4.43}$$

with the estimation error $e(k) = \bar{x}(k) - \hat{x}(k)$. Then, the equivalent representation is:

$$\begin{bmatrix} \bar{x}(k+1) \\ e(k+1) \end{bmatrix} = \begin{bmatrix} A + B_u K & -B_u K \\ 0 & A - \Gamma C_y \end{bmatrix} \begin{bmatrix} \bar{x}(k) \\ e(k) \end{bmatrix} + \begin{bmatrix} B_w \\ B_w \end{bmatrix} \bar{w}(k) \tag{4.44}$$

The closed-loop eigenvalues are the roots of the polynomial:

$$|zI - (A + B_u K)||zI - (A - \Gamma C_y)|$$

Recall that the roots of $|zI - (A + B_u K)|$ are the eigenvalues of $A + B_u K$ and the roots of $|zI - (A - \Gamma C_y)|$ are the eigenvalues of $A - \Gamma C_y$. Furthermore, proposition 1 guarantees that the eigenvalues of both $A + B_u K$ and $A - \Gamma C_y$ are inside the unit disk centered at origin (the stability region). The above discussion points out that the design of the control law (4.40) can be carried out independently of the design of the Luenberger observer (4.41). This is referred to as the *Separation Property*. Note however that, for more complex systems, like uncertain ones, this is generally not

true [5].

The overall control law is, therefore, the aggregation of the state feedback control (4.40) with the state observer (4.41).

As in section 4.3.1, it is necessary to define a matrix D_z to adjust the compromise between the energy allowed for the controlled input and the performance requested on the controlled output. In order to obtain the best performance of the connected state feedback controller - Luenberger observer, both dynamics are separated as much as possible without degrading closed-loop stability. The control action on the output controlled is therefore increased to $D_z = 0.35$. On the other hand, the poles of the full-order observer are placed into a smaller disk with radius $r = 0.7$. Noise level upon 2% on the measured output $y(k)$ was correctly filtered.

After solving the optimization problems (4.23) and (4.30), using the YALMIP matlab interface and the SEDUMI solver [47], gains K and Γ were computed respectively. The system was then simulated in closed-loop. Figure 4-6a shows the output response to the controlled input shown in figure 4-6b. It can be observed that the constraint imposed is well respected. However, since the states are now estimated, the state vector used to compute the flow rate is not the true one, therefore, the output performance is slightly degraded with respect to that one shown in section 4.3.1.

Figure 4-7 shows the open-loop poles in red, the poles of $A + B_u K$ in blue and the poles of $A - \Gamma C_y$ in green. As expected all of them are inside the stability region. In addition, the poles of the observer, correctly placed into the $\mathcal{D}_2$-stability region for $r = 0.7$, are faster than those ones of the state feedback.

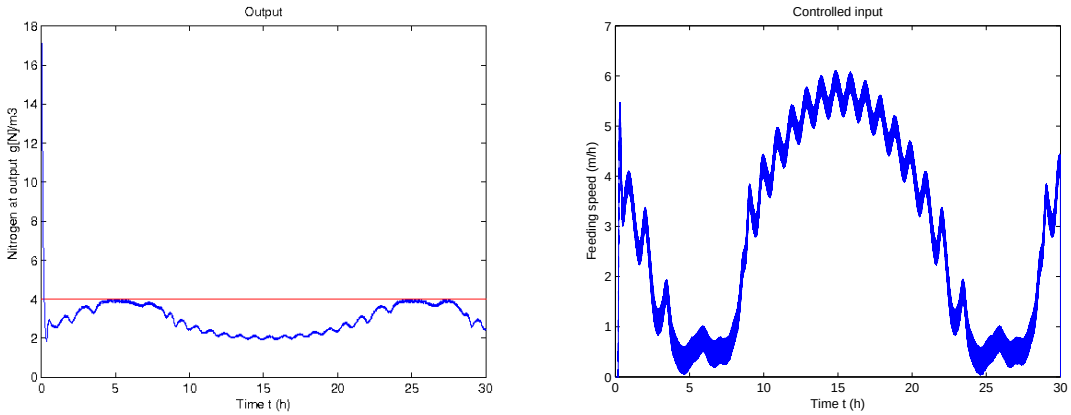

(a) Time-evolution of the nitrogen concentration at the biofilter output. In red the output reference and in blue the real nitrogen concentration.

(b) Time-evolution of the flow rate.

Figure 4-6: Closed-loop time-evolution by considering the full-order observer-based output feedback controller.

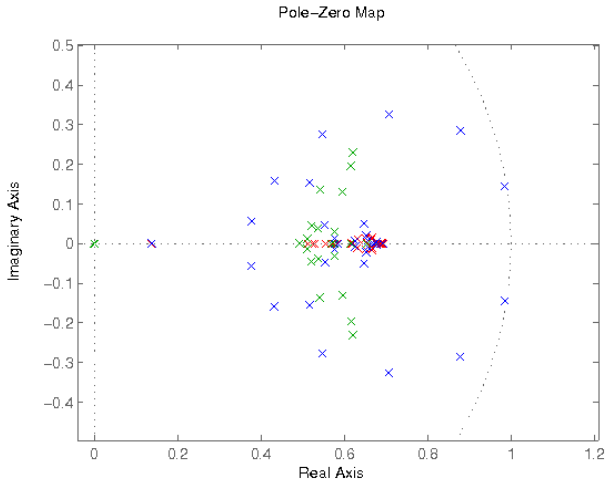

Figure 4-7: Poles of the system controlled by a full-order observer-based output feedback controller. In red, the open-loop poles; in blue the poles of $A + B_u K$; and in green the poles of $A - \Gamma C_y$.

On the other hand, in section 4.3.3 a reduced-order observer has been designed in order to use the measured state variables and to estimate only the remaining state variables. Again, using the separation property, the complete control law is the

aggregation of the state feedback control, but now, with the reduced-order observer.

We know that $\hat{x} = R^{-1}\hat{x}'$, thus $\bar{u} = KR^{-1}\hat{x}'$. By defining $K' = KR^{-1} = [K'_1\ K'_2]$, where $K'_1 \in \mathbb{R}^{m\times l}$ and $K'_2 \in \mathbb{R}^{m\times 3N-l}$, it is obtained:

$$\bar{u}(k) = K'_1\bar{y}(k) + K'_2\hat{x}'_2(k) \tag{4.45}$$

By replacing (4.45) in the reduced-order observer (4.35), it is obtained:

$$\begin{aligned}\hat{x}'_2(k) =&\tilde{\Gamma}\bar{y}(k) + (A'_{21} - \tilde{\Gamma}A'_{11} + (B'_{u2} - \tilde{\Gamma}B'_{u1})K'_1)\bar{y}(k-1)\\ &+ (A'_{22} - \tilde{\Gamma}A'_{12} + (B'_{u2} - \tilde{\Gamma}B_{u1})K'_2)\hat{x}'_2(k-1)\end{aligned} \tag{4.46}$$

Equation (4.46) is used to estimate the part of the system states that is not measured and equation (4.45) is used to compute the controlled input.

Again, like in section 4.3.1, it is necessary to define the matrix D_z to adjust the compromise between the energy allowed for the controlled input and the performance requested on the controlled output. In order to obtain the best performance of the connected state feedback controller - Luenberger observer, both dynamics are separated as much as possible without degrading closed-loop stability. The control action on the output controlled is therefore increased to $D_z = 0.55$. On the other hand, the poles of the reduced-order observer are placed into the same disk with radius $r = 0.8$. Noise level upon 2% on the measured output $y(k)$ was correctly filtered.

After solving the optimization problems (4.23) and (4.39), using the YALMIP matlab inteface and the SEDUMI solver [47], gains K and $\tilde{\Gamma}$ were computed respectively. The system was then simulated in closed-loop. Figure 4-8a shows the output response to the controlled input shown in figure 4-8b. It can be observed that the constraint imposed is almost respected along time, but when the disturbance comes to its highest value, the nitrogen concentration is a little more important than the expected objective.

Figure 4-9 shows the open-loop poles in red, the poles of $A + B_u K$ in blue and the poles of $A'_{22} - \tilde{\Gamma}A'_{12}$ in green. As expected all of them are inside the stability region.

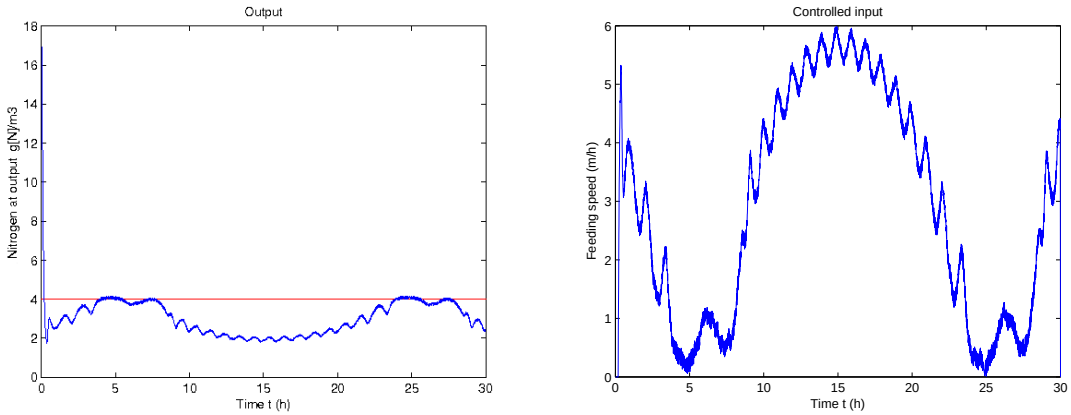

(a) Time-evolution of the nitrogen concentration at the biofilter output. In red the output reference and in blue the real nitrogen concentration.

(b) Time-evolution of the flow rate.

Figure 4-8: Closed-loop time-evolution by considering the reduced-order observer-based output feedback controller.

In addition, the poles of the observer, correctly placed into the $\mathcal{D}_2$-stability region for $r = 0.8$, are faster than those ones of the state feedback.

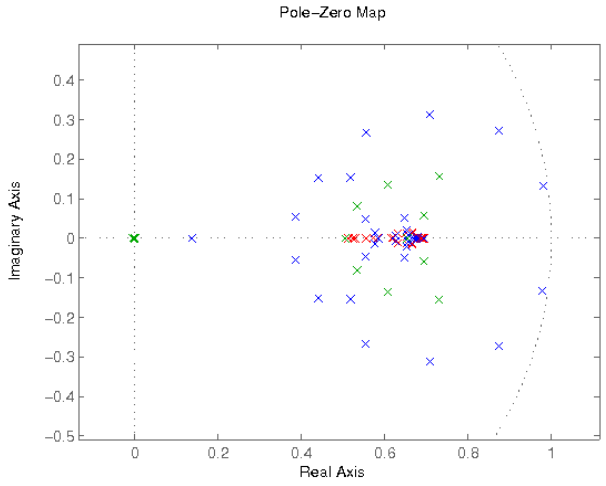

Figure 4-9: Poles of the system controlled by a reduced-order observer-based output feedback controller. In red, the open-loop poles; in blue the poles of $A + B_u K$; and in green the poles of $A'_{22} - \tilde{\Gamma} A'_{12}$.

4.4 Continuous observer-based output feedback linear control

In this section, an observer-based dynamic output feedback controller for the denitrification reactor described by a parabolic PDE system is synthesized. First, a state feedback control law is designed. Following, a full-order Luenberger observer is designed. Finally, by using the separation principle, the state feedback controller is complemented with the observer. Different results about the topics developed are presented in each subsection. The results presented in this section were published in [81] and [82].

In chapter 3 a modal analysis was used to transform the parabolic PDE system (2.1)-(2.3) into an ODE system. The resulting ODE system represents a nonlinear state-space system of the form:

$$\dot{m}(t) = F_{\xi}(m(t), u(t), w(t)) \; ; \;\; m(0) = m_0 \tag{4.47}$$

where $F_{\xi} \in \mathbb{R}^{3N_m}$ is a vector of functions constructed as:

$$F_{\xi}(m(t), u(t), w(t)) = \left[f_{\xi 1}^{1} \; f_{\xi 2}^{1} \; f_{\xi 3}^{1} \; \ldots \; f_{\xi 1}^{N_m} \; f_{\xi 2}^{N_m} \; f_{\xi 3}^{N_m} \right]^T$$

$m \in \mathbb{R}^{3N_m}$ is the vector of modes constructed as:

$$m = \left[m_1^1 \; m_2^1 \; m_3^1 \; \ldots \; m_1^{N_m} \; m_2^{N_m} \; m_3^{N_m} \; \right]^T$$

$u \in \mathbb{R}^m$ is the vector of control inputs and $w \in \mathbb{R}^q$ is the vector of external disturbances.

After linearization around the operating point (m^*, u^*, w^*), system (4.47) can be rewritten in the classic state space form as:

$$\dot{\bar{m}}(t) = A\bar{m}(t) + B_u \bar{u}(t) + B_w \bar{w}(t) \tag{4.48}$$

In all the numerical applications provided in this section, the linear state space model (4.48) is issued from a modal analysis done over the original parabolic PDE model (2.1)-(2.3) by considering eleven discretization points ($N = 11$).

As in section 4.3 the control objective is to maintain the nitrogen concentration at the reactor output around a constraint lower than the European norm while limiting as much as possible the activity of the controlled input. Again, the flow rate is considered as the controlled input, it means $\bar{u}(t) = v(t)$ around a nominal regime determined by $v = 4m/h$ with $m = 1$. The nitrate concentration at the reactor input is again considered as a disturbance, it means $\bar{w}(t) = S_{NO_3,in}(t)$ which values may vary between $14.93g[N]/m^3$ and $18.93g[N]/m^3$ around a nominal regime determined by $S_{NO_3,in} = 16.93g[N]/m^3$ with $q = 1$.

4.4.1 Continuous state feedback H_2 controller

The linear state space equation (4.48) is complemented by (4.3) approximating $\bar{x}(t)$ as:

$$\bar{x}(t) = \Phi_T \bar{m}(t) \tag{4.49}$$

where $\Phi_T \in \mathbb{R}^{3N \times 3N_m}$ is issued from (3.74), to obtain the system:

$$\begin{array}{rcl} \dot{\bar{m}}(t) & = & A\bar{m}(t) + B_u\bar{u}(t) + B_w\bar{w}(t) \\ z(t) & = & C_{zm}\bar{m}(t) + D_z\bar{u}(t) \end{array} \tag{4.50}$$

where $C_{zm} = C_z\Phi_T \in \mathbb{R}^{p \times 3N_m}$.

In order to control the nitrogen concentration at the reactor output C_z is again defined as:

$$C_z = [0 \ \ldots \ 0 \ 1 \ 1 \ 0]$$

and therefore, $p = 1$.

As mentioned in section 4.3.1, matrix D_z is used to tune the closed-loop performance. $D_z = 0.3$ is considered in this section.

A feedback control law $\bar{u}(t) = K\bar{m}(t)$ is then proposed to decrease the influence of the disturbance w on the controlled output z. By replacing it in (4.50) the following system is obtained:

$$\begin{aligned} \dot{\bar{m}}(t) &= (A + B_u K)\bar{m}(t) + B_w \bar{w}(t) \\ z(t) &= (C_{zm} + D_z K)\bar{m}(t) \end{aligned} \tag{4.51}$$

The transfer function of the closed loop system (4.51) from w to z is given by:

$$T_{wz} = \frac{Z(s)}{W(s)} = (C_{zm} + DzK)(sI - (A + B_u K))^{-1} B_w \tag{4.52}$$

Proposition 1 with (4.17) is then used to state the following convex optimal H_2 problem to compute a static feedback controller $K \in \mathbb{R}^{m \times 3N_m}$ for stabilizing the closed-loop dynamics:

$$\begin{aligned} &\min_{W_1, W_2, W_3} trace(W_3) \\ &under \\ &W_1 > 0 \\ &AW_1 + W_1 A^T + BW_2 + W_2^T B^T + B_w B_w^T \leq 0 \\ &\begin{bmatrix} W_1 & W_1 C_{zm}^T + W_2^T D_z^T \\ C_{zm} W_1 + D_z W_2 & W_3 \end{bmatrix} \geq 0 \end{aligned} \tag{4.53}$$

where $W_1 \in \mathbb{R}^{3N_m \times 3N_m}$, $W_2 \in \mathbb{R}^{m \times 3N_m}$ and $W_3 \in \mathbb{R}^{p \times p}$. The controller gain, solution of the optimization problem (4.53), may be then calculated as $K = W_2 W_1^{-1}$ and $\|T_{wz}\|_2 = trace(W_3)$ [6], [69].

Figure 4-10a shows the evolution of the first five modes related to nitrate. Note that, see equation (3.70), the larger the value of j, the faster the convergence of $m_i^j(t)$ to zero. In fact, for $j > 5$ the modes evolve so fast to zero that their contribution to the solution may be neglected. A reduced-order model with five modes is considered

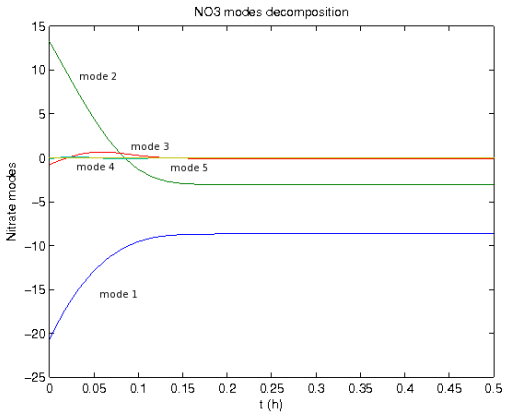

(a) NO_3 modes.

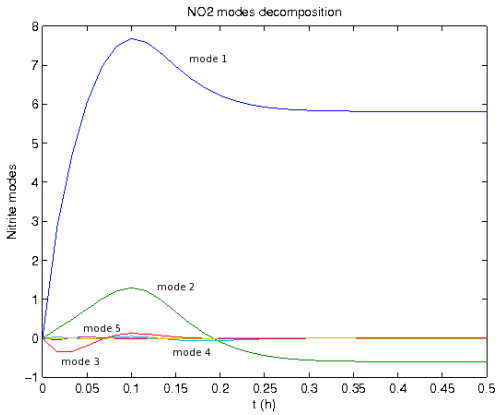

(b) NO_2 modes.

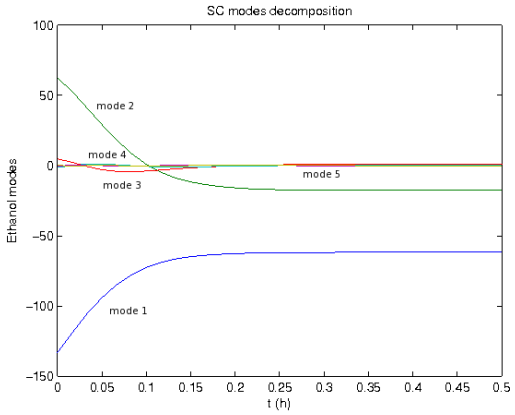

(c) S_C modes.

Figure 4-10: Modes of the state variables for eleven discretization points.

as a good approximation to the real solution. The same behaviour can be shown for the modes associated with the nitrite and the ethanol, figures 4-10b and 4-10c respectively. Therefore $N_m = 5$ is considered in order to compute the state feedback control law. The optimization problem (4.53) is solved by using the YALMIP matlab interface with the SEDUMI solver [47]. A gain $K \in \mathbb{R}^{1\times 3N_m}$ was computed. The flow rate is then computed at each sampling instant considering the values of the first five modes m and the system is simulated in closed-loop.

In order to simulate the closed-loop system, the parabolic PDE system (2.1)-(2.3) is solved by the method of lines and the derivatives terms are approximated by the finite element method, using 151 discretization points.

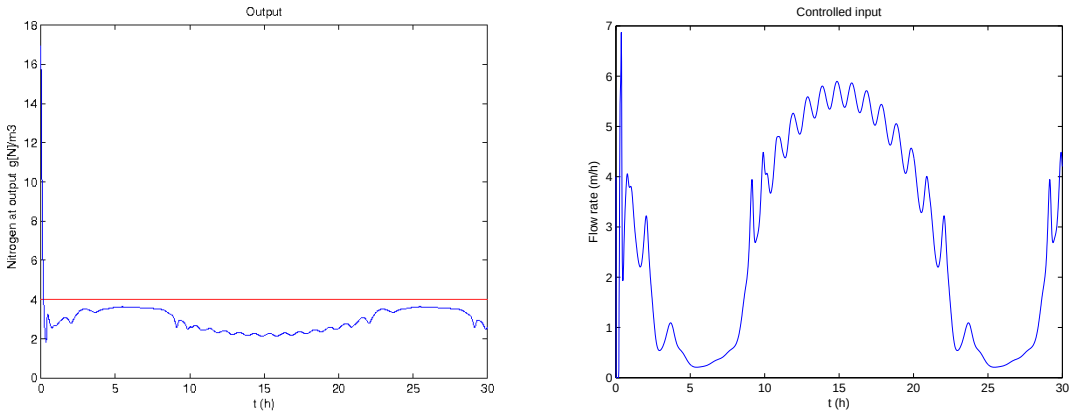

(a) Time-evolution of the nitrogen concentration at the biofilter output. In red the output reference and in blue the real nitrogen concentration.

(b) Time-evolution of the flow rate.

Figure 4-11: Closed-loop time-evolution by considering the modes-based state feedback controller.

Figure 4-11a shows the output response to the controlled input shown in figure 4-11b and the external disturbance shown in figure 4-2a. It is clear that the output in closed-loop is correctly maintained below $4mg[N]/m^3$, respecting the imposed constraint.

4.4.2 Continuous H_2 full-order observer

The state feedback control law uses the modes of the system, which cannot be directly accessible by measurement. It is therefore proposed a full-order observer based on the system modes by using the original measured output. Furthermore, this observer may also be used to estimate the original state variables.

A linear Luenberger observer is proposed in a very similar way as in section 4.3.2, except that, now, for the continuous-time linear representation (4.48) defined as:

$$\dot{\hat{m}}(t) = A\hat{m}(t) + B_u\bar{u}(t) + \Gamma(\bar{y}(t) - \hat{y}(t)) \tag{4.54}$$

where $\hat{m} \in \mathbb{R}^{3N}$ is the vector of estimated modes constructed as:

$$\hat{m} = \left[\hat{m}_1^1\ \hat{m}_2^1\ \hat{m}_3^1\ \ldots\ \hat{m}_1^N\ \hat{m}_2^N\ \hat{m}_3^N\ \right]^T$$

$u \in \mathbb{R}^m$ is the vector of control inputs, $y \in \mathbb{R}^l$ is the vector of measured outputs defined as:

$$\bar{y}(t) = C_y \bar{x}(t) \tag{4.55}$$

By considering (4.49), the following representation for the measured output is obtained:

$$\bar{y}(t) = C_{ym} \bar{m}(t) \tag{4.56}$$

where $C_{ym} = C_y \Phi_T \in \mathbb{R}^{l \times 3N_m}$.

Following the same procedure as in section 4.3.2, but for the continuous-time case, an observer gain Γ to decrease the influence of the disturbance w on the estimation error $e = \bar{m} - \hat{m}$ is then searched. In addition, we can accelerate its dynamics by placing the closed-loop poles into the stability region $\mathcal{D}_3$. Proposition 1 with (4.17), (4.13) and (4.14) are then used to state the following convex optimal H_2 problem to compute the gain Γ:

$$\begin{aligned}
&\min_{W_1, W_2, W_3} trace(W_3) \\
&under \\
&W_1 > 0 \\
&\begin{bmatrix} W_1 A + A^T W_1 + 2dW_1 - W_2 C_{ym} - C_{ym}^T W_2^T & W_1 B_w \\ B_w^T W_1 & -I \end{bmatrix} \leq 0 \\
&\begin{bmatrix} -rW_1 & W_1 A - W_2 C_{ym} \\ A^T W_1 - C_{ym}^T W_2^T & -rW_1 \end{bmatrix} \leq 0 \\
&\begin{bmatrix} W_1 & I \\ I & W_3 \end{bmatrix} \geq 0
\end{aligned} \tag{4.57}$$

where $W_1 \in \mathbb{R}^{3N_m \times 3N_m}$, $W_2 \in \mathbb{R}^{3N_m \times l}$ and $W_3 \in \mathbb{R}^{3N_m \times 3N_m}$, d is the distance between the origin and the vertical strip and r is the radius of the disk. The observer gain, solution of the optimization problem (4.57), is then calculated as $\Gamma = W_1^{-1} W_2$ and $\|T_{we}\|_2 = trace(W_3)$ [69], [16].

To solve the optimization problem (4.57), the matrix C_{ym} is constructed according to the observability test described in appendix B. Considering that only nitrate and nitrite concentrations are accessible to measurements, an observability test has shown that at least six measurement points have to be considered for those two variables to achieve complete observability of the modes vector (of dimension $3N_m$). The pole placement constraint is the stability region $\mathcal{D}_3$ with $d = 10$ and $r = 65$. Using the YALMIP matlab interface with the CSDP solver [47], a gain Γ was computed. The original discretized state variables are reconstructed by using (3.74).

Figure 4-12 shows the nitrate, the nitrite and the ethanol estimations, in blue the true values and in black the estimated ones. The real values of the original state variables are obtained by simulating the parabolic PDE system in open-loop using the method of lines and approximating the derivatives by the finite element method. In addition, noise level upon 5% on the measured output $y(t)$ was correctly filtered.

As shown in figure 4-12, the observer correctly rejects the disturbance and the noise is correctly filtered almost in all positions, except at the reactor input. It can be observed that the ethanol is the best state variable estimated.

4.4.3 Continuous observer-based output feedback H_2 controller

At this moment, a state feedback controller and a full-order observer have been designed. A similar discussion about the separation property like in section 4.3.4 allows to construct the complete control law as the aggregation of the state feedback control with the state observer, that is:

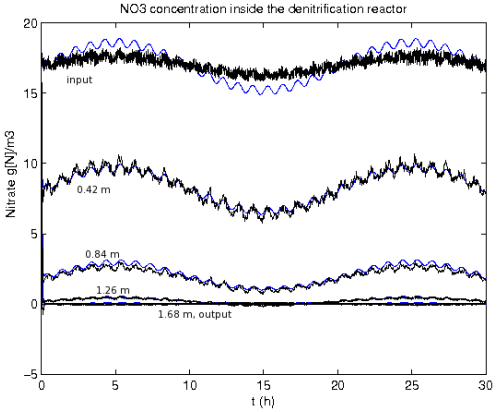

(a) NO_3 estimated.

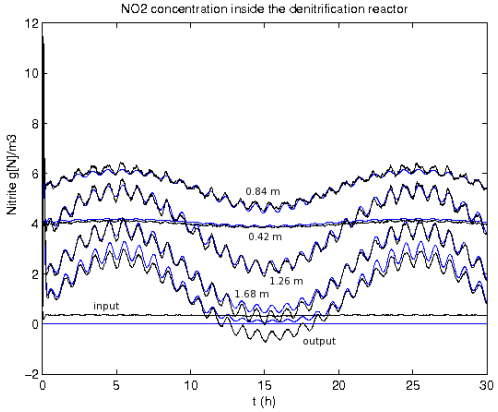

(b) NO_2 estimated.

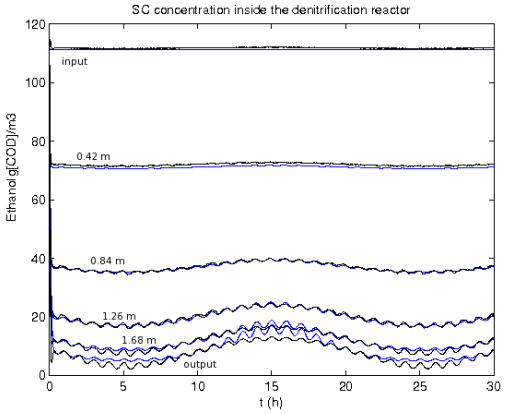

(c) S_C estimated.

Figure 4-12: State variables estimated by considering the full-order observer. In blue the simulated states and in black the estimated ones. Only six locations among the 11 locations used to built the linear state space model are plotted to increase the readability of the figure.

$$\bar{u}(t) = K\hat{m}(t) \tag{4.58}$$

with:

$$\dot{\hat{m}}(t) = (A + B_u K - \Gamma C_{ym})\hat{m}(t) + \Gamma \bar{y}(t) \tag{4.59}$$

Equation (4.59) is used to estimate the modes of the system and equation (4.58) is used to compute the flow rate, which is used in order to simulate the closed-loop parabolic biofilter reactor.

As in section 4.4.1, it is necessary to define a matrix D_z to adjust the compromise between the energy allowed for the controlled input and the performance requested on the controlled output. In order to obtain correct performance of the connected state feedback controller - Luenberger observer, both dynamics are separated as much as possible without degrading closed-loop stability. The control action on the controlled output is therefore increased to $D_z = 0.43$. On the other hand, as in section 4.4.2, the poles of the full-order observer are placed into the stability region $\mathcal{D}_3$, in this case with $d = 5$ and $r = 170$. Furthermore, noise level upon 5% on the measured output $y(t)$ was correctly filtered.

After solving the optimization problems (4.53) and (4.57), using the YALMIP matlab inteface with the SEDUMI and CSDP solvers [47] respectively, gains K and Γ were computed respectively. The system was then simulated in closed loop. Figure 4-13a shows the output response to the controlled input shown in figure 4-13b. It can be observed that the constraint imposed is well respected and the noise is correctly filtered.

Figure 4-14 shows the open-loop poles in red, the poles of $A + B_u K$ in blue and the poles of $A - \Gamma C_{ym}$ in green. As expected all of them are inside the stability region. In addition, the poles of the observer, correctly placed into the $\mathcal{D}_3$-stability region for $d = 5$ and $r = 170$, are faster than those of the state feedback.

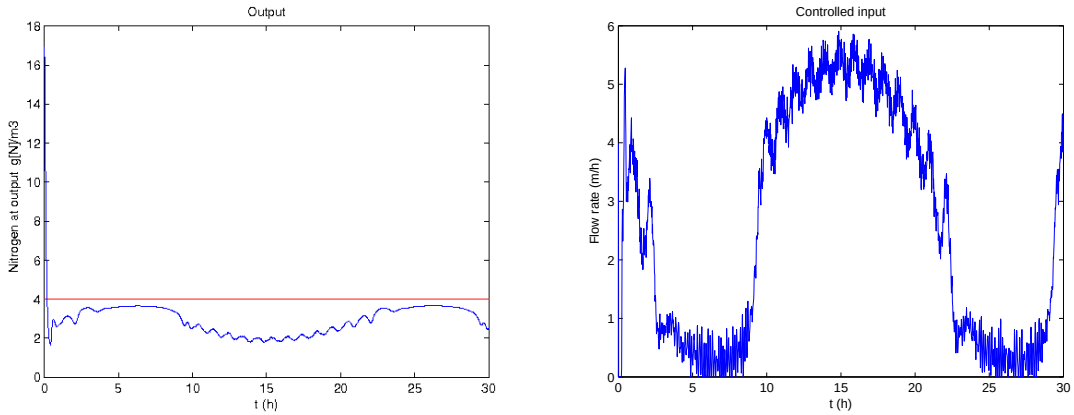

(a) Time-evolution of the nitrogen concentration at the biofilter output. In red the output reference and in blue the real nitrogen concentration.

(b) Time-evolution of the flow rate.

Figure 4-13: Closed-loop time-evolution by considering an observer-based output feedback controller on the system modes.

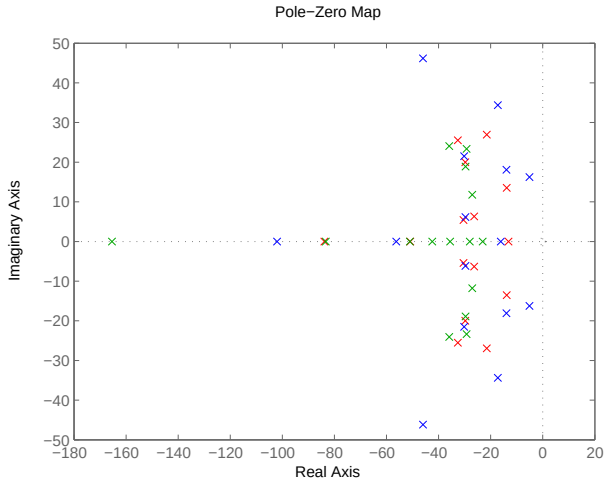

Figure 4-14: Poles of the closed-loop mode system controlled by an observer-based output feedback controller. In red the open-loop poles; in blue the poles of $A + B_u K$; and in green the poles of $A - \Gamma C_{ym}$.

4.5 Conclusions

This chapter presented an early lumping approach to synthesize an observer-based output feedback controller for both denitrification reactor models, i.e. the hyperbolic one and the parabolic one. Since the main objective is to maintain the nitrogen concentration at the reactor output lower than the European norm by reducing the energy of a disturbance at the reactor input ($S_{NO_3,in}$), the H_2 control and the LMI framework were selected as control strategy. In this context, the PDE system representing the denitrificacion process has been first rewritten in the classical state-space form (see chapter 3) before being linearized. Depending on the transformation approach, i.e. the method of characteristics for the hyperbolic system and the modal analysis for the parabolic model, the linear state-space model may be discrete-time or continuous-time. Both H_2 control strategies, for discrete-time systems and for continuous-time systems have been addressed, first in the state feedback context, then extended to a state estimation context, in order to design observer-based output feedback controllers.

The early lumping linear strategies presented in this chapter have been illustrated with a few examples. The main points to be kept in mind are however independent of the particular cases presented.

First, this chapter intended to illustrate that, considering any semi-discretization approach to transform a PDE system into an ODE system followed by a linearization to deal with a linear state space model opens the way to the wide world of (robust) linear control approaches. By extension, other strategies such as output feedback, but also taking uncertainties or saturations into account, could be easily investigated in the same way. The discretization step of the PDE systems results in several forms of ODE systems (dimension, discrete-time or continuous-time, interpretation of the state, etc.) but it has no significant influence on the next steps to follow.

Secondly, the number of discretization points is a key factor to obtain a high performance control law, the more points are taken into account, the better the

system represents the reality. However, in the *LMI* framework, the main disadvantage to face is the matrix dimensions involved in the optimization problem to solve. If the matrix dimensions are large, the solution can be difficult and sometimes impossible to find. A compromise between dimension and precision must be managed. In addition, a reduced-order model may be taken into account. In this context, the nonlinear model based on the most important modes was used to represent the denitrification process in a classical state space form. Such modes are not accessible and a full-order state observer has to be designed. It is however generally of smaller order than the ones obtained by other discretization strategies. As a matter of fact, although reduced-order strategies may be easily studied with a state vector which represents the concentration variables at several locations along the biofilter, the dimension of the observer is generally much larger than the one which results from modal analysis.

Finally, early lumping approaches have been presented in this chapter, whose main advantages are that the control law implementation is a rather direct task since it is provided as a static state-feedback or a dynamic output feedback (state feedback + state observer). On the other hand, this easiness of implementation is counter balanced by the succession of steps which have to be followed to build the control law with a space discretization plus a linearization around a nominal space profile.

In the next chapter a late lumping approach will be presented to attack the same problem but stated as a tracking reference one. Again, observer-based output feedback controllers will be synthesized but now using feedback linearization strategies complemented by a distributed parameter Luenberger observer.

Chapter 5

Late lumping approach techniques

5.1 Introduction

Unlike the early lumping approach, in the late lumping approach the idea is to keep as much as possible the distributed parameter property. Based on the early PDE system stability works [86] and non-linear control theory [60] [35] [39], nonlinear output feedback controllers with control action distributed in the space [18], control action at the boundaries [40] or control action on a derivative term [31], have been developed. In this context, nonlinear feedback controllers complemented by nonlinear observers may be synthesized. Both of them are therefore designed directly on the nonlinear PDEs. In order to implement the observer-based output feedback controller, the resulting PDEs are solved by numerical methods as shown in chapter 3.

In this chapter, nonlinear distributed strategies are investigated in order to design observer-based output feedback controllers by linearizing the output dynamics of the biofilter, first for the hyperbolic PDE model, then for the parabolic one. The relative degree of the PDE system must therefore be analyzed in order to propose a new coordinate system [31]. Linearizing control strategies are then used to synthesize a control law to linearize the output dynamics, assuring closed-loop asymptotic stability [35], [67]. The linearizing feedback controller is complemented by a distributed Luenberger observer, as proposed in [89], to estimate the overall set of state variables distributed

along the reactor, even if at the end, only those ones needed by the nonlinear state feedback control law will be used.

5.2 Problem formulation

Along the chapter, we will be interested in regulating the nitrogen concentration at the reactor output around a constraint lower than the European norm ($5.65g[N]/m^3$) while limiting as much as possible the activity of the controlled input. Again, the flow rate $v(t) = F(t)/A$ is considered as the controlled input. An output function is then defined as the sum of nitrate and nitrite concentrations at the reactor output:

$$y(t) = \vartheta(S) = S_{NO_3}(L,t) + S_{NO_2}(L,t) \tag{5.1}$$

On the other hand, the nitrate concentration at the reactor input $S_{NO_3,in}$ is considered as a disturbance, which values may vary between $14.93g[N]/m^3$ and $18.93g[N]/m^3$.

In order to simulate the closed-loop system, the original (hyperbolic or parabolic) PDE system will be solved by the Method of Lines (MOL) and the spatial derivatives will be approximated by fourth-order finite differences (FDM) by considering $N = 151$ discretization points uniformly distributed throughout the reactor. The values of the parameters used to mimic the biofilter dynamics are given in Table 2.1, with initial conditions given in Table 2.4. Furthermore, in the discrete-time version, a sample period $T = 1\ min$ will be considered.

Finally, we will be also interested in evaluating the robustness of the closed-loop system with respect to the state estimation errors but also to the uncertainties of the model parameters. According to the sensitivity analysis performed in chapter 2, the parameters $\eta_g\mu_{1_{max}}$, $\eta_g\mu_{2_{max}}$, K_{NO_3}, K_{NO_2} and K_C influence the system dynamics. However, the variations of each parameter are aggregated as a variation of the overall μ_1 and μ_2 values. Therefore, in this chapter, we will consider, for all the implementations of the control laws and observers, modified values for the maximum specific

growth rates, proposed as $\mu_{1_{max}} = 0.414\ 1/h$ and $\mu_{2_{max}} = 0.368\ 1/h$.

5.3 Observer-based output feedback linearizing control applied to the hyperbolic PDE model

In this section, an observer-based output feedback linearizing controller for the denitrification reactor described by an hyperbolic PDE system is synthesized. First, a state feedback linearizing control law is designed. Following, a nonlinear distributed parameter observer is designed. Finally, the state feedback controller is complemented with the observer. Different results about the topics developed are presented in each subsection. The results presented in this section were published in [83].

It has been previously shown in chapter 2 that, except during the initial colonization step, the biomass concentration remains almost constant and homogeneously distributed at a value X_{amax} along the biofilter, even after a washing out. The dynamics of the biomass concentration are then cancelled and it is assumed that this concentration remains constant at X_{amax}. Moreover, in the denitrification reactor model considered in this section, the diffusion phenomenon has been neglected, resulting in the following matrix form hyperbolic PDE system:

$$\frac{\partial S}{\partial t} = A_2 \frac{\partial S}{\partial z} + h(S) \tag{5.2}$$

Here $S = [S_{NO_3}\ \ S_{NO_2}\ \ S_C]^T$ is the state vector, defined on the domain $\mathcal{D} = \mathcal{V} \times \mathcal{B} \times \mathcal{T}$ where $\mathcal{V} \in \mathbb{R}$ is the spatial domain with boundary $\mathcal{B}$ and $\mathcal{T}$ is the semiopen time interval $[0, \infty)$. Matrix $A_2 \in \mathbb{R}^{n \times n}$ is a diagonal square matrix whose elements are $v(t)/\epsilon$, $h(S) \in \mathbb{R}^n$ is a vector of non-linear functions and $n = 3$.

5.3.1 Feedback linearizing controller

Differentiating $y(t)$ with respect to time, it is obtained:

$$\dot{y}(t) = L_h\vartheta(S)|_{z=L} - \frac{v(t)}{\epsilon}\left.\frac{\partial\vartheta(S)}{\partial S}\frac{\partial S}{\partial z}\right|_{z=L} \tag{5.3}$$

where $L_h\vartheta(S)$ is the Lie derivative of $\vartheta(S)$ with respect to $h(S)$.

Since for all $t > 0$:

$$\left.\frac{\partial\vartheta(S)}{\partial S}\frac{\partial S}{\partial z}\right|_{z=L} \neq 0$$

the relative degree of the system (5.2)-(5.1) is $r = 1$.

In order to feedback linearize the system (5.2)-(5.1), a new system of coordinates can be introduced [35]:

$$\Phi(S(L,t)) = \begin{pmatrix} \xi_1 \\ \xi_2 \\ \xi_3 \end{pmatrix}$$

with $\xi_1 = y(t)$.

Furthermore, because r is strictly less than n, it is always possible to find $n-r = 2$ additional functions ξ_2, ξ_3 such that [43, p. 910]:

$$\left.\frac{\partial\xi_i}{\partial S}\frac{\partial S}{\partial z}\right|_{z=L} = 0$$

for $i = 2, 3$. In this way, ξ_2 and ξ_3 can be obtained by solving the following two PDE:

$$\left.\frac{\partial\xi_2}{\partial S_{NO_3}}\frac{\partial S_{NO_3}}{\partial z}\right|_{z=L} + \left.\frac{\partial\xi_2}{\partial S_{NO_2}}\frac{\partial S_{NO_3}}{\partial z}\right|_{z=L} + \left.\frac{\partial\xi_2}{\partial S_C}\frac{\partial S_C}{\partial z}\right|_{z=L} = 0 \tag{5.4}$$

$$\left.\frac{\partial\xi_3}{\partial S_{NO_3}}\frac{\partial S_{NO_3}}{\partial z}\right|_{z=L} + \left.\frac{\partial\xi_3}{\partial S_{NO_2}}\frac{\partial S_{NO_2}}{\partial z}\right|_{z=L} + \left.\frac{\partial\xi_3}{\partial S_C}\frac{\partial S_C}{\partial z}\right|_{z=L} = 0 \tag{5.5}$$

It must be pointed out that solving the two PDEs above is a tedious task because they depend on the solution of the state equations.

According to (5.3) and denoting:

$$a(\xi) = L_h \vartheta(S)|_{z=L}$$

$$b(\xi) = \frac{-1}{\epsilon} \frac{\partial \vartheta(S)}{\partial S} \frac{\partial S}{\partial z}\bigg|_{z=L}$$

the following representation is obtained:

$$\frac{d\xi_1}{dt} = \frac{\partial \xi_1}{\partial S}\frac{\partial S}{\partial t} = a(\xi) + b(\xi)v(t) \tag{5.6}$$

Because ξ_2 and ξ_3 have been chosen so that

$$\frac{\partial \xi_i}{\partial S}\frac{\partial S}{\partial z}\bigg|_{z=L} = 0$$

one has,

$$\begin{aligned}
\frac{d\xi_i}{dt} &= \frac{\partial \xi_i}{\partial S}\left(h(S) - \frac{v(t)}{\epsilon}\frac{\partial S}{\partial z}\right)\bigg|_{z=L} \\
&= L_h \xi_i|_{z=L} - \frac{v(t)}{\epsilon}\frac{\partial \xi_i}{\partial S}\frac{\partial S}{\partial z}\bigg|_{z=L} \\
&= L_h \xi_i|_{z=L}
\end{aligned}$$

By setting:

$$q_i(\xi) = L_h \xi_i|_{z=L} \tag{5.7}$$

for $i = 2, 3$, the state space description of the original system (5.2)-(5.1) in the new coordinates may then be written as:

$$\begin{aligned}
\dot{\xi}_1 &= a(\xi) + b(\xi)v(t) \\
\dot{\xi}_2 &= q_2(\xi) \\
\dot{\xi}_3 &= q_3(\xi)
\end{aligned} \tag{5.8}$$

The objective is to build a control law $v(t)$ which stabilizes the closed-loop system and such that the output $y(t)$ tracks a given constant reference y_r while limiting as much as possible the activity of the control input. The tracking error e_0 is defined as

$y(t) - y_r$. As soon as the original system (5.2)-(5.1) is locally exponentially minimum phase and $\alpha_0 > 0$, the state feedback control law:

$$\begin{aligned} v(t) &= \frac{1}{b(\xi)} \left(-a(\xi) - \alpha_0 e_0\right) \\ &= \left(\frac{-\epsilon}{\frac{\partial S_{NO_3}}{\partial z} + \frac{\partial S_{NO_2}}{\partial z}} \right) \Bigg|_{z=L} \\ &\quad \times \left(\frac{1 - Y_{h_2}}{1.71 Y_{h_2} \epsilon} \mu_2(S_{NO_2}, S_C) X_{amax} - \alpha_0 \left(S_{NO_3} + S_{NO_2} - y_r\right) \right) \Bigg|_{z=L} \end{aligned} \tag{5.9}$$

partially linearizes the original system and results in a (locally) exponentially stable closed-loop system [67]. Thus, by inspecting (5.8) the resulting closed-loop dynamics is given by:

$$\dot{y}(t) = -\alpha_0 \left(y(t) - y_r\right) \tag{5.10}$$

because it is sufficient to differentiate once the output function to see explicitly the control input.

The value of α_0 has to be sufficiently small to reject the influence of the S_{NO_3} and S_{NO_2} derivatives at the reactor output in the output dynamics but large enough to bypass the model uncertainties, especially those that come from $\mu_2(S_{NO_2}, S_C)$. In addition to this source of uncertainty, one could also consider parameter uncertainties (on X_{amax}, ϵ, Y_{h_2}), but in some sense, such uncertainties are hidden in that one of μ_2 and therefore they are not directly considered.

The control law is simulated approximating the spatial derivatives by finite differences, that is:

$$\begin{aligned} v(t) &= \left(\frac{-\epsilon}{\frac{\Delta S_{NO_3}}{\Delta z} + \frac{\Delta S_{NO_2}}{\Delta z}} \right) \Bigg|_{z=L} \\ &\quad \times \left(\frac{1 - Y_{h_2}}{1.71 Y_{h_2} \epsilon} \mu_2(S_{NO_2}, S_C) X_{amax} - \alpha_0 \left(S_{NO_3} + S_{NO_2} - y_r\right) \right) \Bigg|_{z=L} \end{aligned} \tag{5.11}$$

with $v(0) = 4m/h$.

As previously mentioned, we are interested in regulating the output $y(t)$ less or equal than the European norm when the system is submitted to the disturbance (influent nitrate concentration) shown in figure 4-2a as in chapter 4. In this application a reference $y_r = 4.0$ is considered.

To calibrate the linearizing controller, a gain $\alpha_0 = 10$ was first proposed. Under the hypothesis that the system is certain, the output converges quickly towards the reference and the disturbance is correctly rejected. However, the controller is strongly susceptible to model uncertainties. α_0 was then increased so as to reduce the influence of model uncertainties. $\alpha_0 = 75$ is then proposed to get robustness over uncertainties in the original model growth terms μ_1 and μ_2 without degradating too much the closed-loop dynamics. A tolerance upon 15% of error on the true μ_1 and μ_2 values was observed.

Figure 5-1a shows the output reference (in red) and the nitrogen concentration at reactor output (in blue) according to the controlled input shown in figure 5-1b computed by using the state feedback linearizing controller designed. It can be seen a transition period of more or less four hours before tracking the reference and well rejecting the disturbance.

5.3.2 Non-linear distributed parameter observer

In order to implement the control law (5.9) it is necessary to know the nitrite and ethanol concentrations to compute $\mu_2(S_{NO_2}, S_C)$ and the spatial derivatives of both the nitrate and the nitrite concentrations, at the reactor output. Since DPS dynamics are characterized by an infinite number of modes, the observer design would in principe require the specification of a large (theoretically infinite) number of tuning parameters. In order to bypass this high-dimensional design problem, a late lumping approach to the construction of distributed parameter observers (DPO) was devel-

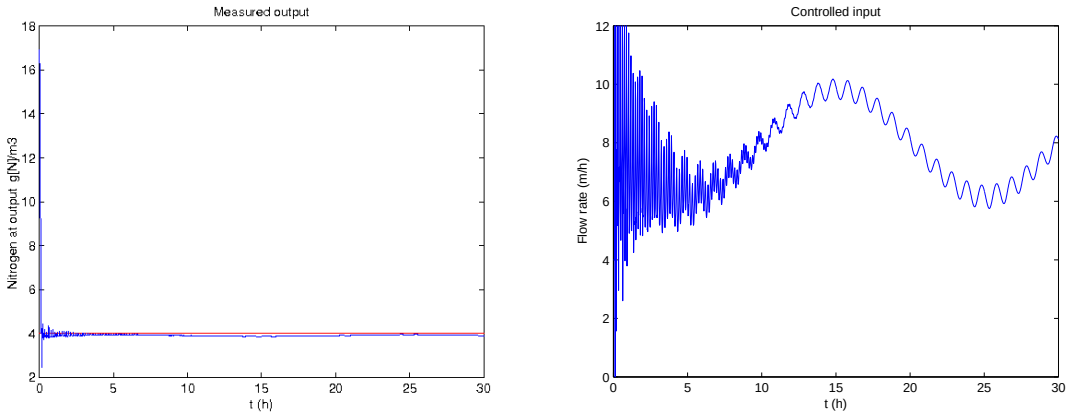

(a) Time-evolution of the nitrogen concentration at the biofilter output. In red the output reference and in blue the real nitrogen concentration.

(b) Time-evolution of the flow rate.

Figure 5-1: Hyperbolic PDE system. Closed-loop time-evolution by considering the state feedback linearizing controller.

oped in [89]. A nonlinear distributed parameter observer (DPO), with a formulation analog to the Luenberger observer, is then designed so as to assign the error dynamics to estimate the concentrations not accessible by measurements:

$$\frac{\partial \hat{S}}{\partial t} = A_2 \frac{\partial \hat{S}}{\partial z} + h(\hat{S}) + \Gamma(\hat{S})\,(y_m - \hat{y}_m) \tag{5.12}$$

with initial condition represented by:

$$\hat{S}(z,0) = \hat{S}(z,0) \tag{5.13}$$

where $\hat{S} = [\hat{S}_1\ \hat{S}_2\ \hat{S}_3]^T$ is the estimated state vector and $\Gamma(\hat{S})$ is the correction term, a square matrix $\in \mathbb{R}^{3\times l}$.

Let us now focus on the measurements to be used for the observer. Nitrate and nitrite concentrations are assumed to be available by measurements at the output of the biofilter. In addition, nitrite at the input is known to be zero and the ethanol concentration is assumed not being accessible at any point of the biofilter. The design of operator Γ is based on the estimation error equation $e(z,t) = \hat{S}(z,t) - S(z,t)$. In order to construct an error vector along of the space domain for each specific time,

interpolation of measured values of the available state variables is performed. Therefore, at least, a pair of state variables measurement is needed [88]. Then, an option to design an observer with the minimum of information consists in measurement, in addition of the output, of the concentration of nitrate at the input, that is $l = 4$. In this way, measured output is defined as:

$$y_m(t) = [S_{NO_3}(0,t)\ S_{NO_2}(0,t)\ S_{NO_3}(L,t)\ S_{NO_2}(L,t)]^T \tag{5.14}$$

Any other options with the measurement of nitrate and nitrite at two or more points along of the reactor would be also admissible. By considering the estimation error $e(z,t)$, its dynamics are given by:

$$\frac{\partial e}{\partial t} = A_2 \frac{\partial e}{\partial z} + h(\hat{S}) - h(S) + \Gamma(\hat{S})\,(y_m - \hat{y}_m) \tag{5.15}$$

$$e(z,0) = \hat{S}(z,0) - S(z,0) \tag{5.16}$$

The linearization of $h(S)$ along the estimated trajectory $\hat{S}(z,t)$ can be done to obtain (see [89]):

$$\frac{\partial e}{\partial t} = A_2 \frac{\partial e}{\partial z} + \left.\frac{\partial h(S)}{\partial S}\right|_{\hat{S}} e + \Gamma(\hat{S})\,(y_m - \hat{y}_m) \tag{5.17}$$

This linearization is justified as soon as the estimation error is assumed sufficiently small, i.e.:

$$\|e(z,0)\| = \|\hat{S}(z,0) - S(z,0)\| << 1 \tag{5.18}$$

In order to stabilize the closed-loop dynamics and to cancel the nonlinear term, physical knowledge about the system is used to design the correction term $\Gamma(\hat{S})\,(y_m - \hat{y}_m)$. Considering the i^{th} PDE, the i^{th} correction term γ_i is constructed in terms of error profile $e(z,t)$ and a tuning parameter row vector $\alpha_i \in \mathbb{R}^{1\times 2}$, i.e.:

$$\gamma_i^T \left(y_m - \hat{y}_m\right) = \left[-\left(\left.\frac{\partial h_i(S)}{\partial S_{NO_3}}\right|_{\hat{S}} + \alpha_{i1} \right) \; -\left(\left.\frac{\partial h_i(S)}{\partial S_{NO_2}}\right|_{\hat{S}} + \alpha_{i2} \right) \; 0 \right] e(z,t) \tag{5.19}$$

for $i = 1, 2, 3$. Initial profile $\hat{S}_0(z)$ as well as error profile $e(z,t)$ along the space in equations above are constructed by linear interpolation of known values at the measurement points.

Remark 7 *The correction term (5.19) is used to compensate the nonlinearities of the i^{th} equation. The resulting observer system is asymptotically stable as soon as $\alpha_{i,j}$ are positive elements high enough. Since measurements about ethanol are not available inside the reactor, their error profile cannot be calculated. Therefore, the error related to this variable is not considered.*

In order to show the convergence of the observer, the estimations started only after a delay of ten hours. In addition, the elements of the matrix α are proposed as:

$$\alpha = \begin{bmatrix} 110 & 0 \\ 100 & 110 \\ 100 & 100 \end{bmatrix}$$

Figure 5-2 shows the time evolution of the 'real' concentrations (in blue) and of the estimated ones (in black), for greated clarity plotted only at six positions along the reactor. It can be observed an acceptable external disturbance rejection. A tolerance upon 15% of error on the true μ_1 and μ_2 values was observed and a noise level upon 1% was well filtered without degradating too much the observer dynamics. It must be noted, however, that the model errors induce a bias in the estimation which is never compensated. Only the effect of the perturbation is correctly evaluated by the observer.

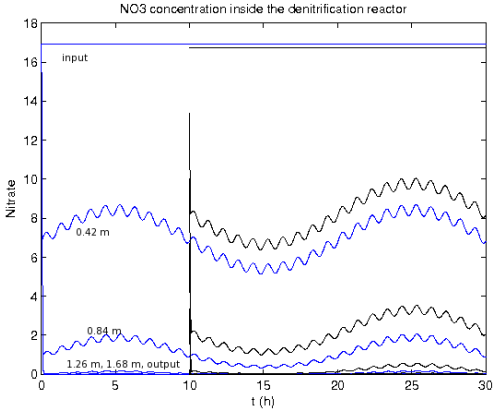

(a) NO_3 concentration.

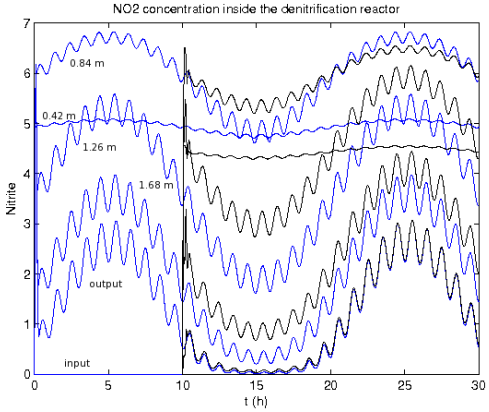

(b) NO_2 concentration.

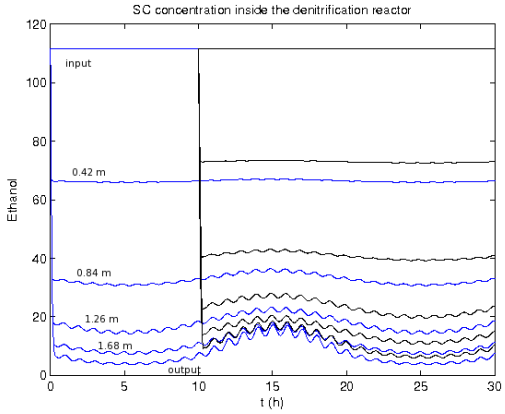

(c) S_C concentration.

Figure 5-2: Hyperbolic PDE model. State variables estimated by considering the distributed parameter observer. In blue the 'real' concentrations and in black the estimated ones. Only six locations are plotted to increase the readability of the figure.

5.3.3 Observer-based output feedback linearizing controller

At this moment a feedback linearizing controller and a distributed parameter observer have been developed by using a late lumping approach over the hyperbolic PDE system (5.2). The overall control law is then the aggregation of the state feedback linearizing control with the distributed parameter observer, approximating the spatial derivatives by finite differences, that is:

$$\begin{aligned} v(t) = & \left(\frac{-\epsilon}{\frac{\Delta \hat{S}_{NO_3}}{\Delta z} + \frac{\Delta \hat{S}_{NO_2}}{\Delta z}} \right) \Bigg|_{z=L} \\ & \times \left(\frac{1 - Y_{h_2}}{1.71 Y_{h_2} \epsilon} \mu_2(\hat{S}_{NO_2}, \hat{S}_C) X_{amax} - \alpha_0 \left(\hat{S}_{NO_3} + \hat{S}_{NO_2} - y_r \right) \right) \Bigg|_{z=L} \end{aligned} \tag{5.20}$$

with $v(0) = 4m/h$ and the $\hat{S}(z,t)$ vector estimated by using (5.12) and (5.19).

Besides the measurements available at the output ($z = L$), the estimates of the concentration at the last point before the output is used. The location of this point depends of the number N of discretization points. However, such an influence is limited as soon as the variation of the concentrations remains smooth enough at the end of the biofilter. In the present configuration with $N = 151$, it is the estimations of nitrate and nitrite concentrations at $z = 2.086m$ which are used to compute the spatial derivatives.

We are interested in regulating the output $y(t)$ at a reference $y_r = 4.0$. In order to keep the distributed parameter observer dynamics faster than the linearizing feedback controller ones, the elements of the matrix α must be proposed large enough. In this section the same α matrix as in section 5.3.2 is considered. It must be pointed out that estimation starts fithteen minutes after the process beginning and the control action starts once the observer has converged (thirty minutes).

Figures 5-3a and 5-3b show both the nitrate and the nitrite derivatives, in blue the 'real' value and in black the estimated one. It can be observed that the estimated

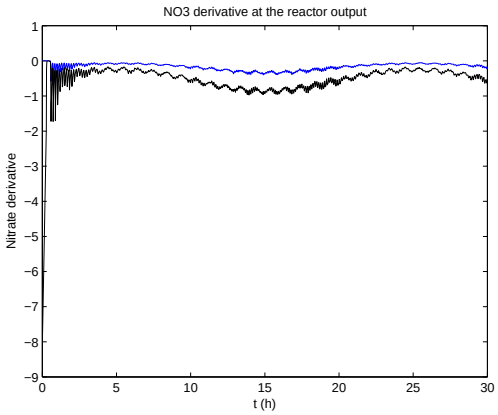

(a) NO_3 derivative at $z = L$.

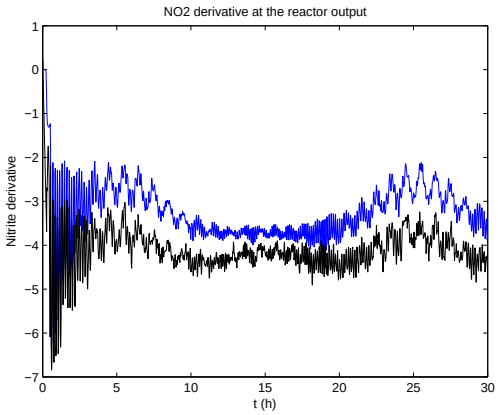

(b) NO_2 derivative at $z = L$.

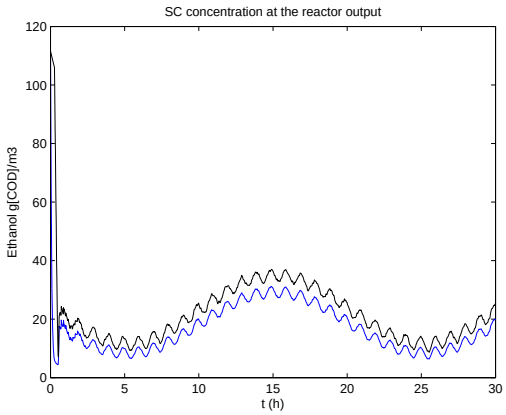

(c) S_C concentration at $z = L$.

Figure 5-3: Hyperbolic PDE model. Estimations needed by the linearizing control law. In blue the 'real' derivative for 5-3a and for 5-3b or concentration for 5-3c and in black the estimated ones, at $z = L$.

values follow correctly the real ones with an expected error because of the estimated values, the uncertainty influence and the noise. Since the concentrations at the reactor output are lower than at the point before, negative slope values are computed.

Figure 5-3c shows in blue the ethanol real value and in black the estimated one at the reactor output. This value is needed to compute the growth term $\mu_2(S_{NO_2}, S_C)$ at the reactor output. The bias in the estimation is related to the model uncertainties and the noise.

The calibration of the output feedback linearizing controller mimics that one of

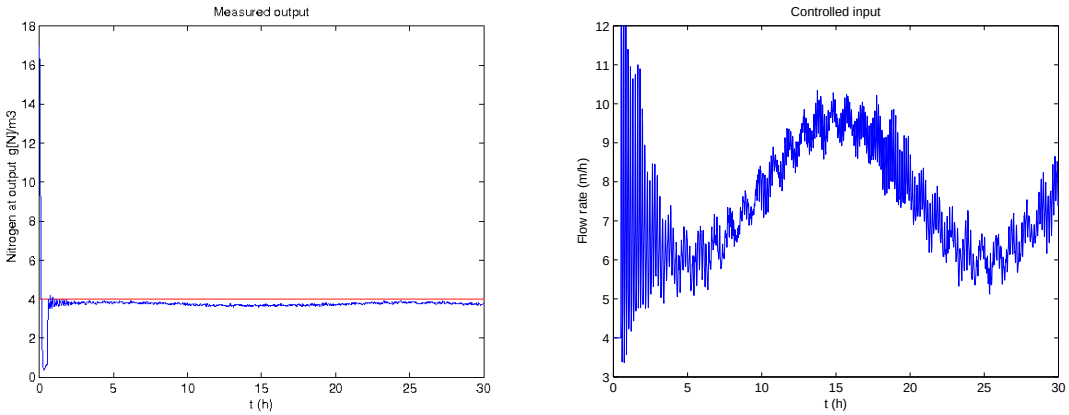

(a) Time-evolution of the nitrogen concentration at the biofilter output. In red the output reference and in blue the real nitrogen concentration.

(b) Time-evolution of the flow rate.

Figure 5-4: Hyperbolic PDE system. Closed-loop time-evolution by considering the observer-based output feedback linearizing controller.

section 5.3.1. The gain α_0 has to be chosen sufficiently high such as to reduce the influence of model uncertainty. $\alpha_0 = 65$ is then proposed to get robustness over uncertainties in the original model growth terms μ_1 and μ_2 without degradating too much the closed-loop dynamics. A tolerance upon 15% of error on the prediction of μ_1 and μ_2 was observed. In addition, a noise level upon 1% was correctly filtered. It must be pointed out that parametric uncertainties of the biofilter model is the most important problem to bypass by the linearizing feedback controller, when the state estimation is sufficiently accurate.

Figure 5-4a shows the output reference (in red) and the nitrogen concentration at the reactor output (in blue) according to the controlled input shown in figure 5-4b, computed by using the observed-based linearizing controller designed. It can be seen a transition period of more or less three hours before tracking the reference and well rejecting the disturbance.

5.4 Observer-based output feedback linearizing control applied to the parabolic PDE model

In this section, an observer-based output feedback linearizing controller for the denitrification reactor described by a parabolic PDE system is synthesized. First, a state feedback linearizing control law is designed. Following, a nonlinear distributed parameter observer is designed. Finally, the state feedback controller is complemented with the observer. Different results about the topics developed are presented in each subsection. The results presented in this section were published in [84].

It has been previously shown in chapter 2 that, when diffusion phenomenon is taken into account, the biofilter model is expressed by the following parabolic PDE system given in matrix form:

$$\frac{\partial S}{\partial t} = A_1 \frac{\partial^2 S}{\partial z^2} + A_2 \frac{\partial S}{\partial z} + h(S) \tag{5.21}$$

As in section 5.3, $S = [S_{NO_3}\ S_{NO_2}\ S_C]^T$ is the state vector, matrices $A_1, A_2 \in \mathbb{R}^{n\times n}$ are diagonal square matrices whose diagonal elements are D_f and v/ϵ respectively, $h(S) \in \mathbb{R}^n$ is a vector of non-linear functions and $n = 3$.

In the next section, the linearizing control strategy presented for the hyperbolic PDE system is extended to the parabolic PDE system.

5.4.1 Feedback linearizing controller

Differentiating $y(t)$ with respect to time and by considering $v(t)$ as the control variable, it is obtained:

$$\dot{y}(t) = D_f \left.\frac{\partial \vartheta(S)}{\partial S}\frac{\partial^2 S}{\partial z^2}\right|_{z=L} + L_h\vartheta(S)|_{z=L} - \frac{v(t)}{\epsilon}\left.\frac{\partial \vartheta(S)}{\partial S}\frac{\partial S}{\partial z}\right|_{z=L} \tag{5.22}$$

where $L_h\vartheta(S)$ is the Lie derivative of $\vartheta(S)$ with respect to $h(S)$.

If Neumann boundary conditions are not considered at the biofilter output, for all

$t > 0$:

$$\left.\frac{\partial \vartheta(S)}{\partial S}\frac{\partial S}{\partial z}\right|_{z=L} \neq 0$$

and therefore, the relative degree of the system (5.21)-(5.1) is $r = 1$.

In order to feedback linearize the system (5.21)-(5.1), a new system of coordinates can be introduced [35]:

$$\Phi(S(L,t)) = \begin{pmatrix} \xi_1 \\ \xi_2 \\ \xi_3 \end{pmatrix}$$

with $\xi_1 = y(t)$.

Furthermore, because r is strictly less than n, it is always possible to find $n-r = 2$ additional functions ξ_2, ξ_3 such that [43, p. 910]:

$$\left.\frac{\partial \xi_i}{\partial S}\frac{\partial S}{\partial z}\right|_{z=L} = 0$$

for $i = 2, 3$. In this way, ξ_2 and ξ_3 can be obtained by solving the following two PDE:

$$\left.\frac{\partial \xi_2}{\partial S_{NO_3}}\frac{\partial S_{NO_3}}{\partial z}\right|_{z=L} + \left.\frac{\partial \xi_2}{\partial S_{NO_2}}\frac{\partial S_{NO_3}}{\partial z}\right|_{z=L} + \left.\frac{\partial \xi_2}{\partial S_C}\frac{\partial S_C}{\partial z}\right|_{z=L} = 0 \tag{5.23}$$

$$\left.\frac{\partial \xi_3}{\partial S_{NO_3}}\frac{\partial S_{NO_3}}{\partial z}\right|_{z=L} + \left.\frac{\partial \xi_3}{\partial S_{NO_2}}\frac{\partial S_{NO_2}}{\partial z}\right|_{z=L} + \left.\frac{\partial \xi_3}{\partial S_C}\frac{\partial S_C}{\partial z}\right|_{z=L} = 0 \tag{5.24}$$

It must be pointed out that solving the two PDEs above is a tedious task because they depend on the solution of the state equations.

According to (5.22) and denoting:

$$a(\xi) = D_f \left.\frac{\partial \vartheta(S)}{\partial S}\frac{\partial^2 S}{\partial z^2}\right|_{z=L} + L_h \vartheta(S)|_{z=L}$$

$$b(\xi) = \frac{-1}{\epsilon} \left. \frac{\partial \vartheta(S)}{\partial S} \frac{\partial S}{\partial z} \right|_{z=L}$$

the following representation is obtained:

$$\frac{d\xi_1}{dt} = \frac{\partial \xi_1}{\partial S} \frac{\partial S}{\partial t} = a(\xi) + b(\xi) v(t) \tag{5.25}$$

Because ξ_2 and ξ_3 have been chosen so that

$$\left. \frac{\partial \xi_i}{\partial S} \frac{\partial S}{\partial z} \right|_{z=L} = 0$$

one has,

$$\begin{aligned} \frac{d\xi_i}{dt} &= \frac{\partial \xi_i}{\partial S} \left(D_f \frac{\partial^2 S}{\partial z^2} + h(S) - \frac{v(t)}{\epsilon} \frac{\partial S}{\partial z} \right) \Big|_{z=L} \\ &= D_f \left. \frac{\partial \xi_i}{\partial S} \frac{\partial^2 S}{\partial z^2} \right|_{z=L} + L_h \xi_i|_{z=L} - \frac{v(t)}{\epsilon} \left. \frac{\partial \xi_i}{\partial S} \frac{\partial S}{\partial z} \right|_{z=L} \\ &= D_f \left. \frac{\partial \xi_i}{\partial S} \frac{\partial^2 S}{\partial z^2} \right|_{z=L} + L_h \xi_i|_{z=L} \end{aligned}$$

By setting:

$$q_i(\xi) = D_f \left. \frac{\partial \xi_i}{\partial S} \frac{\partial^2 S}{\partial z^2} \right|_{z=L} + L_h \xi_i|_{z=L} \tag{5.26}$$

for $i = 2, 3$, the state space description of the original system (5.21)-(5.1) in the new coordinates may then be written as:

$$\begin{aligned} \dot{\xi}_1 &= a(\xi) + b(\xi) v(t) \\ \dot{\xi}_2 &= q_2(\xi) \\ \dot{\xi}_3 &= q_3(\xi) \end{aligned} \tag{5.27}$$

The objective is to build a control law $v(t)$ which stabilizes the closed-loop system and such that the output $y(t)$ tracks a given constant reference y_r while limiting as much as possible the activity of the control input. Let us define the tracking error e_0 as $y(t) - y_r$. As soon as the original system (5.21)-(5.1) is locally exponentially minimum phase and $\alpha_0 > 0$, the state feedback control law:

$$
\begin{aligned}
v(t) &= \frac{1}{b(\xi)}\left(-a(\xi) - \alpha_0 e_0\right) \\
&= \left(\frac{-\epsilon}{\frac{\partial S_{NO_3}}{\partial z} + \frac{\partial S_{NO_2}}{\partial z}}\right)\Bigg|_{z=L} \times \left(D_f \frac{\partial^2 S_{NO_3}}{\partial z^2} + D_f \frac{\partial^2 S_{NO_2}}{\partial z^2}\right. \\
&\quad \left. + \frac{1 - Y_{h_2}}{1.71 Y_{h_2} \epsilon} \mu_2(S_{NO_2}, S_C) X_{amax} - \alpha_0 \left(S_{NO_3} + S_{NO_2} - y_r\right)\right)\Bigg|_{z=L}
\end{aligned}
\tag{5.28}
$$

partially linearizes the original system and results in a (locally) exponentially stable closed-loop system [67]. Thus, by inspecting (5.27) the resulting closed-loop dynamics is given by:

$$
\dot{y}(t) = -\alpha_0 \left(y(t) - y_r\right) \tag{5.29}
$$

because it is sufficient to differentiate once the output function to see explicitly the control input.

The value of α_0 has to be sufficiently small to reject the influence of the S_{NO_3} and S_{NO_2} derivatives at the reactor output in the output dynamics but large enough to bypass the model uncertainties, especially those that come from $\mu_2(S_{NO_2}, S_C)$.

By approximating the spatial derivatives, the control law to simulate is:

$$
\begin{aligned}
v(t) = &\left(\frac{-\epsilon}{\frac{\Delta S_{NO_3}}{\Delta z} + \frac{\Delta S_{NO_2}}{\Delta z}}\right)\Bigg|_{z=L} \times \left(D_f \frac{\Delta^2 S_{NO_3}}{\Delta z^2} + D_f \frac{\Delta^2 S_{NO_2}}{\Delta z^2}\right. \\
&\left. + \frac{1 - Y_{h_2}}{1.71 Y_{h_2} \epsilon} \mu_2(S_{NO_2}, S_C) X_{amax} - \alpha_0 \left(S_{NO_3} + S_{NO_2} - y_r\right)\right)\Bigg|_{z=L}
\end{aligned}
\tag{5.30}
$$

with $v(0) = 4m/h$.

The spatial derivative terms at $z = L$ are approximated by finite differences as:

$$
\frac{\Delta S_{NO_i}}{\Delta z}\Bigg|_{z=L} = \frac{S_{NO_i}(N) - S_{NO_i}(N-1)}{\Delta z}
$$

$$\left.\frac{\Delta^2 S_{NO_i}}{\Delta z^2}\right|_{z=L} = \frac{S_{NO_i}(N) - 2S_{NO_i}(N-1) + S_{NO_i}(N-2)}{\Delta^2 z}$$

for $i = 2, 3$.

It must be pointed out that the parabolic PDE system has to be solved without boundary conditions at the biofilter output since the control law (5.30) needs to compute both the nitrate and the nitrite first derivatives at the output reactor different to zero. As suggested in chapter 2 , in this section we consider Dirichlet + Robin conditions at $z = 0$, that is, both boundary conditions at the reactor input, rather than to use the classical Robin + Neumann conditions at $z = 0$ and $z = L$, respectively. Again, a reference $y_r = 4.0$ is considered.

To calibrate the linearizing controller, a gain $\alpha_0 = 10$ was initially proposed. Under the hypothesis that the system is certain, the output converges quickly towards the reference and the disturbance is correctly rejected. However, the controller is strongly susceptible to model uncertainties. α_0 was then increased so as to reduce the influence of model uncertainties. $\alpha_0 = 50$ is then proposed to get robustness over uncertainties in the original model growth terms μ_1 and μ_2 without degradating too much the closed-loop dynamics. A tolerance upon 15% of error on the real μ_1 and μ_2 values was observed.

Figure 5-5a shows the output reference (in red) and the nitrogen concentration at the reactor output (in blue) according to the controlled input shown in figure 5-5b computed by using the state feedback linearizing controller designed. It can be seen a transition period of more or less two hours before tracking the reference and well rejecting the disturbance.

5.4.2 Non-linear distributed parameter observer

In this section, as it has been done in section 5.3.2, a distributed parameter observer [89] is built to compensate for the lack of measurements. The structure of the DPO

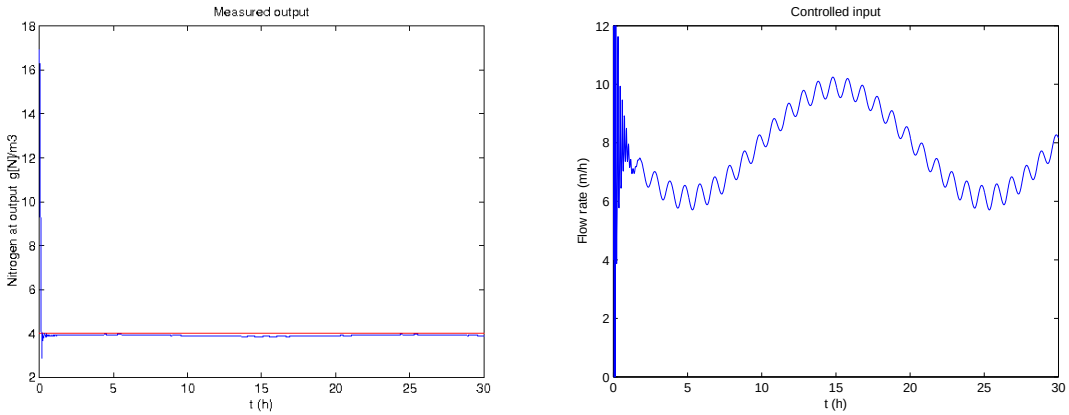

(a) Time-evolution of the nitrogen concentration at the biofilter output. In red the output reference and in blue the real nitrogen concentration.

(b) Time-evolution of the flow rate.

Figure 5-5: Parabolic PDE system. Closed-loop time-evolution by considering the state feedback linearizing controller.

follows from a direct extension of Luenberger's approach to infinite dimensional systems like:

$$\frac{\partial \hat{S}}{\partial t} = A_1 \frac{\partial^2 \hat{S}}{\partial z^2} + A_2 \frac{\partial \hat{S}}{\partial z} + h(\hat{S}) + \Gamma(\hat{S})\,(y_m - \hat{y}_m) \tag{5.31}$$

$$\hat{S}(z,0) = \hat{S}_0(z) \tag{5.32}$$

where $\hat{S} = [\hat{S}_{NO_3}\ \hat{S}_{NO_2}\ \hat{S}_C]^T$ is the estimated state vector and $\Gamma(\hat{S}) \in \mathbb{R}^{3\times l}$ is the correction term. The approach mimics what has been presented in section 5.3.2, but in the current case for the parabolic PDE system. In addition, the same set of available measurements is considered. The design of operator Γ is based on the estimation error equation $e(z,t) = \hat{S}(z,t) - S(z,t)$. It is then obtained:

$$\frac{\partial e}{\partial t} = A_1 \frac{\partial^2 e}{\partial z^2} + A_2 \frac{\partial e}{\partial z} + h(\hat{S}) - h(S) + \Gamma(\hat{S})\,(y_m - \hat{y}_m) \tag{5.33}$$

$$e(z,0) = \hat{S}_0(z) - S_0(z) \tag{5.34}$$

The linearization of $h(S)$ along the estimated trajectory $\hat{S}(z,t)$ may be done to

obtain [89]:

$$\frac{\partial e}{\partial t} = A_1 \frac{\partial^2 e}{\partial z^2} + A_2 \frac{\partial e}{\partial z} + \left.\frac{\partial h(S)}{\partial S}\right|_{\hat{S}} e + \Gamma(\hat{S})\,(y_m - \hat{y}_m) \tag{5.35}$$

This linearization is justified as soon as the estimation error is assumed sufficiently small, i.e.:

$$\|e(z,0)\| = \|\hat{S}_0(z) - S_0(z)\| << 1 \tag{5.36}$$

Physical knowledge about the system is used to design the correction term $\Gamma(\hat{S})\,(y_m - \hat{y}_m)$. Considering the i^{th} PDE, the i^{th} correction term is constructed in terms of error profile $e(z,t)$ and a tuning parameter row vector $\alpha_i \in \mathbb{R}^{1\times 2}$, i.e.:

$$\gamma_i^T\,(y_m - \hat{y}_m) = \left[-\left(\left.\frac{\partial h_i(S)}{\partial S_{NO_3}}\right|_{\hat{S}} + \alpha_{i,1} \right) \; -\left(\left.\frac{\partial h_i(S)}{\partial S_{NO_2}}\right|_{\hat{S}} + \alpha_{i,2} \right) \; 0 \right] e(z,t) \tag{5.37}$$

for $i = 1, 2, 3$. Initial profile $\hat{S}_0(z)$ as well as error profile $e(z,t)$ along the space in equations above are evaluated by linear interpolation of measurement states.

The remark 7 previously stated relative to the selection of the elements of matrix α remains valid. In order to show the convergence of the observer, the estimation is started only after a delay of ten hours. In addition, the elements of the matrix α are proposed as:

$$\alpha = \begin{bmatrix} 110 & 0 \\ 90 & 110 \\ 100 & 100 \end{bmatrix}$$

Figure 5-6 shows the time evolution of the 'real' concentrations (in blue) and the estimated ones (in black), for greated clarity plotted only for six positions along the reactor. It can be observed an acceptable external disturbance rejection. A tolerance upon 15% of error on the true μ_1 and μ_2 values was observed and a noise level of 1% was considered without degradating too much the observer dynamics.

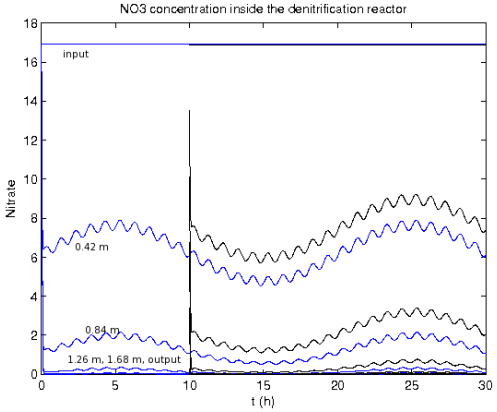

(a) NO_3 concentration.

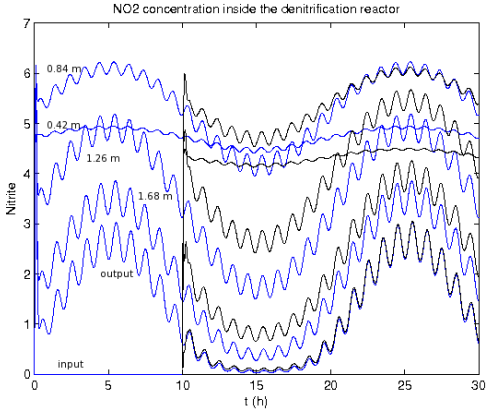

(b) NO_2 concentration.

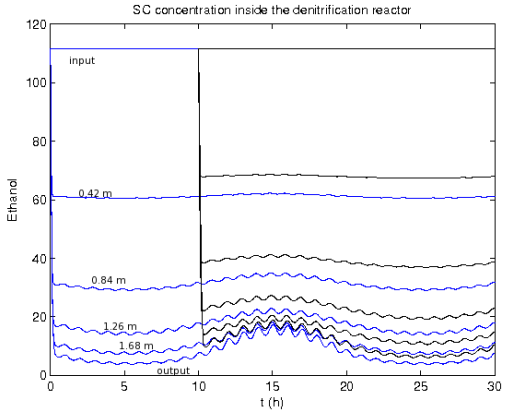

(c) S_C concentration.

Figure 5-6: Parabolic PDE model. State variables estimated by considering the distributed parameter observer. In blue the 'real' concentrations and in black the estimated ones. Only six locations are plotted to increase the readability of the figure.

5.4.3 Observer-based output feedback linearizing controller

At this moment a feedback linearizing controller and a distributed parameter observer have been developed by using a late lumping approach over the hyperbolic PDE system (5.2). The overall control law is then the aggregation of the state feedback linearizing control with the distributed parameter observer, that is:

$$\begin{aligned} v(t) = & \left(\frac{-\epsilon}{\frac{\Delta \hat{S}_{NO_3}}{\Delta z} + \frac{\Delta \hat{S}_{NO_2}}{\Delta z}} \right) \Bigg|_{z=L} \times \Bigg(D_f \frac{\Delta^2 \hat{S}_{NO_3}}{\Delta z^2} + D_f \frac{\Delta^2 \hat{S}_{NO_2}}{\Delta z^2} \\ & + \frac{1 - Y_{h_2}}{1.71 Y_{h_2} \epsilon} \mu_2(\hat{S}_{NO_2}, \hat{S}_C) X_{amax} - \alpha_0 \left(\hat{S}_{NO_3} + \hat{S}_{NO_2} - y_r \right) \Bigg) \Bigg|_{z=L} \end{aligned} \tag{5.38}$$

with $v(0) = 4m/h$ and the $\hat{S}(z,t)$ vector estimated by using (5.31) and (5.37).

The spatial derivative terms at $z = L$ are approximated by finite differences as:

$$\left. \frac{\Delta \hat{S}_{NO_i}}{\Delta z} \right|_{z=L} = \frac{\hat{S}_{NO_i}(N) - \hat{S}_{NO_i}(N-1)}{\Delta z}$$

$$\left. \frac{\Delta^2 \hat{S}_{NO_i}}{\Delta z^2} \right|_{z=L} = \frac{\hat{S}_{NO_i}(N) - 2\hat{S}_{NO_i}(N-1) + \hat{S}_{NO_i}(N-2)}{\Delta^2 z}$$

for $i = 2, 3$.

Besides the measurements available at the output ($z = L$), the estimates of the concentration at the last two points before the output are used. The location of those points depend of the number N of discretization points. However, such an influence is limited as soon as the variation of the concentrations remains smooth enough at the end of the biofilter. In the present configuration with $N = 151$, it is the estimations of nitrate and nitrite concentrations at $z = 2.086m$ and $z = 2.072m$ which are used to compute the spatial derivatives.

We are interested in tracking a reference $y_r = 4.0$. In order to keep the distributed parameter observer dynamics faster than the feedback linearizing controller ones, the

elements of the matrix α must be proposed large enough. In this section the same α matrix as in section 5.4.2 is considered. It must be pointed out that estimation starts fithteen minutes after the process beginning and the control action starts once the observer has converged (thirty minutes).

Figures 5-7a and 5-7b show both the nitrate and the nitrite derivatives, in blue the real value and in black the estimated one. It can be observed that the estimated values follow correctly the real ones with an expected error because of the estimated values, the uncertainty and the noise influence.

Figure 5-7c shows in blue the ethanol real value and in black the estimated one at the reactor output. This value is needed to compute the growth term $\mu_2(S_{NO_2}, S_C)$ at the reactor output. The bias in the estimation is related to the model uncertainties and to the noise.

Keeping in mind the comments done in the previous section 5.4.1, $\alpha_0 = 50$ is selected, large enough to get robustness over uncertainties in the original model growth terms μ_1 and μ_2 without degradating too much the closed-loop dynamics. A tolerance upon 15% of error on the prediction of μ_1 and μ_2 was observed. In addition, a noise level upon 1% was correctly filtered. As previoulsy commented, parametric uncertainties of the biofilter model is the most important problem to bypass by the linearizing feedback controller, when the state estimation is sufficiently accurate.

Figure 5-8a shows the output reference (in red) and the nitrogen concentration at reactor output (in blue) according to the controlled input shown in figure 5-8b computed by using the state feedback linearizing controller designed. It can be seen a transition period of more or less two hours before tracking the reference, well rejecting the disturbance and filtering the noise.

5.5 Conclusions

In this chapter a linearizing state feedback controller complemented by a distributed parameter observer was synthesized both for the hyperbolic and for the parabolic PDE

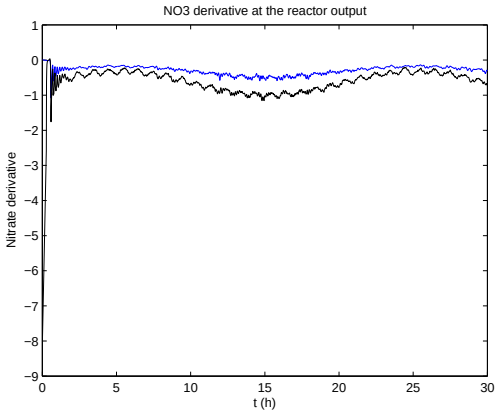

(a) NO_3 derivative at $z = L$.

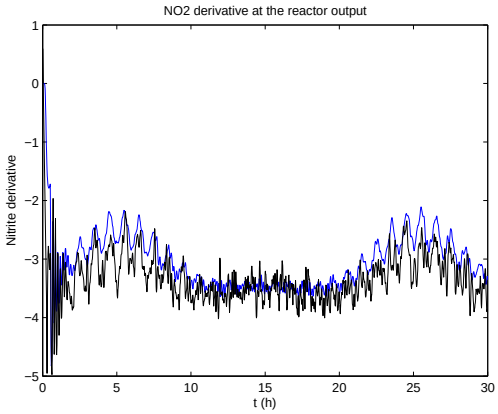

(b) NO_2 derivative at $z = L$.

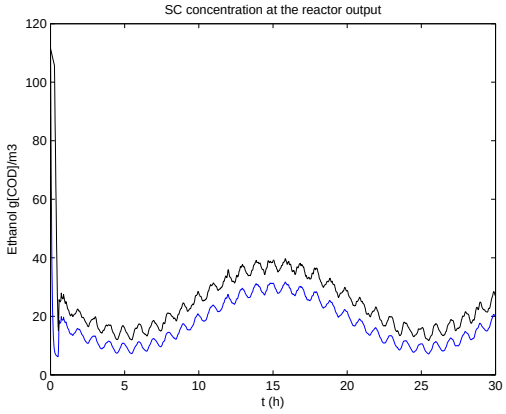

(c) S_C concentration at $z = L$.

Figure 5-7: Parabolic PDE model. Estimations needed by the linearizing control law. In blue the 'real' derivative for 5-7a and for 5-7b or concentration for 5-7c and in black the estimated ones, at $z = L$.

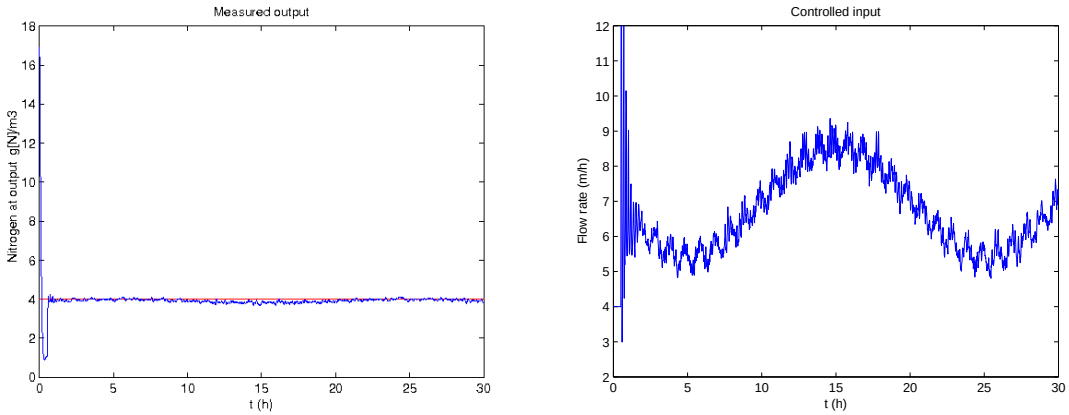

(a) Time-evolution of the nitrogen concentration at the biofilter output. In red the output reference and in blue the real nitrogen concentration.

(b) Time-evolution of the flow rate.

Figure 5-8: Parabolic PDE system. Closed-loop time-evolution by considering the observer-based output feedback linearizing controller.

systems. It must be pointed out that, even if the control laws are different because the diffusion phenomenon is or is not considered, the linear output dynamics resulting are exactly the same in both cases. It can be observed also that the spatial derivative terms do not influence the observer correction term, therefore, both observer are almost the same. The main difference between those two strategies comes from the boundary conditions. Indeed, in the parabolic case, it must be taken care about such boundary conditions, since considering boundary conditions at the reactor output would prevent to apply this strategy.

On the other hand, since it is difficult to demonstrate that both the original system (5.2)-(5.1) for the hyperbolic PDE model and the original system (5.21)-(5.1) for the parabolic PDE model are locally exponentially minimum phase, we have been pragmatics in using the linearizing strategy. Morover, the linearizing control laws synthesized are sensible to model uncertainties. It is natural because the controller is based on the original model and therefore, it takes into account the same parameters, which only approximate the real ones. In addition, large noise perturbating the measured output is not well filtered. However, the disturbance at the reactor input is correctly rejected and the nitrogen concentration at the output kept under its

admissible limit.

Moreover, it must be admitted that, since there is no *Separation Principle* for nonlinear systems, the closed-loop stability of the full observer-based linearizing controlled system is not theoretically supported. Such a perspective of study should most certainly be carried out rather than verify, a posteriori, as it is done here. Anyway, to tune the parameters α_0 and α, it is important to keep in mind that the observer dynamics must be faster than those ones of the state feedback controller, such as to separate, as much as possible, the control activity from the convergence of the observer and to preserve the closed-loop stability of the full system.

Chapter 6

Conclusions and Perspectives

6.1 General conclusion

In this thesis, simulation and control of a denitrification biofilter described by a PDE system have been presented. If the biofilter model takes into account both a diffusion term and a convection term, the resulting model is a parabolic PDE system. On the other hand, if the diffusion term is neglected, the resulting model is an hyperbolic PDE system. Each one of the models needs specific initial and boundary conditions. Hyperbolic PDE systems typically use Dirichlet boundary conditions at the reactor input. Parabolic PDE systems typically consider Robin boundary conditions at the reactor input and Neumann boundary conditions at the reactor output. However, it was discussed that alternative dynamic boundary conditions may be used at the reactor output, which mimic an hyperbolic model at that point. Furthermore, a third boundary condition configuration was also considered to solve a parabolic PDE system, which consisted of Dirichlet + Robin (or equivalently Dirichlet + Neumann) conditions at the reactor input. This set of conditions has allowed us to address the control problem of the parabolic PDE biofilter model with different strategies.

Once the denitrification biofilter model has been defined, it is simulated in order to know its dynamics and to represent the system as an ODE system in state-space form. Several methods are availables to numerically solve a PDE system. The method of

lines is a general technique which may be applied to any PDE classes by approximating the spatial derivatives either by finite differences or by finite elements. The finite difference method is a very simple technique based on truncated Taylor series. Of course, to obtain a correct derivative approximation, a large number of points on the spatial grid must be considered. Fourth-order finite difference approximation has demonstrated excellent results. On the other hand, the finite element method is based on truncated Fourier series of time-depending and space-depending functions. This technique results in a set of matrices to approximate both derivative and integral terms by matrix operations. However, even if the synthesis of FEM matrices is more complex than synthesis of FDM matrices, when compared, the simulation results are almost the same. Both methods result in a set of ODEs to integrate in time.

Another technique used to numerically solve the PDE system describing the biofilter was the method of characteristics. However this method may be used only for the hyperbolic model, which signifies that the diffusion term has been neglected. The solution of the PDE system by using the method of characteristics results in a system of difference equations to be solved in time. Simulation results are very close to those obtained with the method of lines. Since this method results in discrete-time equations to solve, the period of discretization used to develop the final solution is a key point to consider. Of course, the smaller is the period of time, the better is the PDE solution.

Since the spatial operator of the parabolic PDE model has a real discrete spectrum of eigenvalues, a modal analysis can be carried out based on a truncated Fourier series of both spatial-depending and time-depending functions. The spatial-depending functions were calculated off-line by solving an eigenproblem. Because FEM matrices allow to approximate integral and differential operators, the eigenproblem was solved considering them. They were also used to define an operator to project the state variables in the space domain. In this way, an ODE system to compute the time-depending functions (the modes of the system) was obtained. Simulation results by considering the most important modes have shown to be very similar when compared

to the method of lines.

Following, an early lumping approach based on H_2 control and the *LMI* framework was investigated in order to reduce the effect of the influent nitrate concentration along the biofilter and in this way, to maintain the nitrogen concentration at the reactor output under some upper limit concentration. Difference equation system issued from the method of characteristics was considered to synthesize a discrete-time state feedback controller, complemented by a full-order or by a reduced-order Luenberger observer. While the full-order observer better filtered the noise present in the measurements, the reduced-order one presented the advantages of a smaller dimension of the observer synthesized, wich is a key aspect in the *LMI* framework. On the other hand, a very similar strategy has been presented for the control of the parabolic PDE model, but considering now the reduced-order ODE system issued from the modes of the system and a continuous-time version of the observed-based output feedback control strategy. A significant advantage of this strategy is that both the system described by its modes and the associated observer are of much lower orders than the other potential strategies with models issued from MOL or the method of characteristics. This pleads for the use of a parabolic modelling of the biofilter system, that is, considering diffusion phenomena, rather than to use an a priori simpler description of the process without second-order derivatives. The results, very similar to those obtained with a higher order model of the biofilter, demonstrated that the control law synthesized by considering the most important modes satisfied the control objectives.

The main advantage of this early lumping approach is that, it results in a control law easy to implement (linear dynamic system composed by the state-feedback + the state observer), although to the detriment of several manipulations (discretization, linearization, etc.) of the original PDE system to be done before the final controller synthesis. It must be pointed out that the separation principle is verified only in the proposed version which does not consider uncertainties of the linearized system. More complex strategies would have to be carried out to explicitly take into account

additional constraints such as model uncertainty. The results obtained here pave the way, however, for the use of linear control strategies for such PDE nonlinear systems.

Finally, a late lumping approach based on linearizing control was investigated in chapter 5. The control objective, as in chapter 4, was to maintain the nitrogen concentration at the output of the reactor below some given upper bound, in spite of the influent nitrate concentration variations. It was then set as a tracking (nitrogen output reference) and disturbance (influent nitrate concentration) attenuation problem. The strategy followed was to synthesize a feedback controller to linearize the closed-loop dynamics complemented by a distributed parameter observer. It has to be noted that the full observer-based output feedback linearizing control has not been formally proven to be a stabilizing control strategy since the separation principle does not apply for nonlinear system. Moreover, such linearizing control strategy is not very robust to uncertainties of the model parameters, as well associated with a state and parameter observer or not. Its advantage is however that it easily allows to propose a direct feedback strategy without much effort for the synthesis step. In particular, it only involves few parameters to be tuned.

6.2 Perspectives

In this work, two different approaches have been followed in order to synthesize observer-based output feedback controllers to regulate the nitrogen concentration at the output of a denitrification biofilter. Several advantages of the approaches have been brought to the fore, but also several points which will necessitate further investigations. In the case of the early lumping control law based on H_2 control, neither the model parameter uncertainty nor the uncertainty caused by linearization were taken into account, even if they may be easily modeled as a polytope of uncertainty in the *LMI* framework. A short time perspective of this work could then be to consider alternative robust linear control strategies such as dynamic output feedback to be able to deal with model uncertainty. Most of the ideas presented in this thesis will remain valid, but with conditions stated as bilinear matrix inequalities (*BMI*) instead

of *LMI*. On the other hand, in the case of the control law based on the linearization strategy, a theoretical robust analysis must be investigated in order to guarantee, a priori, the stability of the designed controller.

Another subject not handled in this work but also important is the optimal sensor location and the optimal discretizing points location [91], [88], [29]. As a matter of fact, it has been slightly mentioned throughout the chapters on control design that a set of measurements had to be considered to implement state observers, but only from the observability point of view. It may however be expected that the quality of the observation is strongly related, not only to the number of measurements but also to their location.

Finally, in this thesis, the flow rate has been selected as control input. As mentioned in chapter 2, the ethanol concentration at the reactor input is another variable which may be taken into account has control input. This would imply to investigate boundary control strategies such as backsteping control as an alternative nonlinear approach [39], [40].

To go further, one can expect to transfer in the industry some of the ideas presented in this thesis, for process optimization and control of many biological and chemical processes. However, control implementation will imply to deal with different tasks, from Data-Acquisition Systems (DAQ) to Human-Machine Interfaces (HMI). All these tasks are included into two great complementary systems: Supervisory Control And Data Acquisition Systems (SCADA) and Digital Control Systems. A SCADA system generally refers to an industrial control system: a computing system monitoring and controlling a process. Its objective is to centralize information about the process from sensors via industrial networks to data bases in industrial servers. It also sends information to actuators in order to act over others variables. It is then some coordinator of the system, but the control is not computed there. On the other hand, a Digital Control System takes all the information available about the process, filters it, estimates if necessary non-available variables by using observation techniques and then, by applying a control strategy like state feedback or output

feedback, compute the information needed in order to control the process by using a digital system.

Thus, in this work we have studied various control strategies but keeping in mind the idea of their future implementation on embedded computing systems. We have focused in this document on the "control" part of the stack of tasks to be performed. This part will have to be surrounded by the several other lines of research and technological development which have to be considered in the biotechnological process operation, such as:

- further investigations in modelling, estimation and control of biotechnological processes;
- development of DAQ systems to measure biochemical variables;
- development of embedded computing systems based on vectorial architecture processors with standard interfaces (RS-485, USB, Ethernet, etc.) to communicate using standard industrial protocols (Modbus, DNP3, UCA/MMS, TCP/IP, etc.);
- and, finally, development of HMIs based on Information Technology (IT) to manage the complete information about the process to control.

Appendix A

Sensitivity Differential Equations

A.1 Sensitivity equations for the nitrate

The equations describing the nitrate sensitivity with respect to the parameter vector p are given by:

$$\begin{aligned}\frac{\partial s_{11}}{\partial t} =& D_f \frac{\partial^2 s_{11}}{\partial z^2} - \frac{v}{\epsilon}\frac{\partial s_{11}}{\partial z} - \frac{1-Y_{h1}}{1.14 Y_{h1}\epsilon} p_1 \left(\frac{p_3 s_{11}}{(S_{NO_3}+p_3)^2}\right)\left(\frac{S_C}{S_C+p_5}\right) X_a \\ & - \frac{1-Y_{h1}}{1.14 Y_{h1}\epsilon}\left(\frac{S_{NO_3}}{S_{NO_3}+p_3}\right)\left(\frac{S_C}{S_C+p_5}\right) X_a\end{aligned} \tag{A.1}$$

$$\frac{\partial s_{12}}{\partial t} = D_f \frac{\partial^2 s_{12}}{\partial z^2} - \frac{v}{\epsilon}\frac{\partial s_{12}}{\partial z} \tag{A.2}$$

$$\begin{aligned}\frac{\partial s_{13}}{\partial t} =& D_f \frac{\partial^2 s_{13}}{\partial z^2} - \frac{v}{\epsilon}\frac{\partial s_{13}}{\partial z} - \frac{1-Y_{h1}}{1.14 Y_{h1}\epsilon} p_1 \left(\frac{p_3 s_{13}}{(S_{NO_3}+p_3)^2}\right)\left(\frac{S_C}{S_C+p_5}\right) X_a \\ & + \frac{1-Y_{h1}}{1.14 Y_{h1}\epsilon} p_1 \left(\frac{S_{NO_3}}{(S_{NO_3}+p_3)^2}\right)\left(\frac{S_C}{S_C+p_5}\right) X_a\end{aligned} \tag{A.3}$$

$$\frac{\partial s_{14}}{\partial t} = D_f \frac{\partial^2 s_{14}}{\partial z^2} - \frac{v}{\epsilon}\frac{\partial s_{14}}{\partial z} \tag{A.4}$$

$$\begin{aligned}\frac{\partial s_{15}}{\partial t} =& D_f \frac{\partial^2 s_{15}}{\partial z^2} - \frac{v}{\epsilon}\frac{\partial s_{15}}{\partial z} - \frac{1-Y_{h1}}{1.14 Y_{h1}\epsilon} p_1 \left(\frac{p_3 s_{15}}{(S_{NO_3}+p_3)^2}\right)\left(\frac{S_C}{S_C+p_5}\right) X_a \\ &+ \frac{1-Y_{h1}}{1.14 Y_{h1}\epsilon} p_1 \left(\frac{S_{NO_3}}{S_{NO_3}+p_3}\right)\left(\frac{S_C}{(S_C+p_5)^2}\right) X_a\end{aligned} \tag{A.5}$$

A.2 Sensitivity equations for the nitrite

The equations describing the nitrite sensitivity with respect to the parameter vector p are given by:

$$\frac{\partial s_{21}}{\partial t} = D_f \frac{\partial^2 s_{21}}{\partial z^2} - \frac{v}{\epsilon}\frac{\partial s_{21}}{\partial z} + \frac{1-Y_{h1}}{1.14 Y_{h1}\epsilon}\left(\frac{S_{NO_3}}{S_{NO_3}+p_3}\right)\left(\frac{S_C}{S_C+p_5}\right) X_a \tag{A.6}$$

$$\begin{aligned}\frac{\partial s_{22}}{\partial t} =& D_f \frac{\partial^2 s_{22}}{\partial z^2} - \frac{v}{\epsilon}\frac{\partial s_{22}}{\partial z} - \frac{1-Y_{h2}}{1.71 Y_{h2}\epsilon} p_2 \left(\frac{p_4 s_{22}}{(S_{NO_2}+p_4)^2}\right)\left(\frac{S_C}{S_C+p_5}\right) X_a \\ &- \frac{1-Y_{h2}}{1.71 Y_{h2}\epsilon}\left(\frac{S_{NO_2}}{S_{NO_2}+p_4}\right)\left(\frac{S_C}{S_C+p_5}\right) X_a\end{aligned} \tag{A.7}$$

$$\frac{\partial s_{23}}{\partial t} = D_f \frac{\partial^2 s_{23}}{\partial z^2} - \frac{v}{\epsilon}\frac{\partial s_{23}}{\partial z} - \frac{1-Y_{h1}}{1.14 Y_{h1}\epsilon} p_1 \left(\frac{S_{NO_3}}{(S_{NO_3}+p_3)^2}\right)\left(\frac{S_C}{S_C+p_5}\right) X_a \tag{A.8}$$

$$\begin{aligned}\frac{\partial s_{24}}{\partial t} =& D_f \frac{\partial^2 s_{24}}{\partial z^2} - \frac{v}{\epsilon}\frac{\partial s_{24}}{\partial z} - \frac{1-Y_{h2}}{1.71 Y_{h2}\epsilon} p_2 \left(\frac{p_4 s_{24}}{(S_{NO_2}+p_4)^2}\right)\left(\frac{S_C}{S_C+p_5}\right) X_a \\ &- \frac{1-Y_{h2}}{1.71 Y_{h2}\epsilon} p_2 \left(\frac{S_{NO_2}}{(S_{NO_2}+p_4)^2}\right)\left(\frac{S_C}{S_C+p_5}\right) X_a\end{aligned} \tag{A.9}$$

$$\begin{aligned}\frac{\partial s_{25}}{\partial t} =& D_f \frac{\partial^2 s_{25}}{\partial z^2} - \frac{v}{\epsilon}\frac{\partial s_{25}}{\partial z} - \frac{1-Y_{h1}}{1.14 Y_{h1}\epsilon} p_1 \left(\frac{S_{NO_3}}{S_{NO_3}+p_3}\right)\left(\frac{S_C}{(S_C+p_5)^2}\right) X_a \\ & - \frac{1-Y_{h2}}{1.71 Y_{h2}\epsilon} p_2 \left(\frac{S_{NO_2}}{(S_{NO_2}+p_4)^2}\right)\left(\frac{S_C}{S_C+p_5}\right) X_a \\ & + \frac{1-Y_{h2}}{1.71 Y_{h2}\epsilon} p_2 \left(\frac{S_{NO_2}}{S_{NO_2}+p_4}\right)\left(\frac{S_C}{(S_C+p_5)^2}\right) X_a \end{aligned} \tag{A.10}$$

A.3 Sensitivity equations for the ethanol

The equations describing the ethanol sensitivity with respect to the parameter vector p are given by:

$$\begin{aligned}\frac{\partial s_{31}}{\partial t} =& D_f \frac{\partial^2 s_{31}}{\partial z^2} - \frac{v}{\epsilon}\frac{\partial s_{31}}{\partial z} - \frac{1}{Y_{h1}\epsilon} p_1 \left(\frac{S_{NO_3}}{S_{NO_3}+p_3}\right)\left(\frac{p_5 s_{31}}{(S_C+p_5)^2}\right) X_a \\ & - \frac{1}{Y_{h1}\epsilon}\left(\frac{S_{NO_3}}{S_{NO_3}+p_3}\right)\left(\frac{S_C}{S_C+p_5}\right) X_a \\ & - \frac{1}{Y_{h2}\epsilon} p_2 \left(\frac{S_{NO_2}}{S_{NO_2}+p_4}\right)\left(\frac{p_5 s_{31}}{(S_C+p_5)^2}\right) X_a \end{aligned} \tag{A.11}$$

$$\begin{aligned}\frac{\partial s_{32}}{\partial t} =& D_f \frac{\partial^2 s_{32}}{\partial z^2} - \frac{v}{\epsilon}\frac{\partial s_{32}}{\partial z} - \frac{1}{Y_{h1}\epsilon} p_1 \left(\frac{S_{NO_3}}{S_{NO_3}+p_3}\right)\left(\frac{p_5 s_{32}}{(S_C+p_5)^2}\right) X_a \\ & - \frac{1}{Y_{h2}\epsilon} p_2 \left(\frac{S_{NO_2}}{S_{NO_2}+p_4}\right)\left(\frac{p_5 s_{32}}{(S_C+p_5)^2}\right) X_a \\ & - \frac{1}{Y_{h2}\epsilon}\left(\frac{S_{NO_2}}{S_{NO_2}+p_4}\right)\left(\frac{S_C}{S_C+p_5}\right) X_a \end{aligned} \tag{A.12}$$

$$\begin{aligned}\frac{\partial s_{33}}{\partial t} =& D_f \frac{\partial^2 s_{33}}{\partial z^2} - \frac{v}{\epsilon}\frac{\partial s_{33}}{\partial z} - \frac{1}{Y_{h1}\epsilon} p_1 \left(\frac{S_{NO_3}}{S_{NO_3}+p_3}\right)\left(\frac{p_5 s_{33}}{(S_C+p_5)^2}\right) X_a \\ & + \frac{1}{Y_{h1}\epsilon} p_1 \left(\frac{S_{NO_3}}{(S_{NO_3}+p_3)^2}\right)\left(\frac{S_C}{S_C+p_5}\right) X_a \\ & - \frac{1}{Y_{h2}\epsilon} p_2 \left(\frac{S_{NO_2}}{S_{NO_2}+p_4}\right)\left(\frac{p_5 s_{33}}{(S_C+p_5)^2}\right) X_a \end{aligned} \tag{A.13}$$

$$\begin{aligned}\frac{\partial s_{34}}{\partial t} =& D_f \frac{\partial^2 s_{34}}{\partial z^2} - \frac{v}{\epsilon}\frac{\partial s_{34}}{\partial z} - \frac{1}{Y_{h1}\epsilon} p_1 \left(\frac{S_{NO_3}}{S_{NO_3}+p_3}\right)\left(\frac{p_5 s_{34}}{(S_C+p_5)^2}\right) X_a \\ & - \frac{1}{Y_{h2}\epsilon} p_2 \left(\frac{S_{NO_2}}{S_{NO_2}+p_4}\right)\left(\frac{p_5 s_{34}}{(S_C+p_5)^2}\right) X_a \\ & + \frac{1}{Y_{h2}\epsilon} p_2 \left(\frac{S_{NO_2}}{(S_{NO_2}+p_4)^2}\right)\left(\frac{S_C}{S_C+p_5}\right) X_a \end{aligned} \tag{A.14}$$

$$\begin{aligned}\frac{\partial s_{35}}{\partial t} =& D_f \frac{\partial^2 s_{35}}{\partial z^2} - \frac{v}{\epsilon}\frac{\partial s_{35}}{\partial z} - \frac{1}{Y_{h1}\epsilon} p_1 \left(\frac{S_{NO_3}}{S_{NO_3}+p_3}\right)\left(\frac{p_5 s_{35}}{(S_C+p_5)^2}\right) X_a \\ & + \frac{1}{Y_{h1}\epsilon} p_1 \left(\frac{S_{NO_3}}{S_{NO_3}+p_3}\right)\left(\frac{S_C}{(S_C+p_5)^2}\right) X_a \\ & - \frac{1}{Y_{h2}\epsilon} p_2 \left(\frac{S_{NO_2}}{S_{NO_2}+p_4}\right)\left(\frac{p_5 s_{35}}{(S_C+p_5)^2}\right) X_a \\ & + \frac{1}{Y_{h2}\epsilon} p_2 \left(\frac{S_{NO_2}}{S_{NO_2}+p_4}\right)\left(\frac{S_C}{(S_C+p_5)^2}\right) X_a \end{aligned} \tag{A.15}$$

Appendix B

Observability Test

B.1 Observability test for the discrete state space model

The nitrate and the nitrite are variables that can be measured by sensors. An observability test on the pair (A, C_y) is done, by try and error, in order to know the minimum number of measurement points needed and their specific position along the biofilter to be able to estimate the overall set of state variables.

After testing several configurations of the matrix C_y, six measurement points were determined as the minimum number, homogeneously distributed along the biofilter from the input to the output as shown in Table B.1, to obtain a pair (A, C_y) observable.

Measurement point	Position along the reactor
1	input
2	0.42 m
3	0.84 m
4	1.26 m
5	1.68 m
6	output

Table B.1: Measurement points along the biofilter.

B.2 Observability test for the continuous state space model

As mentioned before, the nitrate and the nitrite are variables that can be measured by sensors. An observability test on the pair (A, C_{ym}) is now done, because the linear system is described by the modes, in order to know the minimum number of measurement points needed and their specific position along the biofilter to be able to estimate the overall set of state variables.

After testing several configurations of the matrix C_y and calculating the matrix C_{ym}, six measurement points were determined as the minimum number, homogeneously distributed along the biofilter from the input to the output as shown in Table B.1, to obtain a pair (A, C_{ym}) observable.

Bibliography

[1] F. Acevedo, J. C. Gentina, and A. Illantes, editors. *Fundamentos de ingeniería bioquímica*. Pontificia Universidad Católica de Valparaiso, 2004.

[2] E. Aguilar-Garnica, D. Dochain, V. Alcaraz-González, and V. González-Alvarez. A multivariable control scheme in a two-stage anaerobic digestion system described by partial differential equations. *Journal of process control*, 19:1324–1332, 2009.

[3] J. Alvarez-Ramirez, H. Puebla, and J.A. Ochoa-Tapia. Linear boundary control for a class of nonlinear PDE processes. *System and control letters*, 44:395–403, 2001.

[4] D. R. Andrea. A linear matrix inequality approach to decentralized control of distributed parameter systems. In *Proceedings of the American Control Conference*, pages 1350–1354, 1998.

[5] P. Ansaklis and A. Michel. *Linear Systems*. McGraw-Hill, 2nd. edition, 2006.

[6] H.X. De Araùjo. *Sur la stabilité de systèmes incertains sujets à des contraintes sur l'état et la commande*. PhD thesis, LAAS-CNRS, Université de Toulouse, 1998.

[7] H.T. Banks, R.C. Smith, and Y. Wang. *Smart Material Structures: Modeling, Estimation and Control*. Masson/John Wiley, 1996. Paris/Chichester.

[8] G. Berkooz, P. Holmes, and L. Lumley. The Proper Orthogonal Decomposition in the analysis of turbulent flows. *Ann. Rev. Fluid Mech.*, 25:539–575, 1993.

[9] J. Bernussou, P. L. D. Peres, and J. C. Geromel. A linear programming oriented procedure for quadratic stabilization of uncertain systems. *Systems and Control Letters*, 13(1):65–72, 1989.

[10] O. Boubaker and J. P. Babary. On SISO and MIMO variable structure control of non linear distributed parameter system: aplication to fixed bed reactors. *Journal of process control*, 13:729–737, 2003.

[11] S. Bourrel. *Estimation et commande d'un procédé à paramètres répartis utilisé pour le traitement biologique de l'eau à potabiliser*. PhD thesis, LAAS-CNRS, Université de Toulouse, 1996.

[12] S. Bourrel, D. Dochain, J.P. Babary, and I. Queinnec. Modelling, identification and control of a denitrifying biofilter. *Journal of process Control*, 10:73–91, 2000.

[13] S. Boyd, L. El Ghaoudi, E. Feron, and V. Balakrishnan. *Linear matrix inequalities in system and control theory*. SIAM, 1994.

[14] A. G. Butkovskiy and A. Y. Lerner. The optimal control of systems with distributed parameters. *Automation and Remote Control*, 22(6):472–477, 1960.

[15] C. I. Byners, I. G. Lauko, D. S. Gilliam, and V.I. Shubov. Output regulation for linear distributed parameter systems. *IEEE Transactions on Automatic Control*, 45(12):682–691, 2000.

[16] M. Chilali and P. Gahinet. H_∞ design with pole placement constraints: An LMI approach. *Transactions on automatic control*, 41(3):358–367, 1996.

[17] P. D. Christofides. Robust control of parabolic PDE systems. *Chemical Engineering Science*, 53(16):2949–2965, 1998.

[18] P. D. Christofides. *Nonlinear and robust control of PDE systems - Methods and applications to transport-reaction processes*. Birkhauser, 2001.

[19] P.D. Christofides and P. Daoutidis. Robust control of hyperbolic PDE systems. *Chemical Engineering Science*, 53(1):85–105, 1998.

[20] J. S. Devinny and J. Ramesh. A phenomenological review of biofilter models. *Chemical Engineering Journal*, 113:187–196, 2005.

[21] D. Dochain, J. P. Babary, and N. Tali-Maamar. Modelling and adaptative control of non linear distributed parameter bioreactors via orthogonal collocation. *Automatica*, 28:873–883, 1992.

[22] D. Dochain and P.A. Vanrolleghem. *Dynamical Modelling and Estimation in Wastewater Treatment Processes*. IWA Publishing, 2001.

[23] A. K. Dramé, D. Dochain, and J. J. Winkin. Asymptotic behavior and stability for solutions of a biochemical reactor distributed parameter model. *IEEE Transactions on Automatic Control*, 53(1):412–416, 2008.

[24] F. Fernández-Polanco, E. Méndez, M. A. Urue na, S. Villaverde, and P. A. García. Spatial distribution of heterotrophs and nitrifiers in a submerged biofilter for nitrification. *Water Research*, 34(16):4081–4089, 2000.

[25] P. Gahinet. Explicit controller formulas for LMI-based H_∞ synthesis. *Automatica*, 32(7):1007–1014, 1996.

[26] P. Gahinet and P. Apkarian. A linear matrix inequality approach to H_∞ control. *International Journal of Robust and Nonlinear Control*, 4(4):421–448, 1994.

[27] P. Gahinet, A. Nemirovski, A. J. Laub, and M. Chilali. *LMI control toolbox user's guide*. The Mathworks Inc., 1995.

[28] G. Garcia, J. Daafouz, and J. Bernussou. Output feedback disk pole assignment for systems with positive real uncertainty. *IEEE Transactions on Automatic Control*, 41(9):1385–1391, 1996.

[29] M. R. García, C. Vilas, J. R. Banga, and A. A. Alonso. Optimal field reconstruction of distributed process systems from partial measurements. *Ind. Eng. Chem. Res.*, 46:530–539, 2007.

[30] J. C. Geromel, P. L. D. Peres, and S. R. Souza. H_2 guaranteed cost control for uncertain continuous-time linear systems. *Systems and Control Letters*, 19(1):23–27, 1992.

[31] P. K. Gundepudi and J. C. Friedly. Velocity control of hyperbolic partial differential equation systems with single characteristic variable. *Chemical Engineering Science*, 53(24):4055–4072, 1998.

[32] M. Henze, P. Harremo es, J. Jansen, and E. Arvin. *Wastewater treatment.* Springer, 3er. edition edition, 2002.

[33] T. Hu, Z. Lin, and B. M. Chen. An analysis and design method for linear systems subject to actuator saturation and disturbance. *Automatica*, 32:351–359, 2002.

[34] C. Hua and L. Rodino. General theory of PDE and gevrey classes. *General theory of partial differential equations and microlocal analysis*, 349:6–81, 1995. Series Pitman Research Notes in Mathematics Series.

[35] A. Isidori. *Nonlinear control systems: An introduction.* Springer-Verlag, 2nd. edition, 1989.

[36] T. Iwasaki and R. E. Skelton. All controllers for the general H_∞ control problem: previous LMI existence conditions and state space formulas. *Automatica*, 30(8):1307–1317, 1994.

[37] J. Jacob. *Modelisation et simulation dynamique de procédés de traitement des eaux de type biofiltre: Traitement de systèmes d'équations differentielles partielles et algebraiques (EDPA).* PhD thesis, INP de Toulouse, 1994.

[38] K. Karhunen. Zur spektral theori stochasticher prozesse. *Annales Academiae Scientiarum Fennicae Series A1-Mathematica Phys*, 37, 1946.

[39] H. K. Khalil. *Nonlinear systems.* Prentice-Hall, 2nd. edition edition, 1996.

[40] M. Krstic and A. Smyshlyaev. Backstepping boundary control - a tutorial. In *Proceedings of the American Control Conference*, pages 870–875, 2007.

[41] B. Laroche, Ph. Martin, and P. Rouchon. Motion planning for the heat equation. *International Journal on Robust Nonlinear Control*, 10:629–643, 2000.

[42] R. J. LeVeque. *Finite difference methods for differential equations*. University of Washington, 2005.

[43] W. S. Levine, editor. *The control handbook*. CRC Press Inc., 1996.

[44] C. H. Liang and P. C. Chiang. Mathematical model of the non-steady-state adsorption and biodegradation capacities of bac filters. *Journal of Hazardous Materials*, B139:316–322, 2007.

[45] C. H. Lien. Robust observer-based control of systems with state perturbations via LMI approach. *IEEE Transactions on Automatic Control*, 49(8):1365–1370, 2004.

[46] M. Loeve. Functiona aleatoire de second ordre. *Compt. Rend. Acad. Sci.*, 1945. Paris.

[47] J. Löfberg. YALMIP: A toolbox for modeling and optimization in MATLAB. In *In Proceedings of the CACSD Conference*, 2004. Taipei, Taiwan.

[48] D. Matko, G. Geiger, and W. Gregoritza. Pipeline simulation techniques. *Mathematics and Computers in Simulation*, 52:211–230, 2000.

[49] R. M. M. Mattheij, S.W. Rienstra, and J. H. M. ten Thije Boonkkamp. *Partial Differential Equations: Modeling, Analysis and Computation*. SIAM, 2005.

[50] Y. Nesterov and A. Nemirovskii. *Interior point polynomial algorithms in convex programming*. SIAM, 1994.

[51] R. Oliveira, M. C. de Oliveira, and P. L. D. Peres. Convergent LMI relaxations for robust analysis of uncertain linear systems using lifted polynomial parameter-dependent Lyapunov functions. *Systems and Control Letters*, 57(8):680–689, 2008.

[52] N. Orhanovic, V.K.Tripathi, and P. Wang. Generalized method of characteristics for time domain simulation of multiconductor lossy transmission lines. *IEEE*, pages 2388–2391, 1990.

[53] R. Padhi and Sk. Faruque Ali. An account of chronological developments in control of distributed parameter systems. *Annual Reviews in Control*, (33):59–68, 2009.

[54] D. Peaucelle and D. Arzelier. An efficient numerical solution for H_2 static output feedback synthesis. In *Proceedings of the European Control Conference*, September 2001. Porto (Portugal).

[55] R. Phadi and S. Balakrishnan. Optimal dynamic inversion control design for a class of nonlinear distributed parameter systems with continuous and discrete actuators. *IET Control Theory and Application*, 1(6):1662–1671, 2007.

[56] F. Pourki. *Stabilization and control analysis of distributed parameter systems*. PhD thesis, Purdue University, 1988.

[57] A. J. Pritchard and J. Zabczyk. Stability and stabilizability of infinite dimensional systems. *SIAM Review*, 23(5):25–52, 1981.

[58] I. Queinnec, J.C. Ochoa, A. Vande Wouwer, and E. Paul. Development and calibration of a nitrification PDE model based on experimental data issued from biofilter treating drinking water. *Biotechnology and Bioengineering*, 94(2):209–222, 2006.

[59] H. Rabitz, M. Kramer, and D. Dacol. Sensitivity analysis in chemical kinetics. *Annual Review of Physical Chemistry*, 1983.

[60] W. H. Ray. *Advances process control*. McGraw-Hill, 1981.

[61] J. Reinschke and M. C. Smith. Feedback control of LTI spatially distributed systems. In *Proceedings of the 38th conference on decision and control*, pages 1101–1106, 1999.

[62] Y. Renard, A. Rondepierre, and A. Rouchon. Mathématiques générales. Technical report, INSA, 2010.

[63] E. Rother and P. Cornel. Optimising design, operation and energy consumption of biological aerated filters (BAF) for nitrogen removal of municipal wastewater. *Water Science and Technology*, 50(6):131–139, 2004.

[64] W. J. Rugh. *Mathematical description of linear systems.* Marcel Bekker Inc.

[65] A. Saltelli, K. Chan, and E. M. Scott, editors. *Sensitivity analysis.* Wiley, 2004.

[66] V. Saravanan and T.R. Sreekrishnan. Modelling anaerobic biofilm reactors-a review. *Journal of Environmental Management*, 81:1–18, 2006.

[67] S. Sastry. *Nonlinear systems: analysis, stability and control.* Springer-Verlag, 1999.

[68] H. Satoh, H. Ono, B. Rulin, J. Kamo, S. Okabe, and K. Fukushi. Macroscale and microscale analyses of nitrificacion and denitrification in biofilms attached on membrane aerated biofilm reactors. *Water research*, 38:1633–1641, 2004.

[69] C. Scherer and S. Weiland. *Linear Matrix Inequalities in Control.* Delf University of Technology, 2004.

[70] C. W. Scherer. An efficient solution to multi-objective control problems with LMI objectives. *System and Control Letters*, 40:43–57, 2000.

[71] W. E. Schiesser. *The numerical method of lines.* Academic press, New York, 1991.

[72] W. E. Schiesser. PDE boundary conditions from minimum reduction of the PDE. *Applied Numerical Mathematics*, 20(1-2):171–179, 1996.

[73] H. Shanga, J. F. Forbesb, and M. Guay. Feedback control of hyperbolic distributed parameter systems. *Chemical Engineering Science*, (60):969–980, 2005.

[74] L. Sirovich. Turbulence and the dynamics of coherent structures. Part I: Coherent structures. *Quaterly of Appl. Math.*, 45(3):561–571, 1987.

[75] A. Smyshlyaev and M. Krstic. Closed-form boundary state feedbacks for a class 1-D partial integro-differential equations. *IEEE Transactions in Automatic Control*, 49(12):2185–2202, 2004.

[76] J.F. Sturm. Using SeDuMi 1.02, a MATLAB toolbox for optimization over symmetric cones. *Optimization Methods and Software*, 11-12:625–653, 1999.

[77] S. Tarbouriech, G. Garcia, and A. H. Glattfelder, editors. *Advanced strategies in control systems with input and output constraints*. Springer-Verlag, 2007.

[78] R. Tomovi. *Sensitivity analysis of dynamic systems*, volume 1. McGraw-Hill, 1963.

[79] I. Torres and I. Queinnec. Commande et observation robuste d'un réacteur de dénitrification de type biofiltre. In *Congrès de l'École Doctorale Systèmes*, 2008.

[80] I. Torres and I. Queinnec. Modélisation et commande robuste d'un réacteur de dénitrification de type biofiltre. In *Conférence Internationale Francophone d'Automatique*, 2008.

[81] I. Torres, I. Queinnec, C. Vilas, and A. Vande Wouwer. A linear control strategy applied to a denitrification biofilter. In *IFAC Workshop on Control of Distributed Parameter Systems*, 2009.

[82] I. Torres, I. Queinnec, C. Vilas, and A. Vande Wouwer. Observer-based output feedback linear control applied to a denitrification reactor. In *IEEE American Control Conference*, 2010.

[83] I. Torres, I. Queinnec, and A. Vande Wouwer. Observer-based output feedback linearizing control applied to a denitrification reactor. In *IFAC Computer Applications in Biotechnology*, 2010.

[84] I. Torres, C. Vilas, A. Vande Wouwer, and I. Queinnec. Nonlinear distributed parameter observer applied to a denitrification reactor. In *International Conference on Mathematical Modelling*, 2009.

[85] C. Vilas. *Modelling, simulation and robust control of distributed processes: Application to chemical and biological systems*. PhD thesis, Universidade de Vigo, 2008.

[86] P. K. C. Wang. Asymptotic stability of distributed parameter systems with feedback control. *IEEE Transactions on Automatic Control*, 11:46–54, 1966.

[87] P. K. C. Wang and F. Tung. Optimum control of distributed parameter systems. *Journal of Basic Engineering*, pages 67–79, 1964.

[88] A. Vande Wouwer, N. Point, S. Porteman, and M. Remy. An approach to the selection of optimal sensor locations in distributed parameter systems. *Journal of Process Control*, 10:291–300, 2000.

[89] A. Vande Wouwer and M. Zeitz. State estimation in distributed parameter systems. *Control Systems, Robotics and Automation, Theme in Enzyclopedia of Life Support Systems*, 2003.

[90] W. Wu and C. Lu. Output regulation of two-time-scale hyperbolic PDE system. *Journal of process control*, 11:637–647, 2001.

[91] T. K. Yu and J. H. Seinfeld. Observability and optimal measurment location in linear distributed parameter systems. *International Journal of Control*, 18:785–799, 1973.

[92] S. M. Zarook and A. A. Shaikh. Analysis and comparison of biofilter models. *Chemical Engineering Journal*, 65:55–61, 1997.

[93] K. Zhou, J. Doyle, and K. Glover. *Robust and optimal control*. Prentice Hall, 1996.

[94] O. C. Zienkiewicz, R. L. Taylor, and J. Z. Zhu. *The Finite Element Method: Its Basis and Fundamentals.* Elsevier, Amsterdam, 6^{th} edition, 2005.

[95] D. Zwillinger. *Handbook of differential equations.* Academic Press, 3rd. edition, 1998.